STRUCTURAL ANALYSIS OF THE P85 BH DOMAIN IN COMPLEX WITH BINDING PARTNERS AND EFFECT OF MUTATIONS

A Thesis Submitted to the College of Graduate Studies and Research in Partial Fulfillment of the Requirements of the Degree of
Master of Science
in the Department of Biochemistry
University of Saskatchewan
Saskatoon

by
Jeremy Davin Seiberling Marshall

Permission to Use

In presenting this thesis in partial fulfillment of the requirements for a Postgraduate degree from the University of Saskatchewan, I agree that the Libraries of this University may make it freely available for inspection. I further agree that permission for copying of this thesis in any manner, in whole or in part, for scholarly purposes may be granted by the professor or professors who supervised my thesis work or, in their absence, by the Head of the Department or the Dean of the College under which this thesis work was done. It is understood that any copying or publication or use of this thesis or parts therof for financial gain shall not be allowed without my written permission. It is also understood that due recognition shall be given to me and to the University of Saskatchwan in any scholarly use which may be made of any material in my thesis.

Request for permission to copy or to make other use of materials in this thesis in whole or in part should be addressed to:

Deborah Anderson, Ph.D.
Rm 4D30.2 Health Sciences Bldg
University of Saskatchewan
107 Wiggins Road
Saskatoon, SK Canada S7N 5E5

Abstract

The phosphatidylinositol 3-kinase (PI3K)/PTEN (phosphatase and tensin homologue deleted on chromosome 10) pathway is activated upon stimulation of receptor tyrosine kinases (RTKs) and regulates downstream pathways involved in cell survival, cell growth, cell cycle progression, and protein expression. The protein p85 is uniquely positioned to both positively and negatively regulate the PI3K/PTEN pathway through its interactions with various protein partners including p110, PTEN, and Rab5. The PI3K/PTEN pathway has been shown to be dysregulated in a variety of cancers, including cancers of the breast, prostate, endometrium, and urothelial tract. A better understanding of the interaction between p85 and its various binding partners can further elucidate the mechanisms through which cancer-associated mutations lead to dysregulation of the PI3K/PTEN pathway. To this end we pursued obtaining crystal structure data for the p85 BH domain, alone and in complex with binding partners PTEN and Rab5. Crystal structures were successfully obtained for the bovine p85 BH domain wild-type, individual cancer-associated mutations (E137K, E217K, R262T, E297K), and the engineered mutation R228E. Protein complexes between the p85 BH domain and PTEN or Rab5 were not purified in suitable concentrations for crystallography experiments, and so no structural data was collected for these complexes. Within the p85 BH domain structure a pair of highly coordinated regions of electron density were observed, likely sulfate molecules based on the composition of the crystallization buffer. These regions were coordinated by the p85 residues K224, R228, H234, W237, and Q241. These two highly coordinated regions of electron density were visible for all structures obtained, except the engineered R228E mutant, in which one of these densities was absent. Due to the consist presence of these densities, it was proposed that this region may serve as a potentially uncharacterized binding pocket. Crystallization solutions were prepared exposing crystals of the p85 BH domain to nucleotides, phosphorylated amino acids, or phospholipids, based on the structural similarity between phosphate and sulfate ions. No bound compounds were visible within the determined structures, although high levels of sulfate in the crystallization buffer may have prevented binding of the lower concentration additives. To test p85 for lipid binding in the absence of sulfate, experiments were performed using phosphatidylinositol lipid strips. Direct binding of p85 to lipids present on the lipid strips was detected, with the p85 BH domain alone being sufficient for lipid binding. These results suggest a novel function for the p85 BH domain in direct binding to lipid, which may play a role in regulation of binding partners such as PTEN.

Acknowledgements

I would like to thank my supervisor Dr. Deborah Anderson for her boundless support, and providing another perspective and suggestions that helped lead my research to being the best that it could be. Thanks to Dr. Stanley Moore for guiding me through the intricate path of X-ray crystallography and allowing me to see the world in a way that most never know. Also I would like to thank my other committee members Dr. Linda Chelico, Dr. Erique Lukong, and Dr. Yuliang Wu for their feedback and recommendations across the years. To all the members of the Anderson Lab and Moore Lab I thank you for your help in teaching me new techniques, providing a welcoming forum for trouble-shooting questions or fresh perspective on my tasks at the moment, as well as reminding me the importance of having some fun and not taking myself too seriously. Also, without the assistance of the staff at the Canadian Light Source Synchrotron, and the Protein Characterization and Crystallization Facility on campus, I would not have been able to collect much of the data that is presented within this thesis. Finally, to my family and friends that have been with me over the course of this journey, providing your support, excitement, and energy while I bombarded you with excessive details regarding the various successes and difficulties over the course of my degree, know that your support means the world to me and I cannot thank you enough. I wouldn't be where I am today without all of you.

Dedication

This thesis is dedicated to everyone that has helped and supported me along the path that has lead here. Through the most exciting moments of joy, and the most insufferable moments of frustration, we have made this journey together and I would not be here without all of you.

This mutual journey has brought great magic to my life, and I hope that I have succeeded in capturing a semblance of that magic within these pages to share with you all.

TABLE OF CONTENTS

List of Tables……...Page Number

List of Figures……..Page Number

List of Abbreviations

110B	inter-SH2 domain region important for binding p110
3_{10} Helix	form of α-helical in which 3 residues are present per helix turn and 10 atoms are present between the hydrogen bond donor and acceptor
AEBSF	4-(2-aminoethyl)benzenesulfonyl fluoride hydrochloride
Bad	Bcl-2-associated death promoter
Bcr	Breakpoint cluster region
BH	Breakpoint cluster region homology
BSA	bovine serum albumin
CDK2	cyclin-dependant kinase 2
CLS	Canadian Light Source
CMCF-BM	Canadian Macromolecular Crystallography Facility 08B1-1
CMCF-ID	Canadian Macromolecular Crystallography Facility 08ID-1
CV	column volume
DTT	dithiothreitol
EDTA	Ethylenediaminetetraacetic acid
EEA1	early endosomal antigen-1
FoxO1	forkhead box protein O1
GAP	GTPase activating protein
GDI	guanine nucleotide dissociation inhibitor
GEF	guanine nucleotide exchange factor
GppCp	Guanosine-5`-[(ß,ɣ)-methyleno]triphosphate
GSK3β	glycogen synthase kinase 3 beta
GST	Glutathione S-transferase
GTPase	guanosine triphosphate phosphatase
IPTG	isopropyl ß-D-1-thiogalctopyranoside
MALS	multi-angle light scattering
MDM2	mouse double minute 2 homologue
mTORC1	mammalian target of rapamycin complex 1
MW	molecular weight
p85	85 kDa regulatory subunit of phosphatidylinositol 3-kinase p85α

p85-BH-K224-5E	p85-BH-K224E-K225E
p110	110 kDa catalytic subunit of phosphatidylinositol 3-kinase p110α
pAKT	phosphoAKT
PASE	phosphatase
PBS	phosphate buffered saline
PCCF	Protein Characterization and Crystallization Facility
PDB	Protein Data Bank
PDK1	phosphoinositide-dependent kinase 1
PDZ	post synaptic density protein, Drosophila disc large tumour suppressor, zonula occludens-1 protein
PEG	polyethylene glycol
PIP	phosphatidylinositol phosphate
PI3P	phosphatidylinositol 3-phosphate
PI4P	phosphatidylinositol 4-phosphate
$PI3,4P_2$	phosphatidylinositol 3,4-bisphosphate
$PI4,5P_2$	phosphatidylinositol 4,5-bisphosphate
$PI3,4,5P_3$	phosphatidylinositol 3,4,5-trisphosphate
PTEN	phosphatase and tensin homologue deleted on chromosome 10
PTEN Crystal	PTEN (7-353, Δ286-309)
pTyr	phosphorylated tyrosine
SDS-PAGE	sodium dodecyl sulphate polyacrylamide gel electrophoresis
SEC	size exclusion chromatography
SH2	Src homology 2
SH3	Src homology 3
SNAREs	soluble N-ethylmaleimide-sensitive attachment protein receptors
TCEP-HCl	tns (2-carboxyethyl) phosphine hydrochloride

1.0 Introduction

1.1 Role of signaling pathways in eukaryotic cells

Intracellular and extracellular signaling pathways play critical roles in the monitoring and regulation of countless cellular processes and functions. By monitoring nutrient levels within and outside the cell, detecting hormones and growth factors, and responding to antigens and signs of infection, these signaling pathways trigger many intracellular changes. These responses include alterations to cellular metabolism, import and export of molecules, alterations in gene expression and protein production/degradation, regulating cellular replication, initiating apoptosis, or transmitting information to cells distant from the site of the initial stimulation or signal. Multi-cellular organisms depend upon the well-coordinated transmission of information between different cells.

Disruption of cellular signalling pathways can be detected in a wide variety of human malignancies and diseases, including metabolic syndromes and cancers. Individuals with type 2 diabetes mellitus show decreased sensitivity to insulin signaling for various cells, including adipocytes and skeletal muscle, resulting in the abnormal glucose metabolism observed in the disease (Hojlund, 2014; Kashiwagi *et al.*, 1983). The phosphatidylinositol 3-kinase (PI3K)/PTEN (phosphatase and tensin homologue deleted on chromosome 10) is activated upon stimulation of various receptor tyrosine kinase (RTK) proteins (Liu *et al.*, 2009; Vogt *et al.*, 2010; Yuan and Cantley, 2008; Zhao and Vogt, 2008). Disruption to normal function of the PI3K/PTEN pathway has been shown in cancers of the breast, endometrium, prostate, and urothelial tract (Carnero, 2010; Carracedo and Pandolfi, 2008; Chalhoub and Baker, 2009; Cheung *et al.*, 2011; Liu *et al.*, 2014; Miled *et al.*, 2007; Ross *et al.*, 2013; Vasudevan and Garraway, 2010; Vivanco and Sawyers, 2002).

1.2 Receptor tyrosine kinase signaling

RTK signaling is governed by transmembrane receptor proteins that bind to specific growth factors and hormones. Example RTKs include epidermal growth factor receptor, insulin receptor, and platelet derived growth factor receptor. At least 58 unique RTKs have been identified and they are divided into 20 subfamilies (Gschwind *et al.*, 2004). Across the various subfamilies of RTKs there are conserved structural features shared between the different proteins.

RTKs contain an external ligand binding domain, a transmembrane domain, and an internal tyrosine-kinase domain. A schematic diagram for a general RTK is provided in **Figure 1.1**.

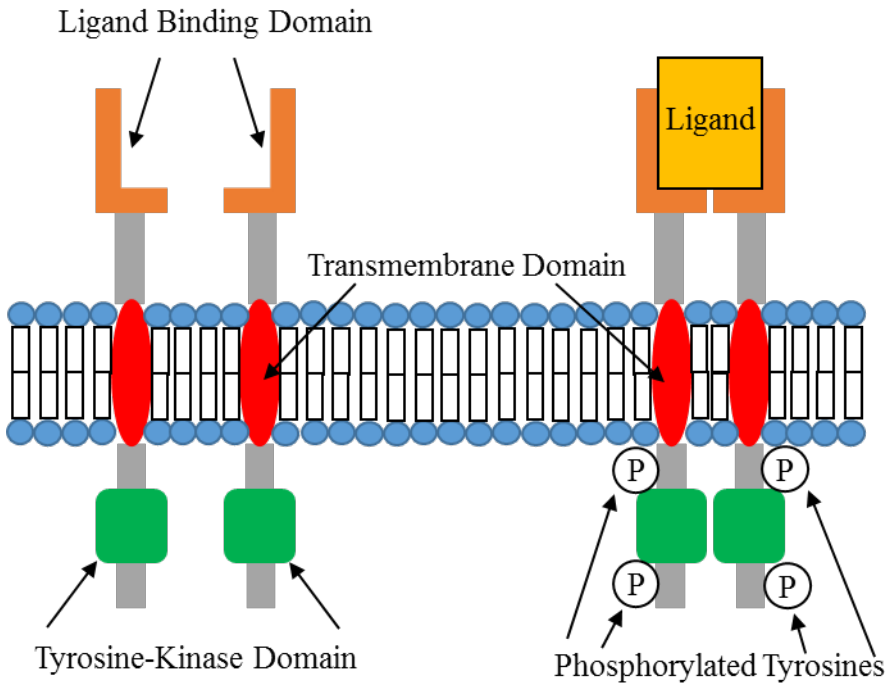

Figure 1.1 Diagram of a RTK. Domain illustration of a general RTK. A RTK has an external ligand binding domain, a transmembrane domain, and an internal tyrosine-kinase domain. Without ligand bound RTKs exist as monomers in the plasma membrane. Ligand binding stimulates dimerization of the RTKs, resulting in auto-phosphorylation of Tyr residues on the receptors. The phosphorylated Tyr residues provide binding sites for proteins containing SH2 domains, resulting in protein relocalization and the activation of various downstream pathways.

When unstimulated, RTKs are present as monomers. Upon binding of their ligand RTKs dimerize, forming homodimers or heterodimers depending on the specific RTKs, through binding to the same ligand complex and/or intermolecular interactions stimulated upon ligand binding (Gschwind *et al.*, 2004). Upon dimerization the tyrosine-kinase domains auto-phosphorylate tyrosine residues present on the other receptor, providing binding sites for proteins that contain SH2 domains. Binding of these proteins then results in changes to the activation of numerous downstream cellular pathways, including pathways important for cell survival and proliferation (Alessi *et al.*, 1997; Stephens *et al.*, 1998).

Due to their role in the regulation of numerous cellular pathways, disruption of RTK signaling regulation is commonly observed in cancers. RTK overexpression and mutations

leading to constitutively active RTKs are observed in leukemia and breast, colorectal, and ovarian cancers (Gschwind *et al.*, 2004). There are also numerous cancers that have dysregulation in the various pathways governed by RTK activation, such as the PI3K/PTEN signaling pathway.

1.2.1 Phosphatidylinositol 3-kinase/PTEN signaling pathway

A proposed model for the PI3K/PTEN signaling pathway is provided in **Figure 1.2**.

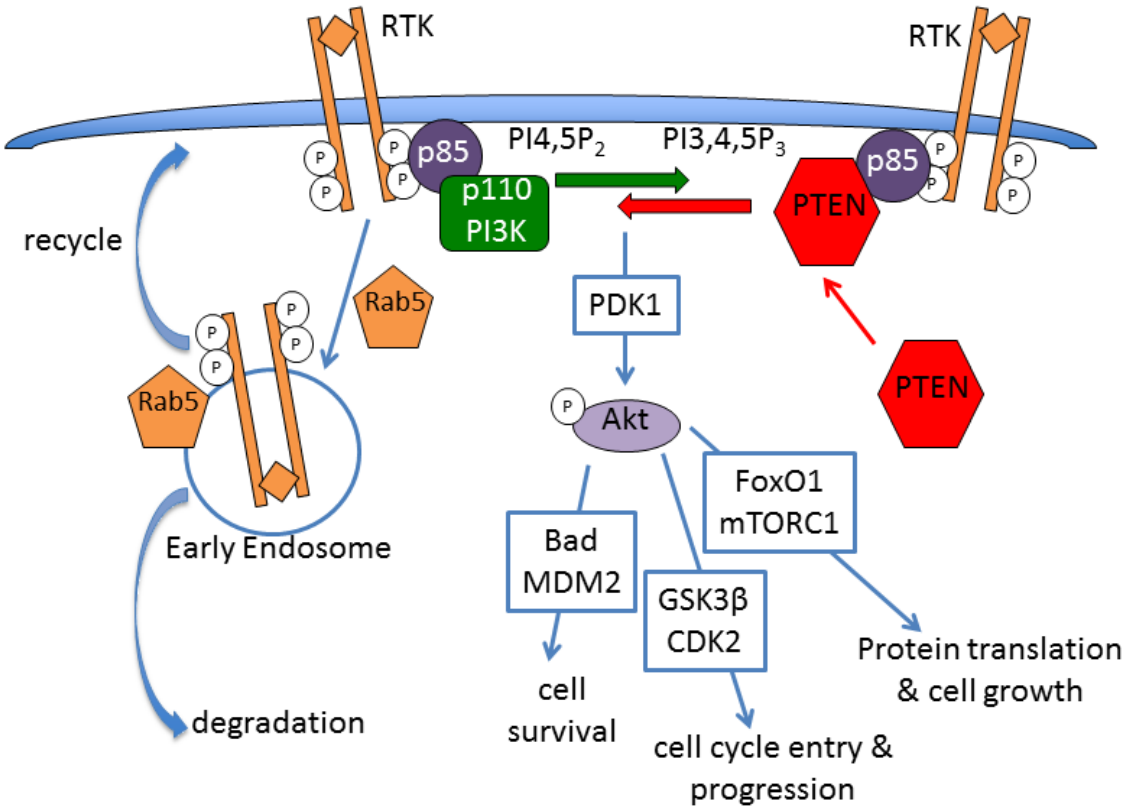

Figure 1.2: Model of the PI3K/PTEN pathway. Activation of the PI3K/PTEN pathway begins with RTK binding their ligand, followed by receptor dimerization and auto-phosphorylation of tyrosine residues. The p85 protein of the PI3K complex binds these pTyr residues, relieves its repressor function on the p110 catalytic subunit of the PI3K complex, and p110 phosphorylates $PI4,5P_2$ to $PI3,4,5P_3$ which serves as a lipid signaling molecule to promote downstream activation of pathways involved in protein translation, cell growth, cell cycle entry and progression, and cell survival. $PI3,4,5P_3$ is converted back to $PI4,5P_2$ by the PTEN lipid phosphatase, preventing sustained downstream activation of the various pathways. The binding of p85 to PTEN has been shown to stimulate PTEN phosphatase activity. Activated RTKs can also be trafficked to early endosomes through Rab-mediated pathways, where they are either recycled back to the cell membrane or else trafficked for degradation in lysosomes. It has been shown that p85 binds to Rab5, a key protein in early endosome trafficking, and stimulates the intrinsic GTPase (guanosine triphosphate phosphatasePAS) activity that converts Rab5 from an active GTP bound form to an inactive GDP bound form.

The PI3K protein complex is composed of a 110 kDa catalytic subunit (p110) and an 85 kDa regulatory subunit (p85).

RTKs including platelet derived growth factor receptor, epidermal growth factor receptor, and insulin receptor, stimulate class 1A PI3Ks which consist of a p85α and p110α subunit (Liu *et al.*, 2009; Vogt *et al.*, 2010; Yuan and Cantley, 2008; Zhao and Vogt, 2008). Binding of their ligands results in receptor auto-phosphorylation of tyrosine residues present on the receptor, which serve as binding sites to allow for the relocalization of the PI3K protein complex to the plasma membrane (Liu *et al.*, 2009; Vogt *et al.*, 2010; Yuan and Cantley, 2008; Zhao and Vogt, 2008). Binding of the p85 protein to the phosphorylated tyrosine (pTyr) residues of the receptor relieves the repression on the associated p110 protein, allowing p110 to phosphorylate the lipid phosphatidylinositol 4,5-bisphosphate ($PI4,5P_2$) to generate phosphatidylinositol 3,4,5-trisphosphate ($PI3,4,5P_3$) (Miled *et al.*, 2007; Yu *et al.*, 1998). $PI3,4,5P_3$ acts as a lipid messenger that binds signaling proteins such as 3-phosphoinositide dependent protein kinase-1 (PDK1) and Akt (also known as protein kinase B), helping them relocate to the plasma membrane (Cantley, 2002; Toker and Cantley, 1997). Once relocated Akt is activated by phosphorylation by PDK1 (Alessi *et al.*, 1997). Phosphorylated Akt then proceeds to phosphorylate various binding partners, leading to downstream activation of various pathways important for cell growth, cell cycle entry and progression, protein translation, and cell survival (Alessi *et al.*, 1997; Stephens *et al.*, 1998). Targets of Akt include: the apoptosis promoting protein Bad (Bcl-2 associated death promoter) preventing Bad from associating with binding partners, the cell cycle regulatory protein CDK2 (cyclin-dependent kinase 2) which plays a role in the G1 to S phase transition in cells, the transcription factor FoxO1 (forkhead box protein O1) which results in localization of FoxO1 to the cytoplasm instead of the nucleus, the regulatory protein GSK3β (glycogen synthase kinase 3 beta) leading to altered cell metabolism and increased survival, the ubiquitin E3 ligase Mdm2 (mouse double minute 2 homologue) which increases degradation of the apoptosis inducing protein p53, and the mTORC1 (mammalian target of rapamycin complex 1) which increases the mTORC1 kinase activity (Brunet *et al.*, 1999; del Peso *et al.*, 1997; Desbois-Mouthon *et al.*, 2002; Ogawara *et al.*, 2002; Rani *et al.*, 1997; Scott *et al.*, 1998).

Activity of the PI3K/PTEN pathway is counteracted by the lipid phosphatase PTEN which dephosphorylates $PI3,4,5P_3$ back to $PI4,5P_2$, preventing sustained downstream activation of the Akt pathway (Myers *et al.*, 1997; Vazquez *et al.*, 2001; Vazquez *et al.*, 2006).

1.2.2 The PI3K/PTEN pathway in cancer

The PI3K/PTEN pathway is dysregulated in a large number of cancers, including those that occur in the breast, endometrium, prostate, and urothelial tract (Cantley, 2002; Carnero, 2010; Carracedo and Pandolfi, 2008; Chalhoub and Baker, 2009; Cheung *et al.*, 2011; Liu *et al.*, 2009; Ross *et al.*, 2013; Vivanco and Sawyers, 2002; Yuan and Cantley, 2008). These activating mutations can occur in various components of the PI3K/PTEN pathway. Oncogenic mutations occur in RTKs leading to constitutive activation, mutations in PI3K catalytic subunit p110α (hereafter referred to as p110) or regulatory subunit p85α (hereafter referred to as p85) that leads to PI3K continuous activation, and mutations leading to a lack of expression or loss of function of PTEN (Carnero, 2010; Carracedo and Pandolfi, 2008; Chalhoub and Baker, 2009; Cheung *et al.*, 2011; Liu *et al.*, 2014; Miled *et al.*, 2007; Ross *et al.*, 2013; Vasudevan and Garraway, 2010; Vivanco and Sawyers, 2002; Vogt *et al.*, 2010; Yuan and Cantley, 2008). Various treatments and drugs have been developed to treat dysregulation of the PI3K/PTEN pathway, many targeting PI3K and other kinases that are often constitutively activated in cancer cells (Garcia-Echeverria and Sellers, 2008; Liu *et al.*, 2009; Wong *et al.*, 2010).

1.2.3 Endocytosis of receptor tyrosine kinases

Reviews of RTK endocytosis by Goh and Sorkin, and of the role of endocytosis in cancers by Mellman and Yarden provide overviews of current understanding towards endocytosis in healthy and disease states (Goh and Sorkin, 2013; Mellman and Yarden, 2013).

Briefly, levels of RTKs found at the cell surface are regulated through the balance between protein expression and receptor transport through endocytosis leading to degradation in lysosomes. In the absence of growth factor stimulation this turnover rate is slower, allowing increased presence of RTKs at the cell surface. Following growth factor stimulation of RTKs the auto-phosphorylation of the receptors provide binding sites for proteins that lead to downstream activation of clathrin-mediated and clathrin-independent endocytosis, transporting the activated RTK to an early endosome (Beattie *et al.*, 2000; Gorden *et al.*, 1978; Haigler *et al.*,

1979; Huang *et al.*, 2004; Orth *et al.*, 2006). From the early endosome the RTK is sorted to either be recycled back to the plasma membrane to be stimulated and signal again, or transported to a lysosome for degradation. This sorting is regulated by various factors, including post-translational modification of the endocytosed RTK such as phosphorylation or ubiquitination, and various protein partners including members of the Rab family GTPases.

Motifs present within the transmembrane domains of the RTKs serve as binding regions for clathrin adaptor protein complexes, leading to the internalization of the RTKs through clathrin-mediated endocytosis (Goh and Sorkin, 2013). Ubiquitination of activated RTKs and interaction with ubiquitin ligase proteins such as Cbl, which binds to phosphorylated RTK directly or indirectly through the adaptor protein Grb2, promotes the internalization of the activated receptors (Huang *et al.*, 2006; Li *et al.*, 2007). Sorting of internalized epidermal growth factor receptor for degradation was decreased by mutations at sites of ubiquitin-conjugation and Cbl binding (Huang *et al.*, 2006). Recycling of RTKs to the plasma membrane can occur for receptor-ligand complexes upon saturation of the degradation pathway resulting in sustained signaling (French *et al.*, 1994; Sorkin *et al.*, 1991). Recycling of RTKs can also occur when ligand dissociates from the receptor following endocytosis, allowing the inactive RTK to be returned to the plasma membrane (Masui *et al.*, 1993).

1.2.4 Rab mediated vesicle trafficking

The Rab family of proteins are small GTPases and contains more than 70 members in humans (Tzeng and Wang, 2016). These proteins, through interactions with a variety of binding partners, play key roles in cell growth, cytoskeleton organization, and numerous stages of cellular vesicle trafficking including both exocytosis of molecules from the trans-Golgi network and endocytosis of molecules from the plasma membrane. The activity of Rab proteins is regulated based on the state of bound nucleotide present, with the proteins active while bound to GTP, and inactive while bound to GDP. Interaction with guanine nucleotide exchange factors (GEF) promotes the exchange of GDP bound to Rab proteins with GTP, converting them to their active forms that interact with downstream effector proteins. GTPase activating proteins (GAP) promote the intrinsic GTPase activity of the Rab proteins, to stimulate the hydrolysis of bound GTP to GDP and switching them to an inactive conformation.

Rab proteins are a unique group of GTPases in that although they are lipid modified to facilitate membrane association, their lipid moiety can be masked through interactions with a guanine nucleotide dissociation inhibitor (GDI) protein, allowing them to come off membranes (Cherfils and Zeghouf, 2013; Soldati *et al.*, 1993). GDI displacement factors are thought to help recruit Rab GTPases to specific membrane locations (Cherfils and Zeghouf, 2013; Ingmundson *et al.*, 2007).

1.2.4.1 Rab5

Rab5 is a small GTPase protein of ~24 kDa. While in a GDP bound inactive form the Rab5 protein is localized within the cytosol of cells. Like other Rab proteins, interaction with GEFs promotes the exchange of GDP with GTP so that Rab5 assumes its active conformation. Active Rab5 localizes to the plasma membrane and the membrane surface of early endosomes (Ali *et al.*, 2004). While present at these membranes GTP-bound Rab5 provides a binding site for effector proteins involved in endocytosis and membrane fusion, such as early endosomal antigen-1 (EEA1). EEA1 is able to bind GTP-bound Rab5 and phosphatidylinositol 3-phosphate (PI3P) lipid present on early endosome membranes through different domains, and serves as a tether between two early endosomes. With the two early endosomes held in close proximity it allows for the membrane bound proteins soluble N-ethylmaleimide-sensitive attachment protein receptors (SNAREs) to interact between membranes to draw the two early endosomes together and mediate membrane fusion (Woodman, 2000).

1.2.4.2 GAP proteins

GAP proteins stimulate the intrinsic GTPase activity of their small GTPase protein binding partners through the contribution of a catalytic Arg residue at the site of catalysis, which serves as an Arg finger to catalyze the conversion of the proteins to their inactive GDP bound state (Bos *et al.*, 2007; Cherfils and Zeghouf, 2013; Peck *et al.*, 2002). Different GAP proteins act on specific small GTPases, and are grouped based on their different binding motifs (Bos *et al.*, 2007; Cherfils and Zeghouf; Peck *et al.*, 2002).

The Breakpoint cluster region (Bcr) protein has a molecular weight (MW) of ~140 kDa, displays GAP activity for the proteins RAC1 and CDC42, and also possesses serine/threonine kinase activity (Diekmann *et al.*, 1991; Maru and Witte, 1991). The Bcr GAP activity was

identified in a C-terminal domain of the protein observed in a number of other proteins that possess GAP activity, providing domains with this structure the name Bcr homology (BH) domains (Bos *et al.*, 2007; Peck *et al.*, 2002). Other proteins that possess BH domains and GAP activity include CDC42GAP, N-chimaerin, GRAF-2, Myosin 9b, and the regulatory subunit of PI3K, p85 (Bos *et al.*, 2007; Peck *et al.*, 2002).

1.3 Phosphatidylinositol 3-kinase

The p110 catalytic subunit of PI3K phosphorylates $PI4,5P_2$ to generate $PI3,4,5P_3$ in the PI3K/PTEN pathway (Carpenter *et al.*, 1990). It is composed of five domains: an N-terminal adaptor binding domain, a Ras binding domain, a C2 domain, a helical domain, and a kinase domain. The p110 protein is mutated in a wide range of cancers, with most mutations found within the helical and kinase domains of the protein and result in increased catalytic activity or loss of regulatory functionality of bound protein partners such as p85 (Liu *et al.*, 2014; Miled *et al.*, 2007; Vogt *et al.*, 2010).

The p85 regulatory subunit of PI3K binds directly to p110 and inhibits the phosphatase activity of p110; this inhibition is relieved upon activation of cellular RTKs (Carpenter *et al.*, 1990; Yu *et al.*, 1998). Other binding partners of p85 include PTEN and Rab5 (Chagpar *et al.*, 2010; Chamberlain *et al.*, 2004). The p85 protein is composed of five domains, a Src homology 3 (SH3), BH, N-terminal Src homology 2 (nSH2), an inter-SH2 domain region important for binding to p110 (110B), and a C-terminal Src homology 2 (cSH2) domain (Backer, 2010). Both the SH3 and BH domains of p85 are involved in the interaction between p85 and PTEN (Chagpar *et al.*, 2010). The nSH2 and cSH2 domains are responsible for p85 binding to the pTyr residues of activated RTKs (Backer, 2010). It has also been shown that the nSH2 and 110B domains interact with p110 to form the PI3K protein complex (Backer, 2010; Huang *et al.*, 2007).

A domain diagram of p85 is shown in **Figure 1.3 A**.

When not bound to other proteins the p85 protein has been shown to homodimerize through two mechanisms as illustrated in **Figure 1.3 B** (Harpur *et al.*, 1999). The first mechanism is through the interaction of the SH3 domain of one p85 protein binding the PXXP motif present in the inter-domain region between the SH3 and BH domains on a second p85 protein, which has a dissociation constant in the µM range (Harpur *et al.*, 1999). The second mechanism is through

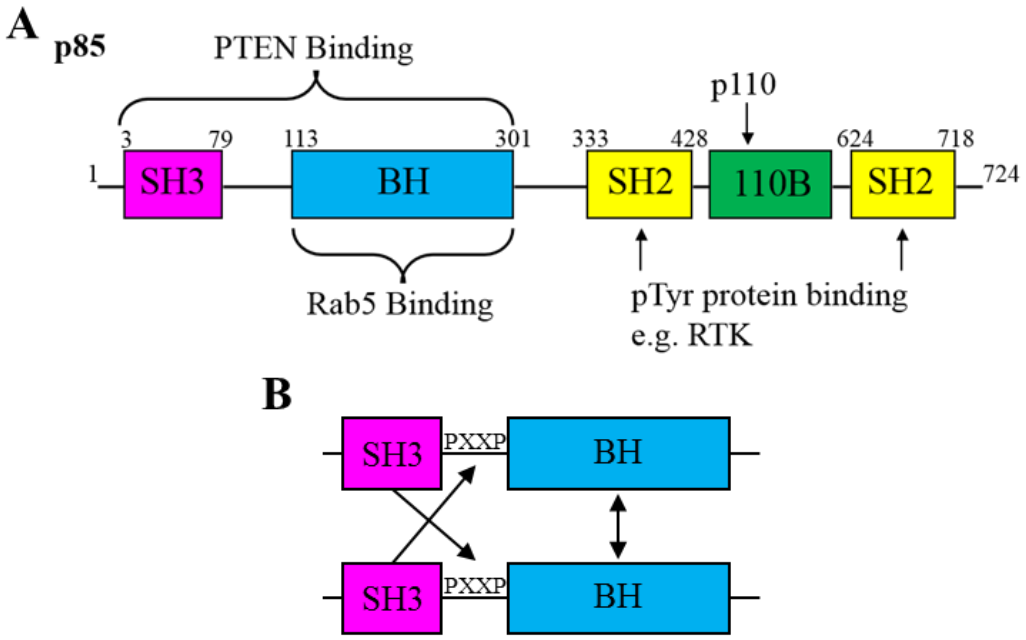

Figure 1.3 Domain diagram and homodimerization of p85. A. Domain diagram of p85 displaying amino acid ranges and regions important for binding protein partners. **B.** Diagram of the two different mechanisms behind p85 homodimerization. One involves the binding of one p85 SH3 domain with the PXXP motif present in the inter-domain linker of the other p85. The other mechanism is through direct interaction between the BH domain of each protein.

interaction of two BH domains on separate p85 proteins forming a relatively weak interaction with a dissociation constant in the mM range (Harpur *et al.*, 1999).

Regulation of the PI3K protein complex is achieved through protein interaction between the p85 regulatory and p110 catalytic protein subunits. Binding of p85 to p110 represses the catalytic activity of p110 until binding to the pTyr residues of activated RTKs relieves this repression (Miled *et al.*, 2007; Yu *et al.*, 1998). In the absence of binding p85, the p110 protein has been shown to be unstable, leading to rapid degradation within cells (Yu *et al.*, 1998). Binding of p85 to p110 stabilizes the p110 protein, resulting in a decreased rate of degradation and more prolonged presence within the cell (Yu *et al.*, 1998).

1.4 Phosphatase PTEN

PTEN is an ~55 kDa protein with dual lipid/protein phosphatase activity, with substrates including the focal adhesion kinase and $PI3,4,5P_3$ (Myers *et al.*, 1997; Tamura *et al.*, 1998). PTEN is comprised of 5 domains: a plasma membrane binding domain that binds $PI4,5P_2$, a dual lipid/protein phosphatase domain, a C2 domain, a Ser/Thr rich regulatory domain, and a PDZ

(post synaptic density protein, Drosophila disc large tumour suppressor, zonula occludens-1 protein) binding domain. A domain diagram of PTEN is shown in **Figure 1.4**.

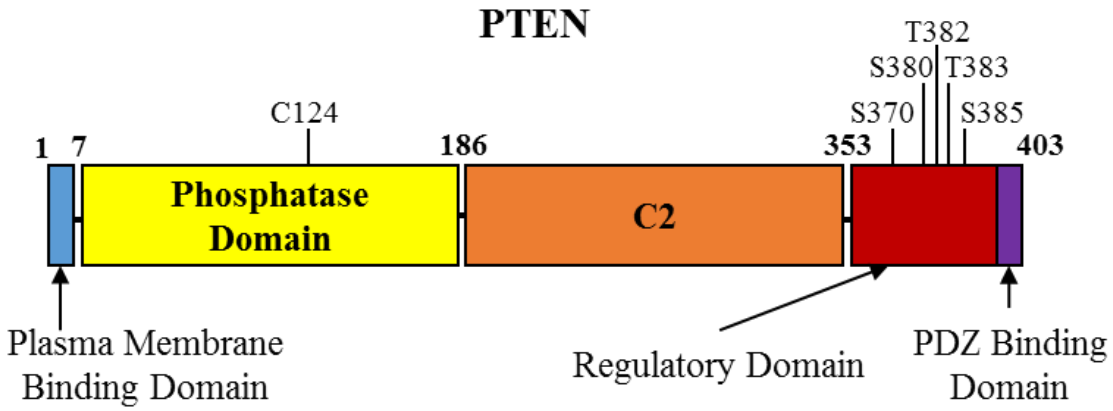

Figure 1.4 Domain diagram of PTEN. PTEN is composed of five domains: an N-terminal plasma membrane binding domain that binds $PI4,5P_2$, a catalytic phosphatase domain, a C2 domain, a regulatory domain rich in Ser/Thr residues which can be phosphorylated, and a C-terminal PDZ binding motif. The catalytic C124 residue in the phosphatase domain and Ser/Thr residues that are phosphorylated in the regulatory domain are indicated.

In the absence of growth factor stimulation, PTEN is constitutively phosphorylated on residues S370, S380, T382, T383, and S385 within the PTEN regulatory domain by casein kinase 2, GSK3ß, PICT-1, and ROCK kinases (Tamguney and Stokoe, 2007). These phosphorylated residues interact with basic residues found in the phosphatase (R161, K163, K164) and C2 (K260, K263, K266, K267, K269) domains to form a closed conformation (Rahdar *et al.*, 2009). The closed conformation of PTEN keeps it localized in the cytosol and increases the stability of the protein (Vazquez *et al.*, 2001). Stimulation from upstream activating signals triggers the dephosphorylation of PTEN which assumes an open conformation for interacting with lipids at the plasma membrane (Das *et al.*, 2003; Lee *et al.*, 1999; Rahdar *et al.*, 2009; Vazquez *et al.*, 2001; Vazquez *et al.*, 2006). Relocalization of PTEN to the plasma membrane is mediated by the PTEN plasma membrane binding domain (binding to $PI4,5P_2$ lipids) and electrostatic interactions between negatively charged membrane lipids and basic residues in the phosphatase (PASE) domain (R161, K163, and K164) (Das *et al.*, 2003; Rahdar *et al.*, 2009). The PTEN PDZ binding motif can also interact with a variety of scaffold proteins that contain PDZ domains. These scaffold proteins also bind to activated RTKs, further localizing PTEN to sites of $PI3,4,5P_3$

lipid generation (Bonifant *et al.*, 2007; Takahashi *et al.*, 2006; Tolkacheva *et al.*, 2001; Wu *et al.*, 2000a; Wu *et al.*, 2000b).

Following its relocalization, the PTEN protein dephosphorylates the 3-position of $PI3,4,5P_3$ to $PI4,5P_2$, and turning off the PI3K/PTEN pathway by preventing downstream activation of Akt (Myers *et al.*, 1997; Vazquez *et al.*, 2001; Vazquez *et al.*, 2006). PTEN has also been shown to dephosphorylate proteins such as focal adhesion kinase, inactivating the protein and preventing promotion of cellular mobility (Tamura *et al.*, 1998).

1.5 Structural studies of p85 and binding partners

All five domains of the human p85 protein have had their crystal structures solved individually, and the nSH2 domain and 110B domain were cocrystallized together with the p110 catalytic subunit of PI3K although the nSH2 was not visible within the crystal structure (Hoedemaeker *et al.*, 1999; Huang *et al.*, 2007; Liang *et al.*, 1996; Musacchio *et al.*, 1996; Nolte *et al.*, 1996).

The human p85 SH3 domain (**Figure 1.5 A-B**) is composed of five beta strands, one alpha helix, and two 3_{10} helices (form of α-helix with three residues per helix turn and 10 atoms between the hydrogen bond donor and acceptor) connected by flexible loop regions (Liang *et al.*, 1996). SH3 domains serve as sites of protein-protein interactions through their binding to proline rich motifs (e.g. PXXP where X is any amino acid) and are found in a variety of proteins including tyrosine kinases such as Src, adaptor proteins such as Grb2, regulatory proteins such as GAPs and p85, and structural proteins such as α-spectrin (Pawson and Gish, 1992). The SH3 domain has also had its crystal structure solved bound to a proline-rich peptide, revealing minimal conformational changes upon ligand binding (Figure 1.5B) (Batra-Safferling *et al.*, 2010).

The human p85 BH domain (**Figure 1.5 C-D**) is composed of eight alpha helices and one 3_{10} helix which are connected by flexible loop regions (Musacchio *et al.*, 1996). In the p85 BH domain crystal structure a homodimer of BH domains was observed, with the M176 of one monomer interacting with a hydrophobic pocket formed by the L161, I177, and V181 of the other monomer (Musacchio *et al.*, 1996). In the bovine sequence of p85, residue 177 is a phenylalanine in place of the isoleucine, preserving the hydrophobic nature of this residue.

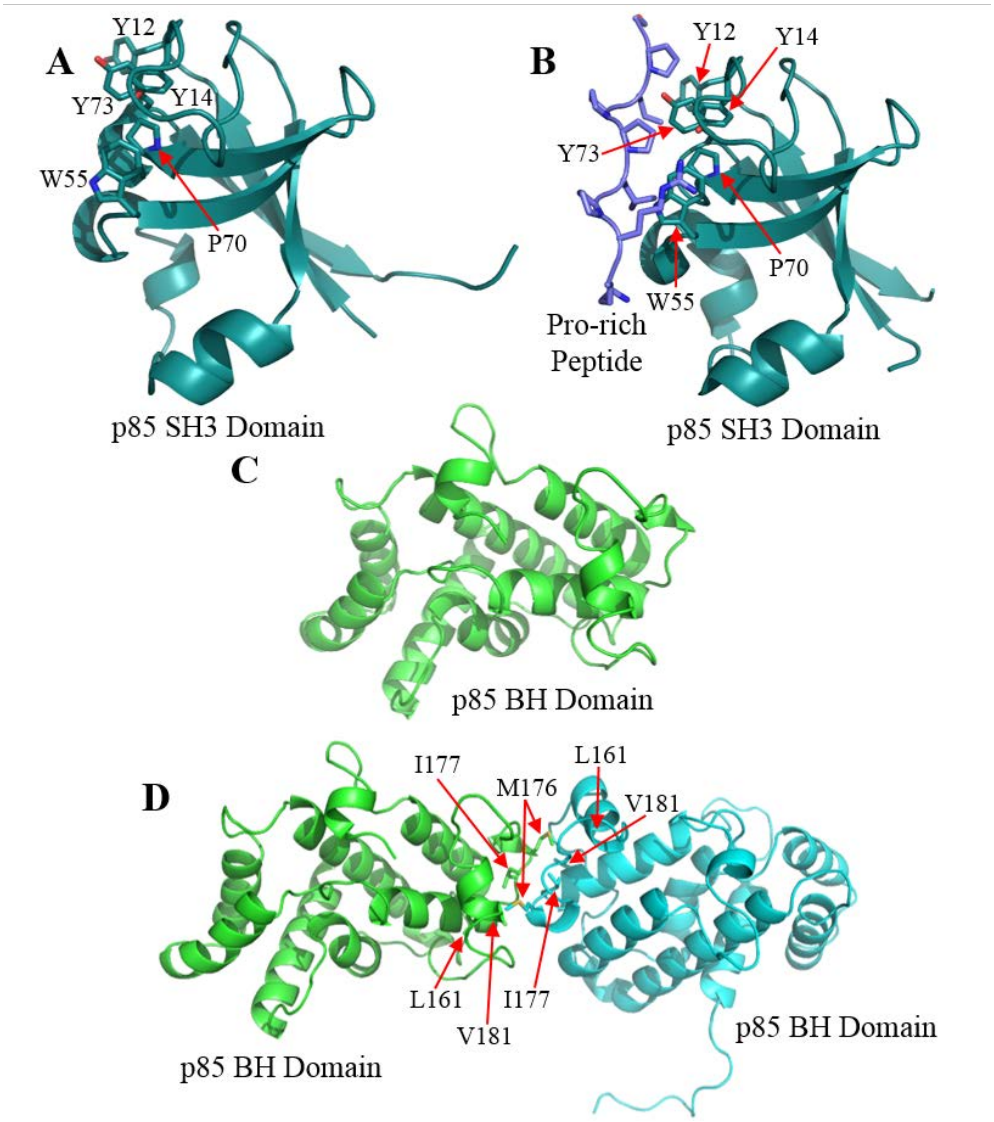

Figure 1.5 Crystal structures of human p85 SH3 and BH domains. Crystal structures of the: p85 SH3 domain (**A**, PDB ID# 1PHT; Liang *et al.*, 1996), p85 SH3 with bound Pro-rich peptide (**B**, PDB ID# 3I5R; Batra-Safferling *et al.*, 2010), p85 BH domain monomer and homodimer (**C** and **D**, PDB ID# 1PBW; Musacchio *et al.*, 1996). Residues important for ligand binding in SH3 domains, and homodimerization in BH domains, are indicated and shown in stick format. Pro-rich peptide is shown in stick format in violet.

The human p85 nSH2 domain (**Figure 1.6**) is composed of 4 beta strands, 4 alpha helices, and one 3_{10} helix connected by flexible loop regions (Nolte *et al.*, 1996). The human p85 cSH2 domain (**Figure 1.6**) is composed of six beta strands, two alpha helices, and two 3_{10} helices connected by flexible loop regions (Hoedemaeker *et al.*, 1999). Both SH2 domains were shown to be able to bind proteins containing pTyr residues, with the nSH2 structure determined both

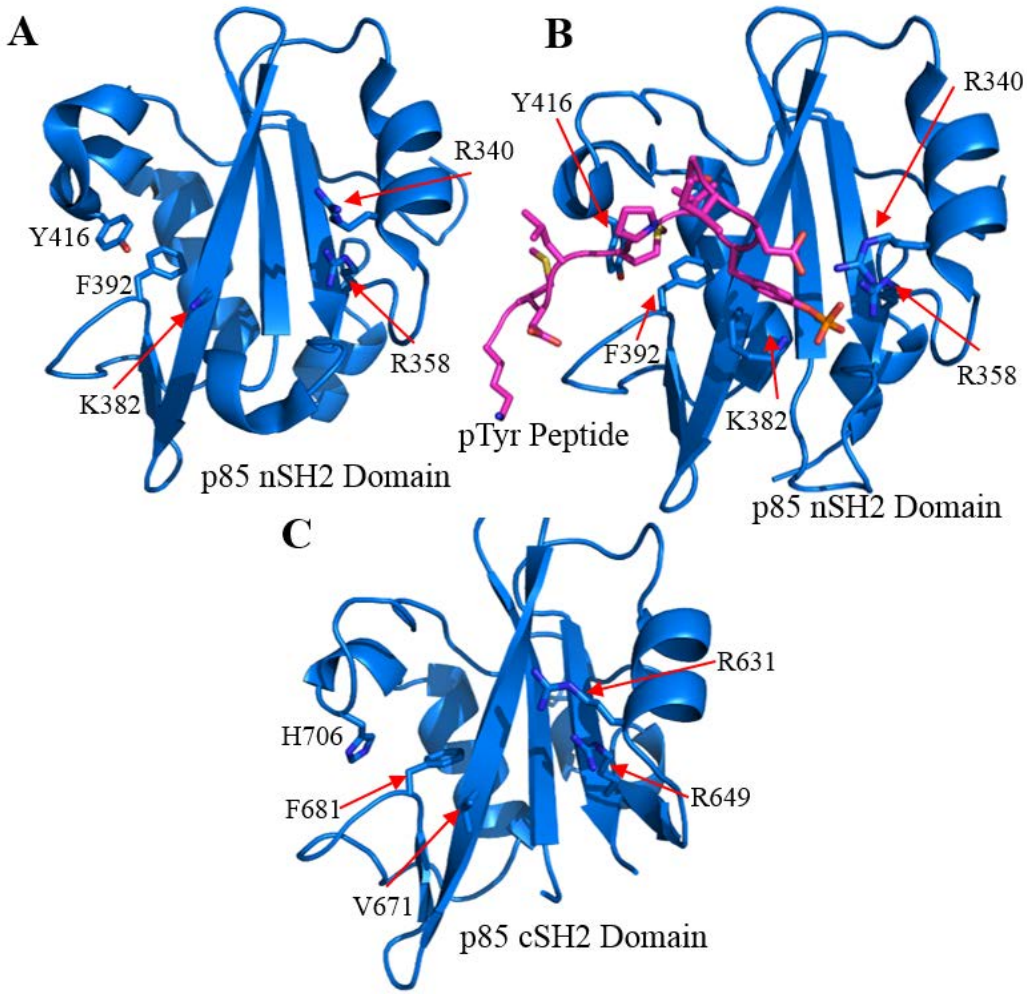

Figure 1.6 Crystal structures of human p85 SH2 domains. Crystal structures of the: p85 nSH2 domain without peptide (**A**, PDB ID# 2IUG; Nolte *et al.*, 1996) and with a pTyr peptide bound (**B**, PDB ID# 2IUI; Nolte *et al.*, 1996), and the p85 cSH2 domain (**C**, PDB ID# 1QAD; Hoedemaeker *et al.*, 1999). Residues important for ligand binding are indicated and shown in stick format. The pTyr peptide is shown in stick format in magenta.

with and without bound phosphopeptide (Hoedemaeker *et al.*, 1999; Nolte *et al.*, 1996). The cSH2 domain was crystallized in the absence of ligand and had a very similar structure to the nSH2 domain (Hoedemaeker *et al.*, 1999).

1.5.1 Structural studies of p110

The human p110 protein has been crystallized in complex with a human p85 fragment containing the nSH2 and 110B regions, although the nSH2 domain was not visible within the structure, to examine the regions and residues important for complex formation between the two

proteins (Huang *et al.*, 2007). The crystal structure is shown in **Figure 1.7**. Examination of cancer-associated mutations within p110 was used to determine if these mutations likely affected binding between the two proteins, such as p110 residues N345 and Q453 being located at the interface between p110 and the coiled-coiled p85 110B region (Huang *et al.*, 2007). Using this structural data they also examined suspected regions important for p110 binding to the plasma membrane, and which residues of p85 are nearest to the p110 catalytic site (Huang *et al.*, 2007).

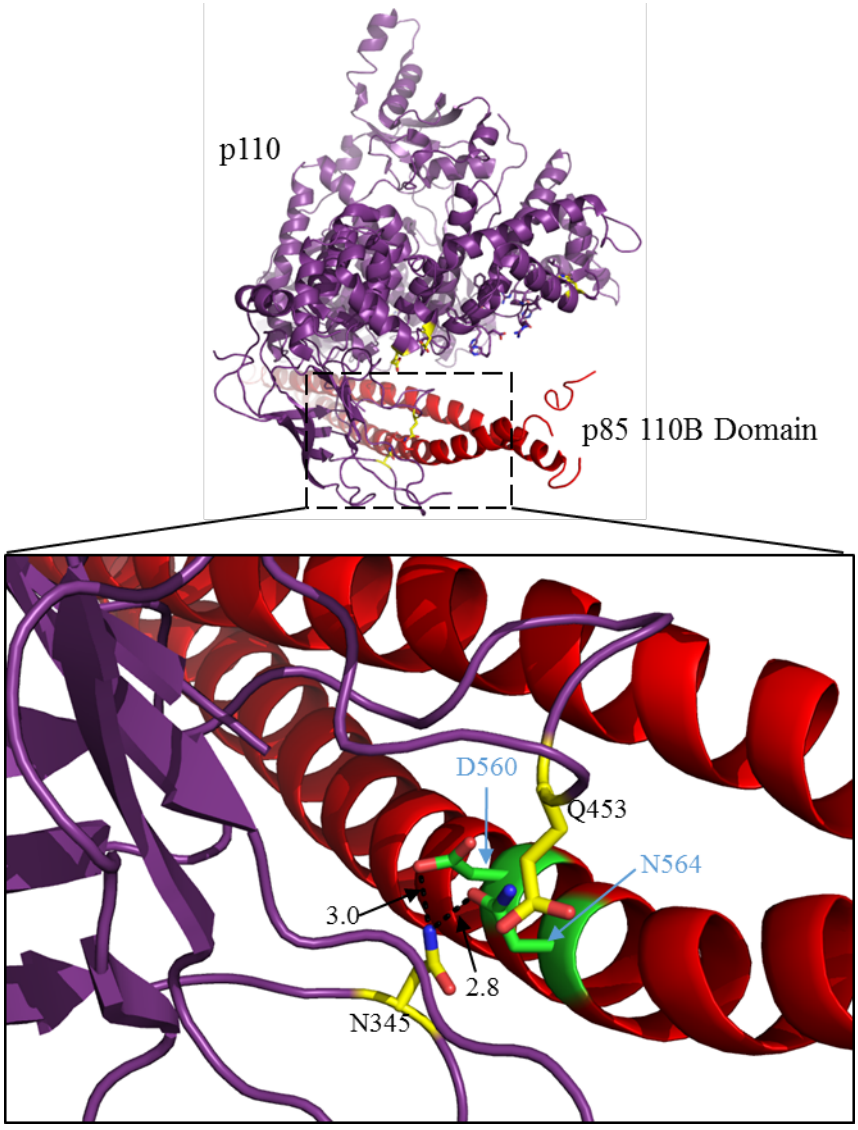

Figure 1.7 Crystal structure of human p85 110B domain in complex with human p110. Crystal structure of the p85 110B domain (red) in complex with p110 (purple) (PDB ID# 2RD0; Huang *et al.*, 2007) including a close up view of the interface region. Cancer associated mutants in p110 are shown in yellow, p85 interface residues are in green, p110 residues are labelled in black, p85 residues are labelled in blue, and bond distances are in Angstroms.

Miled *et al.* used a combination of crystallographic and biochemical analysis to examine mutations in p110 and p85 to understand the mechanisms behind oncogenic mutations and identify important contact residues (Miled *et al.*, 2007). They crystallized the adaptor binding domain of bovine p110 with the 110B domain of human p85 to examine the residues important for the interaction between the two regions, and the location of oncogenic p110 mutants (Miled *et al.*, 2007). This crystal structure is shown in **Figure 1.8**.

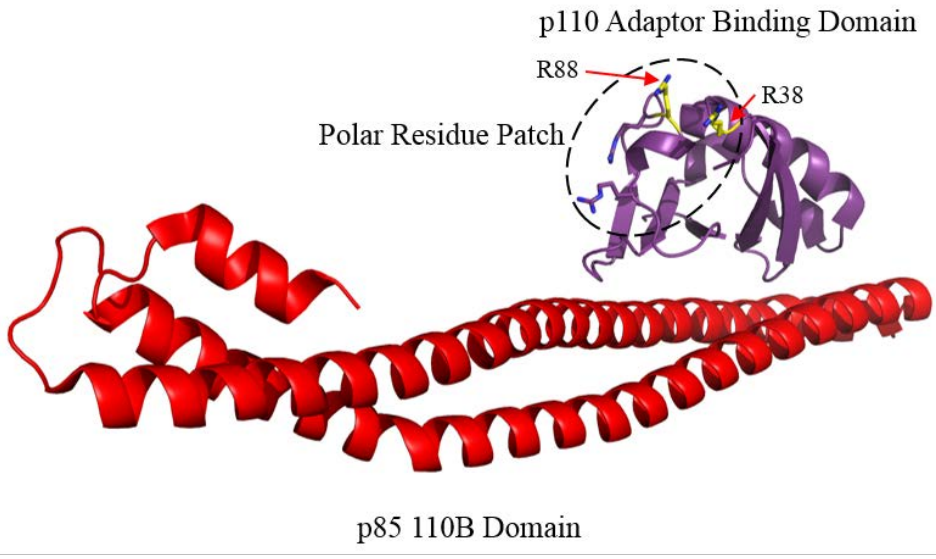

Figure 1.8 Crystal structure of human p85 110B in complex with bovine p110 adaptor binding domain. Crystal structure of the p85 110B domain (red) in complex with the p110 adaptor binding domain (purple) (PDB ID# 2V1Y; Miled *et al*., 2007). The polar residue patch identified in the p110 adaptor binding domain is indicated, with cancer-associated mutations shown in yellow.

Two residues of oncogenic p110 mutations, R38 and R88, were present within a highly conserved patch of mostly polar residues on the p110 adaptor binding domain surface apart from the interaction region with p85 110B domain, where the oncogenic mutations could interfere with proper association between this surface region and other domains of the p110 protein (Miled *et al.*, 2007). Lipid kinase assays of full-length p110 with a p85 fragment containing the nSH2 and 110B domains was used to identify important residues in the p85 nSH2 domain through testing charge reversal mutants (Miled *et al.*, 2007). These experiments demonstrated that p85 mutants R340E and K379E no longer performed their inhibitory role upon binding to p110, suggesting they form critical inhibitory contacts with p110 (Miled *et al.*, 2007). They also demonstrated that

the p85 nSH2 and 110B fragment containing K379E mutant was able to restore its inhibitory function upon binding to p110 E545K oncogenic mutant, where wild-type nSH2 and 110B p85 showed no inhibitory function, with this charge reversal restoring the critical inhibitory contact site (Miled *et al.*, 2007).

1.5.2 Structural studies of PTEN

A crystal structure of human PTEN (7-353, Δ286-309) containing the phosphatase and C2 domains has been previously determined with a tartrate molecule bound within the phosphatase catalytic pocket (Lee *et al.*, 1999). Tartrate was included due to its similar structure to a portion of the phosphatidylinositol lipid head group. The crystal structure of PTEN (7-353, Δ286-309) including a closer examination of the phosphatase pocket is shown in **Figure 1.9**.

The catalytic pocket within the PTEN phosphatase domain is composed of residues D92, H93, K125, A126, G127, K128, T167, I168, and Q171, with a catalytic C124 residue (Lee *et al.*, 1999). Bound within the catalytic pocket was a tartrate molecule which helped to determine the residues responsible for forming the pocket and coordinating potential substrate molecules (Lee *et al.*, 1999). Cancer associated mutants that alter PTEN catalytic activity, including C124S which completely disables PTEN phosphatase activity and G129E which disables PTEN lipid phosphatase activity but maintains activity for phosphorylated peptides, are commonly located in the PTEN catalytic pocket or the surrounding region (Liaw *et al.*, 1997; Myers *et al.*, 1997). Mutation to the basic residues in the phosphatase domain (R161, K163, K164, **Figure 1.9**) can reduce the ability of PTEN to localize to the plasma membrane (Das *et al.*, 2003).

Dimerization of PTEN has been shown to play a role in its lipid phosphatase activity, with mutations that inhibit this activity functioning in a dominant negative fashion (Papa *et al.*, 2014). It has also been shown that the p85 interacts directly with PTEN and that this interaction improves the stability and stimulates the catalytic activity of the PTEN protein (Chagpar *et al.*, 2010; Cheung *et al.*, 2015; Rabinovsky *et al.*, 2009). The recent study by Cheung *et al.* further identified that the PTEN protein binds specifically to p85 homodimers, and that disruption of p85 homodimerization prevents binding to PTEN (Cheung *et al.*, 2015). Using deletion mutants of various domains of the two proteins it was shown that the SH3 and BH domains of p85, and the phosphatase domain for PTEN, were important for the interaction between the two proteins (Chagpar *et al.*, 2010; Cheung *et al.*, 2015).

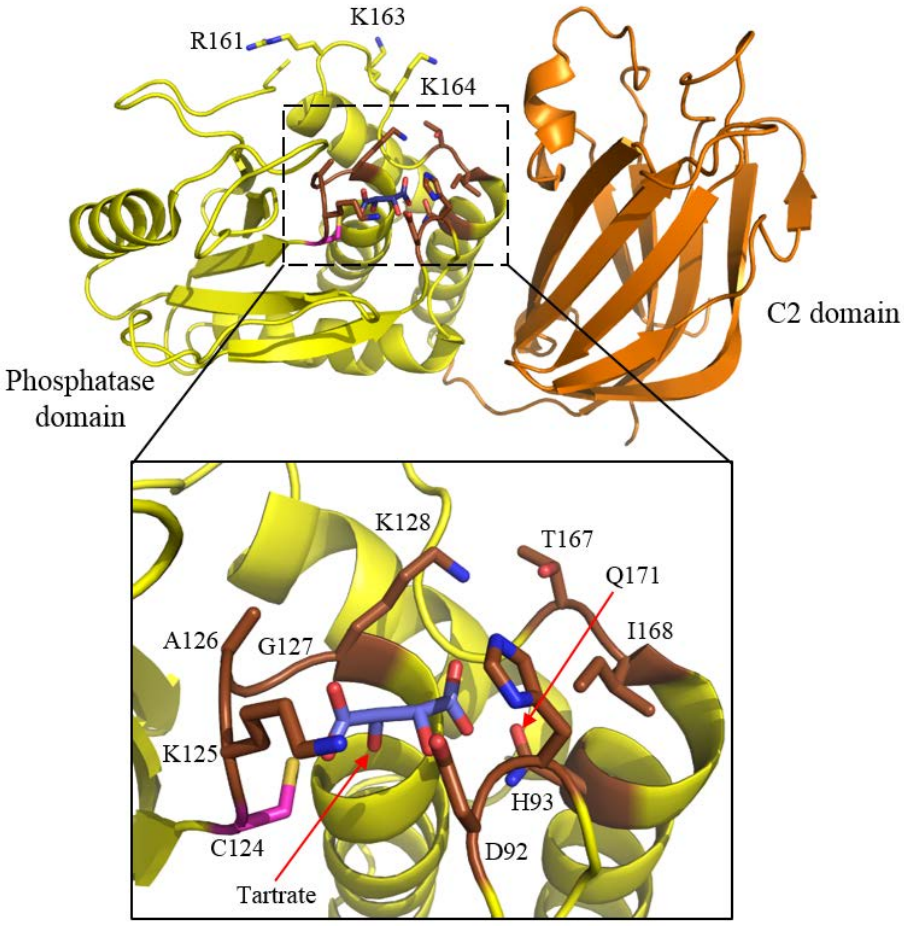

Figure 1.9 Crystal structure of human PTEN (7-353, Δ286-309) and the catalytic pocket. Crystal structure or PTEN (7-353, Δ286-309) solved by Lee *et al.* PDB ID# 1D5R (Lee *et al.*, 1999). The phosphatase domain is shown in yellow and the C2 domain is shown in orange. Residues important for lipid binding and that form the catalytic pocket are shown in stick format, with catalytic pocket forming residues shown in brown and the catalytic C124 residue in magenta. The tartrate molecule bound in the catalytic pocket is shown in violet.

Determining the amino acids important for p85 and PTEN binding would allow for a better understanding of the interaction interface between the two proteins. To this end Xuan Ruan, Dielle Whitecross, and Dr. Paul Mellor of the Anderson lab generated a series of tagged p85 mutants that were either FLAG-tagged and transfected into COS-1 cells and pull-down experiments performed using cell lysates, or the mutant proteins were GST-tagged, expressed in BL21 bacteria, purified, the GST-tag cleaved, and then used for pull-down experiments. All pull-down experiments were performed using Glutathione S-transferase (GST)-tagged PTEN, or GST

alone as a control. The results of these experiments are shown in **Figure 1.10** (Ruan *et al.*, Unpublished Data).

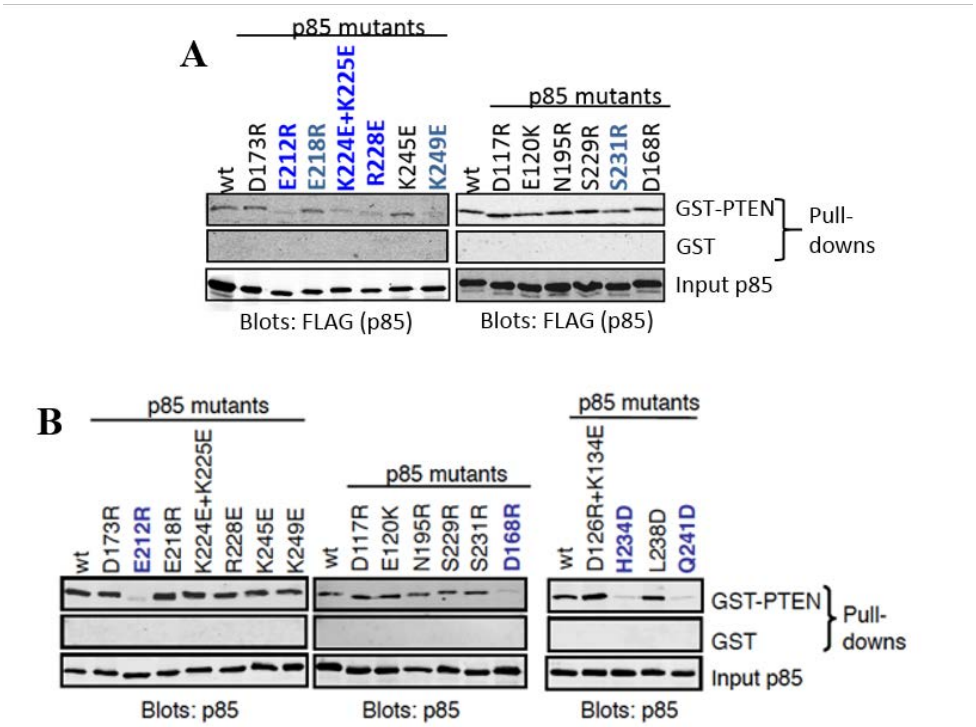

Figure 1.10 Altered PTEN binding of p85 mutants. Pull-down experiments of p85 proteins containing various mutants bound by GST-tagged PTEN, or GST alone as a negative control. Protein was detected through western blot analysis using an anti-FLAG or anti-p85 primary antibody and an infrared-linked secondary antibody (Ruan *et al.*, Unpublished Data). **A**. FLAG-tagged p85 wild-type or mutant proteins were expressed in COS-1 cells, the cells lysed and the lysate used for pull-down analysis. Mutants in dark blue showed consistent decreases in binding, while those in light blue showed larger variation between experiments. **B**. GST-tagged p85 wild-type or mutant proteins were expressed in BL21 bacteria cells, purified, cleaved from GST and the purified protein used for pull-down analysis.

Results of initial pull-down experiments using COS-1 cell lysates showed several p85 mutants that had decreased PTEN binding: E212R, K224E+K225E, R228E, and K249E. As COS-1 cells still possess some endogenous p85 there were concerns that dimerization between mutant p85 and wild-type endogenous p85 could affect the results of the experiments, such as masking the effects that some mutations might have upon PTEN binding through the formation of a p85 mutant and p85 wild-type heterodimer. To this end further pull-down experiments were performed using GST-tagged p85 wild-type and mutant proteins purified from *Escherichia coli*

(*E. coli*) strain BL21 bacterial cells and cleaved from GST. Using purified p85 protein resulted in a smaller number of mutants showing a decrease in PTEN binding: D168R, E212R, H234D, and Q241D, with three in common between the two experimental approaches.

In addition to their mutagenesis studies Cheung *et al.* also pursued structural modeling of the p85 SH3 and BH domains, followed by modeling this arrangement of the p85 BH domain with PTEN (Cheung *et al.*, 2015). Since small angle X-ray scattering data for the p85 SH3 and BH domain together was not available, they generated simulated small angle X-ray scattering results and performed several modeling iterations to obtain this model. Further experimental analysis will be required to validate the accuracy of the suggested orientation. Determination of the crystal structure of the p85 BH domain in complex with PTEN would provide direct experimental identification of residues important for the interaction between these two proteins. The structure of the complex would also help identify p85 residues that stimulate PTEN catalytic activity, similar to the insights provided by Huang *et al.* structure of p85 110B region in complex with p110 (Huang *et al.*, 2007).

1.5.3 Structural studies of Rab5

The crystal structure of the human Rab5 GTPase domain (amino acids 15-184) has been solved for the protein alone, as well as in complex with fragments of effector binding partners EEA1 and Rabaptin5 (Mishra *et al.*, 2010; Terzyan *et al.*, 2004; Zhu *et al.*, 2003; Zhu *et al.*, 2004). The solved crystal structures are shown in **Figure 1.11**.

The Rab5 GTPase domain is composed of five alpha helices and two beta sheets that each contain three beta strands, with the catalytic pocket of the protein composed of various flexible loops including 2 switch loops that change orientation based on binding GDP or GTP (Zhu *et al.*, 2003). A magnesium ion is present within the catalytic pocket of Rab5, and conformational changes are observed in the switch loops that help form the catalytic pocket depending on if GTP or GDP is bound by the protein (Zhu *et al.*, 2003). Mutation of A30 present in one of the loops that form the catalytic pocket to an arginine residue resulted in an increased rate of conversion of GTP to GDP, but this increase in catalysis was inferior to that observed from the arginine finger provided by bound GAP proteins (Zhu *et al.*, 2003).

Structural data obtained for Rab5 in complex with its effector Rabaptin5 C-terminal domain identified residues important for protein-protein interactions, which allowed mutagenesis

studies and pull-down experiments to validate these observations (Zhu *et al.*, 2004). Based on these observations they generated a Y82A mutant of Rab5, transfected cells with this mutant, and showed that it impaired Rab5 endosomal fusion activity (Zhu *et al.*, 2004). Comparison of the structure of Rab5-GTP bound to Rabaptin5 with the structure of Rab5-GDP also allowed for the observation of conformational changes that occur in the different nucleotide-bound states of Rab5, providing potential reasons for the specificity of Rabaptin5 only binding to GTP-bound Rab5 and not the GDP-bound protein (Zhu *et al.*, 2004).

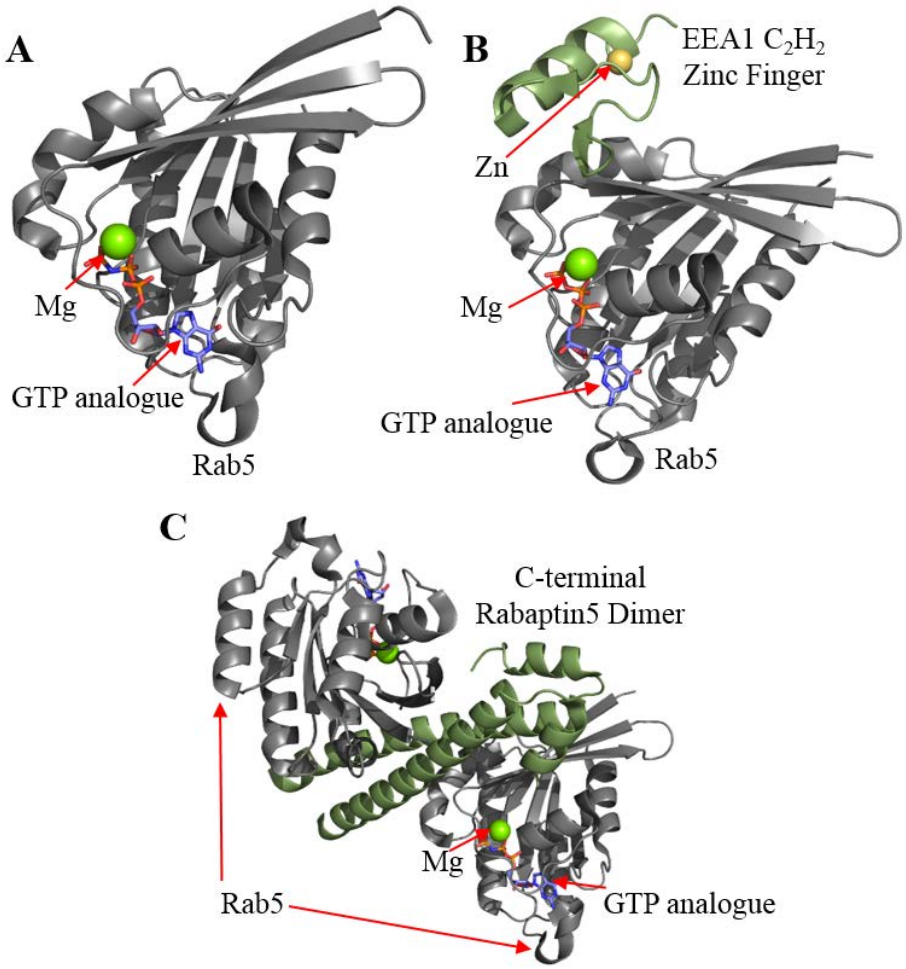

Figure 1.11 Crystal structures of human Rab5 alone and in complex with effector binding partners. Crystal structures of: Rab5 (15-184) with bound GTP analogue (**A**, PDB ID# 1N6H; Zhu *et al*., 2003), Rab5 (15-184) in complex with the C_2H_2 zinc finger of human EEA1 (**B**, PDB ID# 3MJH; Mishra *et al.*, 2010), and two Rab5 (15-184) molecules in complex with a dimer of the C-terminal domain of human Rabaptin 5 (**C**, PDB ID# 1TU3; Zhu *et al*., 2004). Magnesium ions are shown as green spheres, zinc ions are shown as gold spheres, and bound GTP analogues are shown in violet.

The crystal structure determined for Rab5 in complex with the EEA1 C_2H_2 zinc finger domain allowed for the closer examination of Rab5 binding to an effector proteins that plays an important role in endosome fusion. This allowed for further characterization of residues important for interaction between the two proteins, as well as conserved binding interface regions between Rab5 and binding partners that take advantage of conserved hydrophobic residues present on one of the switch regions of Rab5 (L85 and M88) (Mishra *et al.*, 2010). Based on these observed structural contact points mutagenesis and binding experiments were performed to observe the effects mutation of these residues had on Rab5:EEA1 binding in order to further support their role in binding (Mishra *et al.*, 2010). In addition to their structural studies, Mishra *et al.* also performed binding affinity experiments to compare the binding of EEA1 with Rab5 and other members of the Rab protein family, showing that EEA1 binds with high specificity to Rab5 and had much weaker binding with other Rab proteins, including those that are most closely related to Rab5 (Mishra *et al.*, 2010).

The p85 protein has been shown to bind Rab5 and serve as a GAP to stimulate the intrinsic GTPase activity of Rab5 (Chamberlain *et al.*, 2004). There are currently no crystal structures for Rab5 in complex with one of its GAP proteins. Crystal structures of human p85 BH domain and the BH domains of other GAP proteins have been solved individually for Myosin 9b (PDB ID# 5C5S) and N-chimaerin (PDB ID# 2OSA), and a crystal structure of CDC42GAP in complex with CDC42 (PDB ID# 2NGR) was also solved (Kong *et al.*, 2015; Nassar *et al.*, 1998) (Walker *et al.*, Unpublished). A comparison of the BH domain structures of p85, Myosin 9b, N-chimaerin, and CDC42GAP is shown in **Figure 1.12**. Cheung *et al.* modeled a potential interaction between p85 and Rab5 based on superimposing the crystal structures of the p85 BH domain and Rab5 over the crystal structure of CDC42 bound to CDC42GAP (Cheung *et al.*, 2015). This potential orientation placed p85 residue R151 at the interface to serve as the catalytic residue stimulating Rab5 GTPase activity. Previous mutagenesis studies performed had shown that mutation of R151 lead to a slight decrease in p85 GAP activity, while mutating R274 completely removed p85 GAP activity, leading to the interpretation that R274 was the catalytically critical residue (Chamberlain *et al.*, 2004). A potential orientation of the p85 BH domain and Rab5, generated based on overlaying these structures with the CDC42 and CDC42GAP structure as performed by Cheung *et al.*, with R151 and R274 of p85 indicated is shown in **Figure 1.13**. The R274 residue is located distant from the Rab5 catalytic site, positioned between several helices and loops. It is possible

that mutation of this residue resulted in a destabilization of structural elements of the p85 BH domain, leading to the observed loss of GAP activity. Determination of a crystal structure between the p85 BH domain and Rab5 would better determine the accuracy of this model, identify specific residues important for the interaction, confirm the identity of the catalytic Arg, and how mutations affect binding.

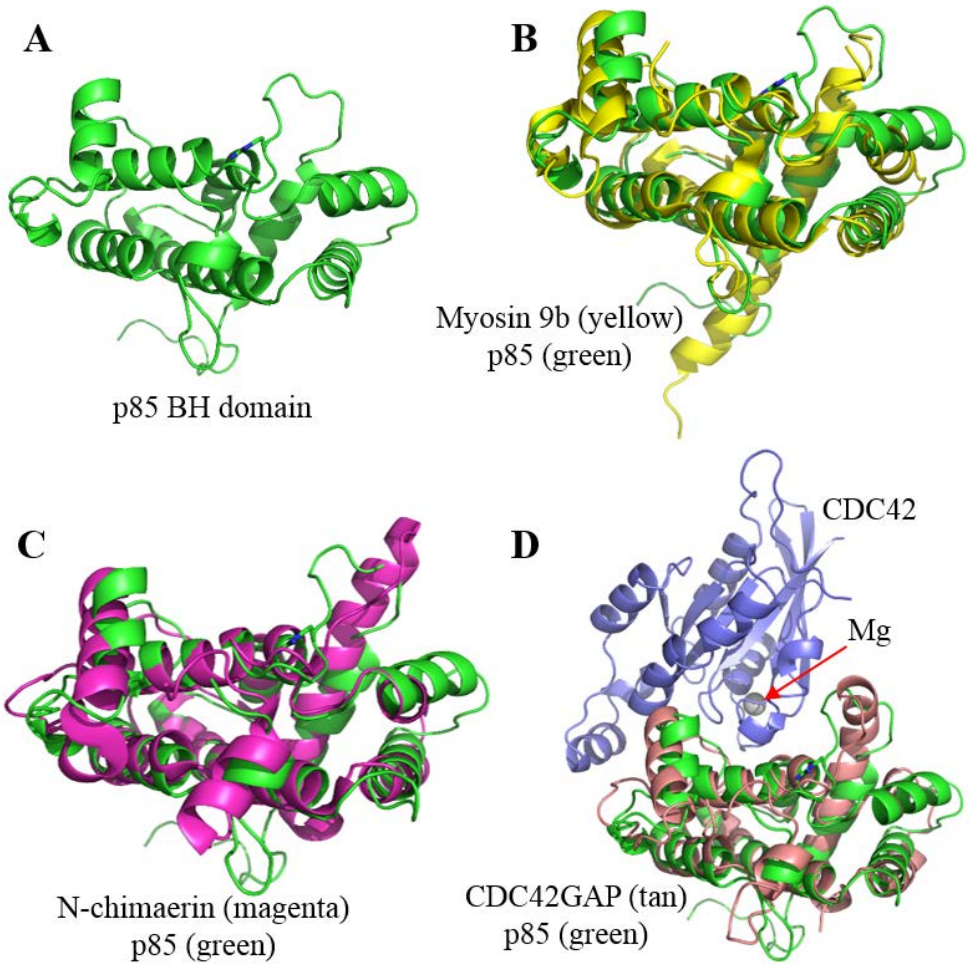

Figure 1.12 Comparison of the human p85 BH domain with BH domains of other GAP proteins. A. The p85 BH domain (green) alone, PDB ID# 1PBW (Musacchio *et al*., 1996). **B.** Overlay of the p85 BH domain and the human Myosin 9b BH domain (yellow), PDB ID# 5C5S (Kong *et al*., 2015). **C.** Overlay of the p85 BH domain and the human N-chimaerin BH domain (magenta), PDB ID# 2OSA (Walker *et al*., Unpublished). **D.** Overlay of the p85 BH domain with the human CDC42GAP BH domain (tan) bound to human CDC42 (purple), PDB ID# 2NGR (Nassar *et al*., 1998). The magnesium ion in the CDC42 binding site is shown as a grey sphere.

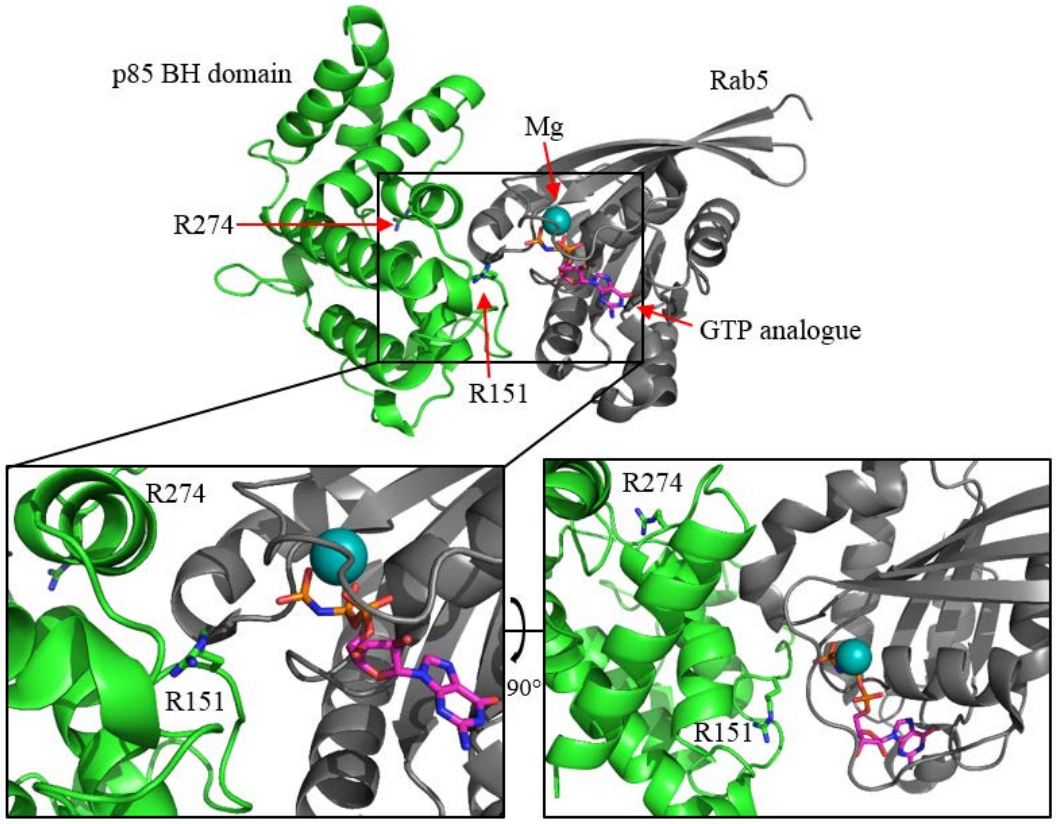

Figure 1.13 Potential interface region between p85 BH domain and Rab5. Possible orientation of the p85 BH domain and Rab5 complex, determined by aligning the crystal structures of the p85 BH domain (green, PDB ID# 1PBW; Musacchio *et al*., 1996) and Rab5 (gray, PDB ID# 1N6H; Zhu *et al*., 2003) with the crystal structure of CDC42 bound to CDC42GAP (PDB ID# 2NGR; Nassar *et al*., 1998; structure not shown). R151, located at the potential interface, and R274, the previously proposed GAP catalytic residue, are shown in stick format, with magnesium shown as a teal sphere and the bound GTP analogue shown in magenta.

2.0 Hypothesis and Objectives

2.1 Rationale

Combining high-resolution structural data with results of biochemical experiments can provide a deeper insight into the mechanisms of function and disease. The crystal structures of p85 110B domain in complex with the p110 adaptor binding domain or the full-length p110 protein were used to examine how known cancer-associated mutations could alter the binding of the two proteins based on their positions within the structure, and additional biochemical experiments to characterized binding residues (Huang *et al.*, 2007; Miled *et al.*, 2007). The p85 BH domain and its known binding partners PTEN and Rab5 have not seen the same examination, with recent modeling and biochemical analysis by Cheung *et al.* beginning a deeper examination (Cheung *et al.,* 2015). High resolution structural data of the interactions between these protein complexes can allow for greater understanding of the residues involved and how cancer-associated mutations affect their binding and function.

2.2 Hypothesis

Detailed structural information for the p85 BH domain, several cancer-associated and engineered mutants, and complexes involving binding partners PTEN and Rab5, will allow us to better understand the function and regulation of this protein.

2.3 Objectives

1. Obtain crystal structure data for the p85 BH domain wild-type, and containing a number of cancer-associated and engineered mutations.
2. Determine the crystal structure of the p85 BH domain in complex with the previously crystallized PTEN (7-353, Δ286-309) or Rab5 (15-184) protein fragments.
3. Determine the effect of various cancer-associated and engineered mutations on p85 dimerization.

3.0 Materials and Methods

3.1 Materials

3.1.1 Bacterial cells and culture

DNA amplification was performed within *E. coli* strain TOP10 [F^-, *mcr*A, D(*mrr-hsd*RMS-*mcr*BC), f80*lac*ZDM15 D*lac*X74, *deo*R, *rec*A, *ara*D139 D(*ara-leu*)7697, *gal*K, *rps*L(StrR), *end*A1, *nup*G] cells (Invitrogen). GST-fusion proteins were overexpressed in protease-deficient BL21 [*E. coli* B, F^-, *dcm*, *ompT*, *hsdS*(*rb-ms-*), *gal*] cells (Amersham). Both strains were grown in Miller Luria Bertani Broth (LB, EMD Millipore; Billerica, MA), supplemented with 100 µg/mL ampicillin (Sigma-Aldrich), at 37°C in a shaking incubator. For obtaining higher yields of GST-fusion proteins some batches of BL21 bacteria were grown in Hyper Broth (AthenaES; Baltimore, MD), supplemented with 100 µg/mL ampicillin, at 37°C in a shaking incubator. GST-fusion proteins of PTEN (7-353, Δ286-309) and Rab5 (15-184) were also overexpressed in protease-deficient Rosetta [F^- *ompT hsdS*$_B$($r_B^-m_B^-$) *gal dcm* pRARE (Cam^R)] cells (Novagen). Rosetta cells were grown in LB or Hyper Broth media supplemented with 100 µg/mL ampicillin and 34 µg/mL chloramphenicol, at 37°C in a shaking incubator.

3.1.2 Plasmids

The various cDNAs used were subcloned separately into the pGEX6P1 vector (Amersham). All GST-p85 mutants and GST-PTEN (7-353, Δ286-309 C124S) were generated within this plasmid.

3.1.3 Primers

Table 3.1 Sequencing primers. All primers were custom-ordered through Invitrogen Life Sciences. The GST-seq primers were used for sequencing all pGEX6P1 plasmids.

Sequencing Primers	
Primer Name	**Sequence**
5`-GST-seq	TTTGCAGGGCTGGCAAGC
3`-GST-seq	TTCACCGTCATCACC

Table 3.2 Primers for p85, Rab5, and PTEN fragment generation. The 5`-p85 primer was previously purchased from the University of Alberta oligonucleotide synthesis service (Edmonton, AB). All other primers were custom-ordered through Invitrogen Life Technologies. Restriction enzyme sites for cloning into desired vectors are indicated with the recognition site underlined. Codons are separated by spaces.

Primer Name	Sequence
Primers for p85	
5`-p85	TCAGGATCC ATG AGT GCC GAG GGG TA
5-BamHI-p85bv-105	TCAGGATCC GAA GCA GAC AGT GAG CA
3-p85bv-319+stopEco	CGAGAATTC TCA GTT GGC TAC AGT AGT GGG
5`BCR	ACCACAAAGGATCC GGA AGG AAA AAG ATC TCG CCT CCC A
Primers for PTEN	
5-PTENhu-BamHI-7	GCAGGATCC GAG ATC GTT AGC AGA AAC
3-PTENhu-EcoRI-353	CGGGAATTC TCA CTC CTC TAC TGT TTT TGT G
Primers for Rab5	
5-Rab5hu-BamHI-15	GCAGGATCC GGA AAT AAA ATA TGC CAG
3-Rab5dog-EcoRI-184	CCAGAATTC TCA GTT CTT TGG CAA CTT TTT AGC

Table 3.3 Primers for GST-p85 and GST-PTEN mutagenesis. All primers were custom-ordered through Invitrogen Life Technologies. All mutagenesis primers were utilized in sense-antisense pairs. The mutation site is indicated by the nucleotide(s) underlined. Codons are separated by spaces.

Primer Name	Sequence
Mutagenesis Primers for p85	
5-p85hE137K	C AAG CTC GTG AAA GCC ATT G
3-p85hE137K	C AAT GGC TTT CAC GAG CTT G
5-p85bv-F177N	GAC TTG GAG ATG AAC GAT GTG CAC
3-p85bv-F177N	GTG CAC ATC GTT CAT CTC CAA GTC
5-p85bv-E217K	G CAG AGT TCT AAA GAA TAC ATC CAG
3-p85bv-E217K	CTG GAT GTA TTC TTT AGA ACT CTG C
5-p85bv-R262T	CTG AAT GCA ACA GTA CTT TCT GAA C
3-p85bv-R262T	G TTC AGA AAG TAC TGT TGC ATT CAG
5-p85bv-K288Q	CAC CTC ATA CAA ATT ATA GAA ATC
3-p85bv-K288Q	GAT TTC TAT AAT TTG TAT GAG GTG
5-p85bv-E297K	ATC TCC ACC AAA TGG AAT GAA CGC
3-p85bv-E297K	GCG TTC ATT CCA TTT GGT GGA GAT
Mutagenesis Primers for PTEN	
5` PTEN C124S	GCA ATT CAC AGT AAA GCT GG
3` PTEN C124S	CC AGC TTT ACT GTG AAT TGC

3.1.4 Antibodies

The anti-p85 BH primary antibody was generated in a rabbit by our laboratory to a protein peptide corresponding to a region of the p85 BH domain (amino acids 78-332) (Chagpar *et al.*, 2010). These anti-p85 BH antibodies were purified from rabbit serum first by isolating all IgGs, then by affinity purification through binding and elution to the protein antigen used for the antibody generation. The anti-Rab5 antibodies were purchased from Cell Signaling Technology. Secondary antibodies used were goat anti-rabbit conjugated to infrared dye (LI-COR Biosciences; Lincoln, NB) and were visualized using LICOR ODYSSEY infrared scanner and analyzed using ODYSSEY software V3.0. Antibodies used are summarized in **Table 3.4**.

Table 3.4 Primary and secondary antibodies used

Antibody Name, species	Company and Cat. #	Figure(s)	Concentration
Anti-p85 BH, rabbit	Lab generated	4.11, 4.15, 4.16	0.726 µg/mL
Anti-Rab5, rabbit	Cell Signaling Technology, 2143	4.11	1:1000
IRDye 680 anti-rabbit, goat	LI-COR Biosciences, 926-32221	4.11, 4.15, 4.16	0.132 µg/mL

3.1.5 Crystallization condition screening kits

The following commercially available sparse matrix crystallization conditions screening kits were used during initial crystallization trials: WIZARD I (Rigaku Reagents), WIZARD II (Rigaku Reagents), Pact Suite (QIAGEN), Index Suite HR2-144 (Hampton Research), PEG-Ion (Hampton Research), Crystal Screen HR2-110 (Hampton Research), JCSG+ Suite (QIAGEN), and $AmSO_4$ Crystal Screen (QIAGEN).

3.1.6 Other reagents

Phosphatidylinositol phosphate (PIP) strips were purchased from Echelon Biosciences Inc. (Salt Lake City, UT). Non-hydrolyzable GTP analogue GppCP was purchased from Jena Bioscience. It was obtained as a sodium salt and dissolved in water. All other chemicals and reagents were purchased from Sigma-Aldrich or VWR and were analytical grade or higher unless otherwise specified.

3.2 Methods

3.2.1 Generation of GST-tagged protein fragments

3.2.1.1 Generation of GST-tagged bovine p85 protein fragments

Previously Dr. Deborah Anderson had generated a pGEX6P1 vector containing a cDNA coding for the full length bovine p85, which possesses 96.8% sequence identity with the human protein (701 of 724 amino acids). Using this plasmid as a template I PCR generated p85 fragments coding for amino acids 1-319 (primers 5`-p85 and 3-p85bv-319+stopEco), 78-319 (primers 5` BCR and 3-p85bv-319+stopEco), or 105-319 (primers 5-BamHI-p85bv-105 and 3-p85bv-319+stopEco), with all primers used found in **Table 3.2**. The bovine p85 (1-319) protein fragment has 94.4% sequence identity with the human (301 of 319 amino acids), the p85 (78-319) has 93.0% sequence identity (225 of 242 amino acids), and the p85 (105-319) has 92.6% sequence identity (199 of 215 amino acids). The PCR reaction mixtures contained KOD Hot Start DNA Polymerase Buffer (EMD Millipore), 1.5 mM $MgSO_4$, 0.2 mM each dNTP, 0.3 µM each of 5` and 3` primers, 10 ng template DNA, 1 µL KOD Hot Start Enzyme (EMD Millipore), and water up to a total volume of 50 µL. All PCR reactions were performed in an Applied Biosystems 2720 Thermo Cycler with polymerase activation by 2 mins at 95°C, followed by 30 cycles of 95°C for 20 seconds for DNA denaturing, 43°C for 10 seconds for primer annealing, and 70°C for 20 seconds for extension, followed by storage at 4°C. These DNA fragments were purified following the PCR using a clean-up kit (QIAgen) and restriction digested with 10 U *BamH*I and 10 U *EcoR*I for 1 hour at 37°C. The digested fragments were removed from enzyme and buffer using the clean-up kit. The digested DNA was ligated into *BamH*I and *EcoR*I digested pGEX6P1 vector using 1 µL Quick Ligase (New England Biolabs) in Quick ligation buffer (New England Biolabs) to a final volume of 20 µL, incubated at 25°C for 30 minutes. The ligated DNA was transformed into competent TOP10 cells (Hanahan *et al.*, 1991), that were grown on LB plates supplemented with 100 µg/mL ampicillin for selection. Plasmid DNA from the resulting colonies was isolated using a QIAgen Plasmid Miniprep Kit (QIAgen) and sent for sequence verification of the entire insert region at the Plant Biosciences Institute using the 5`-GST-seq and 3`-GST-seq primers (**Table 3.1**). Sequence confirmed plasmids were transformed into BL21 competent cells for later use in protein expression and purification.

3.2.1.2 Generation of GST-tagged p85 mutants

Six point-mutations were introduced into the pGEX6P1-p85 (105-319) vector using Pfu DNA polymerase (Thermo Scientific). The reaction mixture contained Pfu buffer with $MgSO_4$, 100 ng template DNA, 125 ng 5` mutagenic primer and 125 ng 3` mutagenic primer (**Table 3.3**), 2 mM dNTPs, and 2.5 U/mL Pfu DNA polymerase to a final volume of 50 µL. Mutagenesis reaction mixtures were heated to 95°C for 30 seconds for the initial denaturation of the DNA, followed by 16 cycles of; 95°C for 30 seconds for DNA denaturation, 55°C for 1 minute for primer annealing, and 68°C for 5 minutes for DNA extension in an Applied Biosystems 2720 Thermo Cycler. The DNA was treated with 10 U *Dpn*I at 37°C for 1 hour to digest the methylated wild type DNA used as the template. Following *Dpn*I digestion 40 µL of the DNA amplification reaction was used for transformation and sequence verification as described above.

3.2.1.3 Generation of GST-tagged PTEN (7-353, Δ286-309 C124S)

Previously the Anderson lab generated a pGEX6P1 vector containing the cDNA coding for human PTEN (7-353, Δ286-309), the fragment previously used for PTEN crystallization studies (Lee *et al.*, 1999). It has been shown in other phosphatases possessing conserved active site sequence (I/V HCXAGXXR S/T G) that mutation of the active site Cys residue inactivates the protein phosphatase activity while still allowing binding to target ligand (Jia *et al.*, 1995; Streuli *et al.*, 1989). Based on this knowledge we generated a fragment coding for PTEN (7-353, Δ286-309, C124S) (PTEN Crystal) via mutagenesis using pGEX6P1-PTEN (7-353, Δ286-309) as the template, and the mutagenesis primers 5` PTEN C124S and 3` PTEN C124S (**Table 3.3**) to assist in complex formation experiments. Mutagenesis reaction mixture, DNA treatment, bacterial transformation, and sequencing were performed as described above.

Sequence confirmed plasmids were also transformed into Rosetta cells for later use in protein expression and purification to maximize the yield of soluble protein.

3.2.1.4 Generation of GST-tagged Rab5 (15-184)

Previously the Anderson lab generated a pGEX6P1 vector containing the cDNA coding for the full length canine Rab5 protein. Using this plasmid as a template I PCR generated a fragment encoding Rab5 (15-184), the same fragment used in previous crystallization studies of Rab5 (Zhu *et al.*, 2003). Human and canine Rab5 share 100% amino acid identity across this

region. Primers used were 5-Rab5hu-BamHI-15 and 3-Rab5dog-EcoRI-184 (**Table 3.2**). Purification, bacterial transformation, and sequencing were performed as described above.

Sequence confirmed plasmids were also transformed into Rosetta cells for later use in protein expression and purification to maximize yield of soluble protein.

3.2.2 Protein expression, purification, and tag cleavage of GST-tagged protein fragments

3.2.2.1 Individual batch protein purification

BL21 cells transformed with our protein expression vectors of interest were used to inoculate 100 mL cultures of LB supplemented with 100 µg/mL ampicillin and grown for 16 hours at 37°C in a shaking incubator. These 100 mL cultures were then used to inoculate 1 L cultures of LB supplemented with 100 µg/mL ampicillin and incubated at 37°C until they reached an optical density at 600 nm of between 0.6-0.8, determined using a Pharmacia Biotech Ultrospec 300 UV/Visible Light Spectrophotometer. Protein overexpression was induced with addition of 0.1 mM isopropyl ß-D-1-thiogalactopyranoside (IPTG). The culture was incubated for 16 hours at 25°C. Cultures were centrifuged at 6000 X g for 15 mins at 4°C in a JA-10 rotor using an Avanti J-E Centrifuge (Beckman Coulter). Pellets were collected and their weight recorded.

For PTEN Crystal and Rab5 (15-184) being expressed in Rosetta cells, these bacteria were used to inoculate 100 mL cultures of LB supplemented with 100 µg/mL ampicillin and 34 µg/mL chloramphenicol. Other growth conditions and pelleting were performed as described above for the BL21 cells.

Bacterial pellets were lysed using Prescission buffer (50 mM Tris pH 7.0, 150 mM NaCl, 1 mM Ethylenediaminetetraacetic acid (EDTA), 1 mM dithiothreitol (DTT), the protease inhibitors 10 µg/mL aprotinin, 10 µg/mL leupeptin, and 1 mM 4-(2-aminoethyl)benzenesulfonyl fluoride hydrochloride (AEBSF)) with 1 µg/mL lysozyme. Following resuspension of the bacterial pellet in lysis buffer they were incubated at 4°C for 1 hour. The bacteria were further lysed and the viscosity was reduced via sonication on ice. Six 10 second sonications were performed with 60 seconds between each sonication, using a setting of 2.5 on a Branson Sonifier 450. The sonicated cell debris was pelleted via centrifugation at 24000 X g for 30 mins at 4°C in a JA-25.5 rotor using an Avanti J-E Centrifuge. The lysate was filtered through 0.8 µm Nalgene syringe filters (Thermo Scientific).

For every 40 mL of protein lysate we added 1 mL of 50% Glutathione-Sepharose beads in phosphate buffered saline (PBS, 137 mM NaCl, 2.7 mM KCl, 4.3 mM Na_2HPO_4, 1.4 mM KH_2PO_4, pH 7.3). The GST-tagged proteins were allowed to bind to the beads for 1 hour at 4°C. Samples were centrifuged at 500 X g for 5 minutes at 4°C using an Eppendorf Centrifuge 5810 R. Supernatant was aspirated, and the beads were washed 5 times using 40 mL Prescission buffer (50 mM Tris pH 7.0, 150 mM NaCl, 1 mM EDTA, and 1 mM DTT). Washed beads were transferred to microcentrifuge tubes with addition of 900 µL Prescission buffer for every 500 µL of packed Glutathione-Sepharose beads. To every tube we added 60 µL of 3C Prescission Protease (Sigma-Aldrich), and the samples were incubated for 72 hours at 4°C. 3C Prescission Protease is a genetically engineered fusion of human rhinovirus 3C protease and GST that cleaves between the Gln and Gly residues of the recognition sequence LEVLFQGP.

Samples were centrifuged at 500 X g for 5 minutes at 4°C and supernatant containing the cleaved protein was collected. Beads had 1 mL cold Prescission buffer added and were agitated at 4°C for 15 minutes before centrifuging and the supernatant containing the cleaved protein was collected. We collected 5 washes from the beads to recover additional cleaved protein.

Samples and each wash were analyzed using sodium dodecyl sulphate polyacrylamide gel electrophoresis (SDS-PAGE) with Coomassie Blue staining to check for protein purity and yield. Pooled samples were concentrated and buffer exchanged into the desired storage buffer using Millipore Amicon 10 kDa centrifugal filter units. Proteins were stored at 4°C until further purification or experiments.

3.2.2.2 Large scale ÄKTA Purifier Glutathione-Sepharose column purification

Initial bacterial culture growth and lysis was performed as per **3.2.2.1 Individual batch protein purification**. For larger protein yields the larger 1 L cultures were grown in Hyper Broth to obtain larger bacterial pellets.

Following filtration through the 0.8 µm Nalgene syringe filters, the bacterial lysate was loaded into a Superloop (GE Healthcare) equilibrated in PBS. The Superloop was connected to the ÄKTA Purifier attached to an HR 16/10 column loaded with Glutathione-Sepharose high performance media (GE Healthcare, column bed height 8.0 cm, column bed diameter 1.6 cm, column volume 16 mL). The lysate was injected onto the column with PBS buffer, using protocol settings of 1 mL/min flow rate, pressure limit of 0.5 MPa, and collecting 5 mL fractions while

unbound proteins were washed off across 5 Column Volumes (CV) buffer. Washing was maintained until the A280 UV absorbance was less than 20 mAU, to ensure non-specifically bound protein had all been removed from the column. The collected fractions allowed analysis to ensure our GST-tagged protein of interest was not being removed from the column during washing steps.

GST-tagged proteins were eluted from the column using Elution Buffer (50 mM Tris pH 8.0, 150 mM NaCl, and 10 mM reduced glutathione). This elution step was performed at the same flow rate and pressure limit as protein binding, and was performed over 5 CV while collecting 2 mL fractions.

Presence of desired protein was confirmed using SDS-PAGE analysis with Coomassie Blue staining.

Fractions containing protein were pooled and transferred to Spectra/Por molecularporous membrane tubing (Spectrum Medical Industries Inc.; Los Angeles, CA) with a MW cut-off of 6000-8000 Da. The protein was then dialyzed for 16 hours in 50 mM Tris pH 8.0, 150 mM NaCl, 1 mM EDTA buffer. Following dialysis we added 60 µL 3C Prescission Protease and incubated the samples for 72 hours at 4°C.

We purified our liberated protein from the cleaved GST-tag using the HR 16/10 Glutathione-Sepharose column used previously by binding the GST portion to the column and allowing the desired cleaved protein to flow through without binding. Samples were added to the column using PBS buffer, with a flow rate of 1 mL/min, pressure limit of 0.5 MPa, and collecting 1 mL fractions. Fractions collected containing the desired cleaved protein were checked for protein purity and yield using SDS-PAGE with Coomassie Blue staining. Samples containing purified protein were concentrated and buffer exchanged into the desired storage buffer using Millipore Amicon 10 kDa centrifugal filter units. Proteins were stored at 4°C until further purification or experiments.

3.2.2.3 Anion exchange chromatography of p85 protein fragments

Proteins purified using Glutathione-Sepharose affinity chromatography were further purified using anion exchange chromatography. Protein samples were buffer exchanged into Source Q Anion A Buffer (50 mM Tris pH 8.0, 50 mM NaCl, 2 mM DTT) and loaded onto an HR 16/10 Column packed with Source Q Anion Exchange Media (GE Healthcare, column bed

height 10 cm, column bed diameter 1.6 cm, column volume 20.1 mL). Protein was injected onto the column and washed with 2 CV Source Q Anion A Buffer to remove unbound protein with a flow rate of 3 mL/min and a pressure limit of 0.5 MPa. Bound protein was eluted starting from Source Q Anion A Buffer across a gradient of 0-100% Source Q Anion B Buffer (50 mM Tris pH 8.0, 1 M NaCl, 2 mM DTT) across 3 CV while collecting 1 mL fractions. After completing the gradient an additional 2 CV of Source Q Anion B Buffer were used to ensure full elution of any remaining bound proteins.

Fractions were analyzed using SDS-PAGE analysis and Coomassie Blue staining to verify protein purity and yield. Fractions containing purified protein were pooled and concentrated and buffer exchanged into the desired storage buffer using Millipore Amicon 10 kDa centrifugal filter units. Proteins were stored at 4°C until used for experiments.

3.2.3 Protein Visualization and concentration determination

3.2.3.1 Coomassie Blue staining

Proteins were visualized using SDS-PAGE (7.5, 10, or 15% acrylamide, Fisher Scientific) (Laemmli, 1970) and Coomassie blue staining (0.14% [w/v] Coomassie Blue R-250 [Bio-Rad], 41.4% [v/v] methanol, and 5.4% [v/v] acetic acid). Unbound Coomassie blue was removed by washing the gels with destain solution (41.4% [v/v] methanol, 5.4% [v/v] acetic acid). Following cleavage of the GST-tag, bands corresponding to the following MW were expected for each protein: p85 (1-319; ~36 kDa), p85 (78-319; ~27 kDa), p85 (105-319) (p85-BH; ~24 kDa), Rab5 (1-215 ~24 kDa), Rab5 (15-184; ~19 kDa), and PTEN (7-353 Δ286-309; ~38 kDa). Presence of other bands were interpreted as presence of contaminating proteins, presence of cleaved GST, or signs of protein degradation. Gel images were recorded using a ChemiDoc imaging system (Bio-Rad).

3.2.3.2 Western blot analysis

For western blot analysis protein resolved by SDS-PAGE were transferred to a nitrocellulose membrane (Amersham) in transfer buffer (48 mM Tris-HCl pH 9.2, 0.028% [w/v] SDS, and 20% [v/v] methanol) using a Trans-Blot Turbo Transfer System (Bio-Rad). The transfer was arrayed as follows: 3 pieces of 3 mm filter paper (Whatman) soaked in transfer buffer, nitrocellulose membrane hydrated with water, SDS-PAGE gel, and 3 pieces of 3 mm filter

paper soaked in transfer buffer. Any air bubbles present were removed by applying a roller across the top. The system was operated at 2.5 A, 25 V for 20 minutes to perform the transfer.

The nitrocellulose membrane was incubated in blocking solution (5% [w/v] Carnation skim milk powder [Safeway] in PBS) for 1 hour at room temperature with agitation. The membrane was then incubated with 10 mL primary antibody (appropriate primary antibody from **Table 3.4** in blocking solution above) solution for 1 hour at room temperature. The blot was washed three times for 10 minutes in PBST. The IRDye 560 anti-rabbit secondary antibody (**Table 3.4**) was prepared in 10 mL blocking solution and the membrane incubated in secondary antibody for 1 hour at room temperature in the dark. The membrane was washed as above, in the dark, with an additional wash performed using PBS. The membrane was scanned using a LI-COR ODYSSEY infrared scanner (LI-COR Biosciences) and analyzed with the ODYSSEY V3.0 software.

3.2.3.3 Nano drop protein concentration determination

Concentrations of purified proteins were determined by measuring UV absorbance at 280 nm with a Nanodrop 2000c Spectrophotometer (Thermo Scientific) with corresponding extinction coefficients calculated based on protein sequence using the ExPASy ProtParam tool. The corresponding protein storage buffer was used as a blank for the machine prior to analysis of the purified proteins. Determined protein concentrations were confirmed by SDS-PAGE and Coomassie blue staining compared to known concentrations of bovine serum albumin (BSA).

Protein fragments, calculated MW, and extinction coefficients are provided in **Table 3.5**.

Table 3.5 Protein fragments, calculated MW, and extinction coefficients

Protein Fragment Name	Calculated MW (kDa)	Extinction Coefficient (M^{-1} cm^{-1})
GST	24.50	42860
p85 full-length	83.60	99130
p85 (1-319)	35.72	35870
p85 (78-319)	26.98	19940
p85 (105-319)	24.15	19940
Rab5 (1-215)	23.66	18450
Rab5 (15-184)	18.97	18450
PTEN (7-353, Δ286-309)	38.43	42290

3.2.4 Crystallization condition screening for bovine p85 protein fragments

3.2.4.1 Automated sparse matrix screens

Identification of initial crystal conditions was performed via preparation of sitting drop vapour diffusion screens of commercially available sparse matrix crystallization condition screening kits against 15 mg/mL samples of our protein of interest. These sparse matrix screens were set up using the GRYPHON robot (Art Robbins Instruments) operated by the Protein Characterization and Crystallization Facility (PCCF) of the University of Saskatchewan. Training on the operation of the GRYPHON robot was provided by Dr. Maia Cherney and Dr. Michal Boniecki of the PCCF. The GRYPHON robot generated 0.4 µL sitting drops by mixing 0.2 µL protein solution in crystal holding buffer (20 mM Bis-Tris Propane pH 6.5, 100 mM NaCl, 2 mM tns [2-carboxyethyl] phosphine hydrochloride [TCEP-HCl]) with 0.2 µL crystallization mother liquor in 96-well 2-well intelliplates (Art Robbins Instruments) with 100 µL of crystallization mother liquor deposited in the well reservoir. Plates were sealed with clear cellophane tape to prevent evaporation. Plates were incubated at room temperature and crystal growth was monitored using a Nikon SMZ1000 light microscope. Promising conditions were used as the basis for hanging-drop vapour diffusion condition optimization screens.

3.2.4.2 Hanging-drop vapour diffusion condition optimization screens

Larger volume hanging-drop vapour diffusion condition optimization screens discussed in (McPherson, 1976) were prepared using 24-well VDX plates with sealant (Hampton Research). Using promising conditions from the sparse matrix screens, these screens altered pH values, salt concentrations, and presence/levels of additives such as glycerol or polyethylene glycols (PEG) of various MW. Altering these conditions allowed for improved crystal growth in order to obtain crystals suitable for X-ray diffraction data collection. The crystallization drops were formed on plastic cover slips with the mixture of 1 µL 5-15 mg/mL purified protein solution in crystal holding buffer added to 1 µL crystallization mother liquor and sealed above 1 mL of crystallization mother liquor. Plates were incubated at room temperature and crystal growth was monitored using a Nikon SMZ1000 light microscope.

Conditions that yielded crystals for our p85-BH fragment and mutants were 0.1 M Sodium Cacodylate pH 6.0-6.2, 1.3-1.7 M Li_2SO_4, and 4-8% Glycerol.

3.2.4.3 Crystal seeding and streak seeding

Some mutants of p85 produced small crystals or showers of very small crystals under the initial crystallization conditions. Crystal seeding and streak seeding were used to obtain larger crystals more suitable for diffraction data collection.

For crystal seeding a single small crystal was extracted from the existing crystallization drop and transferred to a fresh drop of crystallization mother liquor to rinse the crystal and remove any small crystals that may have been present on its edges. This washed crystal was then transferred to a fresh drop containing protein and crystallization mother liquor as a seed crystal for further hanging-drop vapour diffusion crystallization. The seed crystal serves as a scaffold for additional protein to crystallize on, resulting in the growth of a larger crystal.

For streak seeding multiple very small crystals were transferred to a fresh crystallization drop containing protein and crystallization mother liquor by moving the whisker of a cat from one side of the initial crystal drop to the other, and then immediately moving the cat whisker through the fresh drop. This streak seeded drop was then sealed and incubated using the hanging-drop vapour diffusion method. The very small crystals introduced to this fresh drop serve as nucleation sites to encourage additional crystal growth, resulting in the production of larger crystals.

3.2.5 X-ray diffraction data collection, processing, and structure refinement

3.2.5.1 X-ray diffraction data collection and processing

Crystals were taken to the Canadian Light Source (CLS, Saskatoon, SK) to collect diffraction data. Diffraction data was collected using the Canadian Macromolecular Crystallography Facility 08B1-1 (CMCF-BM) (Fodje *et al.*, 2014), or the Canadian Macromolecular Crystallography Facility 08ID-1 (CMCF-ID) (Grochulski *et al.*, 2011) beamlines. Drops containing crystals to be analyzed had cryoprotectant solution (0.1 M Sodium Cacodylate pH 6.0, 1.5 M Li_2SO_4, 18% [w/v] glycerol) added prior to data collection. Crystals were extracted using nylon loops attached to mounting pins, which were then connected to the goniometer.

Diffraction data were collected with a detector distance of 280 mm, in 0.5° or 1° wedges for a total collection of 180°. No beam attenuation was applied for data collected using CMCF-BM, while 40-50% beam attenuation was applied for data collected using CMCF-ID. X-ray

detectors equipped at the beamlines were a Rayonix MX300 HE CCD for the CMCF-BM and a Rayonix MX300 CCD for the CMCF-ID. Processing of collected data was performed using HKL2000 software (Otwinowski and Minor, 1997) installed at the CLS.

3.2.5.2 Structure refinement using PHENIX and *Coot* software

Using the files generated following HKL2000 processing structure determination was performed using PHENIX software (Adams *et al.*, 2010). As the human p85 BH domain crystal structure has previously been solved (Musacchio *et al.*, 1996) we used molecular replacement with PDB structure 1PBW as the initial probe to determine the phases of the collected data by determining the best agreement of the calculated diffraction data from the probe and the observed diffraction data experimentally collected. Determined structures were examined using *Coot* software (Emsley *et al.*, 2010) and manual adjustments applied to increase agreement with the observed electron density. Repeated cycles of phenix.refine and manual adjustments in *Coot* were performed to further improve the structure. Improvement to the structure was determined by examining validation tools in *Coot* and the Rfree score following phenix.refine.

After determination of the p85-BH structure, this was used as the starting structure for refinement of other structural data collected.

3.2.5.3 PyMOL image generation

Final images of obtained crystal structures were generated using the PyMOL Molecular Graphics System, Version 1.4.1 Schrödinger, LLC.

3.2.5.4 Generation of electron density maps in CCP4 for visualization in PyMOL

To generate electron density maps for use in PyMOL for visualization we used CCP4 version 6.5.008 (Winn *et al.*, 2011) using *fft* (Immirzi, 1966; Eyck, 1973; Read and Schierbeek, 1988). Generated 2Fo-Fc maps that covered all atoms present within the source PDB files. 2Fo-Fc maps presented in PyMOL were contoured to 1.0 Sigma.

3.2.6 Size exclusion chromatography and Native PAGE

3.2.6.1 Complex formation experiments between p85-BH and Rab5

Before any co-crystallization trials could be performed we first needed to show complex formation between p85-BH and Rab5, as well as purify yields of this complex suitable for crystallization trials. Equimolar amounts of p85-BH and Rab5 purified protein solutions were mixed and incubated at room temperature for 5 or 20 mins, then underwent size exclusion chromatography (SEC). Using a Superdex 200 Increase column (column bed height= 30 cm, column bed diameter= 1 cm, Total Volume= 24 mL, Void Volume= 8 mL, GE Healthcare) connected to an ÄKTA Purifier unit 0.5 mL of this protein mixture at a concentration of 4 mg/mL was loaded. SEC was performed using a buffer of 50 mM Tris pH 7.0, 250 mM NaCl, and 2 mM DTT, at a flow rate of 0.750 mL/min, a pressure limit of 3.80 MPa, and collecting 0.5 mL fractions. A chromatogram was recorded based on the absorbance at 280 nm for each fraction.

MW of observe absorption peaks were determined using the formulas below:

$$K_{av} = (\text{Elution Volume} - \text{Void Volume})/(\text{Total Volume} - \text{Void Volume}) \quad \textbf{(3.1)}$$

$$\text{LogMW} = -3.199(K_{av}) + 3.0564 \quad \textbf{(3.2)}$$

Void Volume and Total Volume are determined based on the column used (8 mL and 24 mL respectively for our Superdex 200 Increase). The numerical values found in **Equation 3.2** were determined by observing the elution volumes of several known MW proteins (ß-amylase, alcohol dehydrogenase, BSA, carbonic anhydrase, and cytochrome c) that were used to calibrate the Superdex 200 Increase column.

Due to the similar MW of the p85-BH (~24 kDa) and Rab5 (~24 kDa) determination of which proteins were present in the various fractions was done using Western blot analysis as described above.

3.2.6.2 Oligomerization determination of recombinant full-length human p85 and mutants

In order to determine potential oligomeric states of our p85 proteins, and the changes that mutations may have on these arrangements, we used SEC. Using our Superdex 200 Increase column connected to an ÄKTA Purifier unit 0.5 mL of protein at a concentration of 0.7 mg/mL was loaded. This protein underwent SEC using the same buffer and conditions as described above. A chromatogram was recorded based on the absorption at 280 nm for each fraction.

In order to confirm the MW determined by SEC and verify the oligomerization of the proteins, we used Native PAGE. Samples of the SEC protein input and the peak fraction were loaded onto Native PAGE 4-16% Bis-Tris gradient Gels (Life Technologies) and were electrophoresed at 150 V for 95 mins. Protein was fixed in the gels with addition of destain solution and microwaved for 45 seconds, then incubated at room temperature with agitation for 30 minutes. The gels were treated with Coomassie blue stain to visualize the protein, microwaved and incubated as above. To remove unbound Coomassie blue stain from the gels destain was added, gels were microwaved as above, and incubated at room temperature with agitation until protein bands were clearly visible. Gel images were recorded using a ChemiDoc imaging system (Bio-Rad).

3.2.7 Multi-angle light scattering

Multi-angle light scattering (MALS) experiments were performed using the MALS-RI (Wyatt Technology) operated by the PCCF, with training and experimental assistance by Dr. Michal Boniecki. The MALS-RI was connected with the PCCF ÄKTA Purifier to allow for SEC-MALS tandem experiments. Protein solutions of 4 mg/mL, 2 mg/mL, 1 mg/mL, 0.7 mg/mL or 0.5 mg/mL were injected onto the Superdex 200 Increase (dimensions provided above) column using a buffer of PBS with 250 mM NaCl, a flow rate of 0.5 mL/min, and a pressure limit of 4.00 MPa. Data analysis and processing, using the mean square radius of the proteins present across the various elutions to determine their corresponding MW, was performed using ASTRA 6.1.2.84 software.

3.2.8 Phosphatidylinositol phosphate lipid strip analysis

PIP lipid strips were used to test protein fragments for the ability to bind various lipids that were immobilized on nitrocellulose. The PIP strips are spotted with 15 different lipids (lysophosphatidic acid; lysophosphocholine; sphingosine-1-phosphate; PI; PI3P; PI4P; PI5P; $PI3,4P_2$; $PI3,5P_2$; $PI4,5P_2$; $PI3,4,5P_3$; phosphatidylethanolamine; phosphatidylcholine; phosphatidic acid; phosphatidylserine) at 100 pmol per lipid spot. PIP strips were incubated in blocking buffer (3% [w/v] fatty acid free BSA [Sigma-Aldrich, Cat#A6003], 10 mM Tris pH 8.0, 150 mM NaCl, 0.01% Tween-20) for 1 hour at room temperature with agitation. All incubations for PIP strips were performed in the dark. The PIP strips were incubated for 16 hours at 4°C with

the protein fragment of interest diluted in blocking buffer. PIP strips were washed 6 times, each wash lasting 5 minutes at room temperature, in PBST. PIP strip were probed with anti-p85 BH primary antibody (**Table 3.4**) in blocking buffer for 1 hour at room temperature with agitation. The PIP strips were washed as described above. PIP strips were incubated in IRDYE 680 anti-rabbit secondary antibody (**Table 3.4**) in blocking buffer for 90 mins at room temperature with agitation. The PIP strips were washed as described above. Protein bound to the PIP strips were detected and visualized using a LI-COR ODYSSEY infrared scanner and analyzed with the ODYSSEY V3.0 software.

4.0 Results

4.1 Purification and crystallization trials for GST-tagged bovine p85 protein fragments

The primary objectives of my research were to **1)** obtain crystal structure data for the SH3 and BH domains of the bovine p85 protein wild-type, **2)** obtain crystal structure data for the p85 BH domain containing cancer-associated point mutations, and **3)** obtain crystal structure data for the p85 BH domain containing mutations to residues important for interaction with the PTEN protein. To accomplish these objectives we generated and purified GST-tagged protein fragments of varying amino acid length as well as containing various cancer-associated or engineered point mutations. Cancer-associated mutations were identified through bioinformatics analysis of cancerous tissues against wild-type matched tissues (Cheung *et al.*, 2011; Ross *et al.*, 2013). Initial crystallization trials were performed using the automated Arts Robbins Instrument GRYPHON Robot for rapid screening of commercially available sparse matrix screen crystallization condition suites. Promising conditions were used as the basis of manually prepared optimization screens that utilized the hanging-drop vapour diffusion method of crystal growth. Crystals were taken to the CLS for data collection using the beamlines of the Canadian Macromolecular Crystallography Facility. Diffraction data was processed on site using HKL2000 software, and crystal structures were refined and processed using PHENIX and COOT software. Images were generated using PyMOL.

A sequence alignment of the SH3 and BH domains of the p85 human and bovine proteins is provided in **Figure 4.1** generated using MacVector version 12.5.0, indicating locations of cancer-associated point mutations and residues where mutations affect p85 binding to PTEN.

A summary of the progress made for the various bovine p85 fragments can be found in **Table 4.1**.

4.1.1 Crystallization of p85 fragments containing SH3 and BH domains, and the BH domain alone

Initial crystallization experiments were performed on bovine p85 protein fragments containing amino acids 1-310 or 1-319. Small rectangular prism-shaped crystals, commonly forming in clusters, were obtained for both fragments using 0.1 M Sodium Cacodylate pH 6.0-6.3, 1.5 M Li_2SO_4, and 4% (w/v) glycerol. Manipulation of the p85 (1-310) crystals resulted in

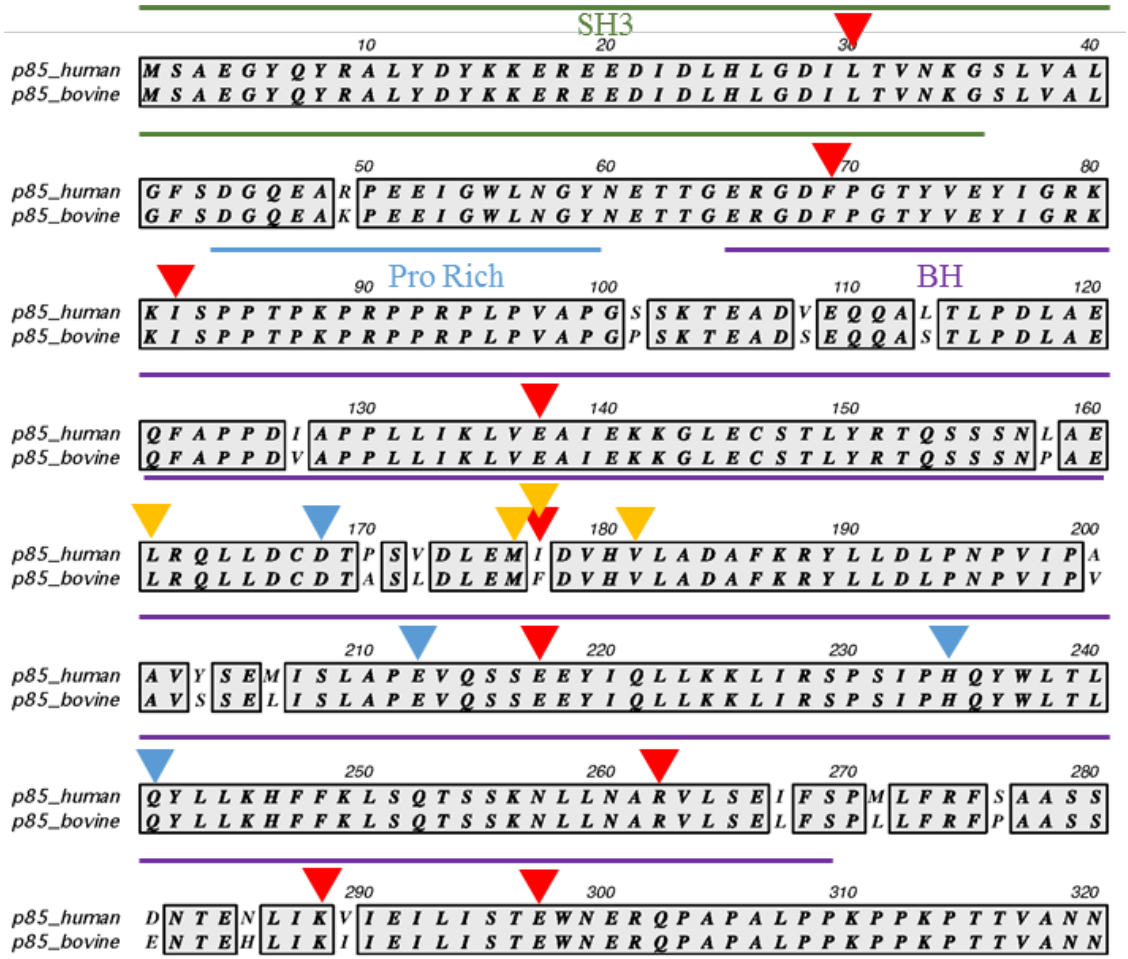

Figure 4.1 Sequence alignment of human and bovine p85 N-terminal domains. Alignment generated using MacVector version 12.5.0 displaying the first 320 amino acids for the human and bovine p85 proteins. The SH3 domain is labeled in green and the BH domain is labelled in purple. The proline rich region important for SH3 domain based p85 homodimerization is labelled in blue. Residues that form the BH domain homodimerization interface are indicated using yellow triangles. Cancer-associated mutations sites are indicated using red triangles. Residues shown to reduce PTEN binding are indicated using blue triangles.

the crystals crumbling so further optimization was only performed using p85 (1-319). Initial p85 (1-319) crystals reached maximum dimensions of approximately 100 µm by 50 µm by 50 µm after 7-10 days of incubation at room temperature. These crystals were used for crystal seeding, and following an additional 7 days of incubation they reached final dimensions of approximately 500 µm by 100 µm by 100 µm. Crystals are shown in **Figure 4.2 A**. The analyzed crystal had unit cell dimensions of 83.92, 92, 50, 92.98, 90, 90, 90; had $P2_12_12_1$ symmetry, and diffracted to 2.70 Å.

Table 4.1: Summary of crystallization results for bovine p85 fragments

Protein	Plasmid Made	Protein Purification Optimized	Crystal Trial Progress	Crystal Resolution (Å)	R-merge (Highest resolution shell in brackets)
p85 (105-319)	Y	Y	Y	2.45	8.5 (60.2)
p85 (105-319) [p85-BH] + PI4P				2.25	9.4 (65.9)
p85 (78-319) + $PI4,5P_2$	Y	Y	Y	3.1	13.5 (73.1)
p85-BH-I177N	Y	Y	In Progress		
p85-BH-E137K	Y	Y	Y	2.40	7.0 (45.3)
p85-BH-E217K	Y	Y	Y	2.20	6.0 (42.0)
p85-BH-R262T	Y	Y	Y	2.70	8.9 (50.1)
p85-BH-K288Q	Y	Y	N		
p85-BH-E297K	Y	Y	Y	2.30	6.9 (42.6)
p85-BH-K224-5E	Y	Y	Y		
p85-BH-R228E	Y	Y	Y	2.40	8.5 (60.1)
p85-BH-H234D	Y	Y	Y		
p85-BH-Q241D	Y	Y	Y		

Amino acids 113-297 of p85 were visible forming a homodimer within the solved crystal structure. This corresponded to the BH domain dimer visualized in the human p85 BH domain structure previously solved (Musacchio *et al.*, 1996). The SH3 domain of the protein was not visible in the structure. The crystal structure determined is shown in **Figure 4.2 B**.

Within the observed structure a pair of highly coordinated SO_4 ions from the crystallization solution could be seen near residues K224, R228, H234, W237, and Q241. As the conditions used to crystallize the human p85 BH domain were 3.6 M sodium formate, pH 5.0, there were no SO_4 molecules visible within their structure. The highly coordinated nature of the

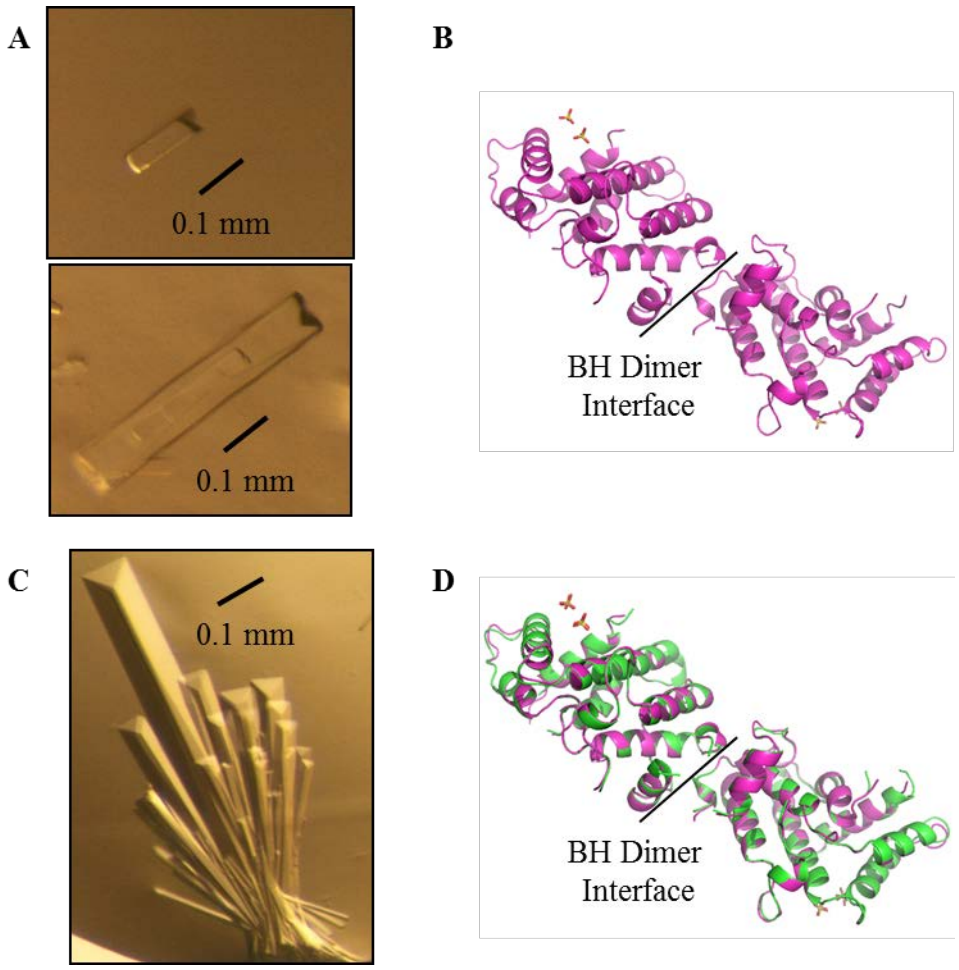

Figure 4.2 Crystals and crystal structures for bovine p85 (1-319) and p85 (105-319). A. Initial protein crystals obtained for the bovine p85 (1-319) protein fragment were small (top) and used as seed crystals to generate the larger crystals used for X-ray diffraction data collection (bottom). **B.** Crystal structure with a resolution of 2.70 Å obtained from p85 (1-319) crystals. A homodimer of BH domains were visible containing residues 113-297 for both components of the dimer. Residues corresponding to the SH3 domain did not have solvable electron densities. **C.** Example cluster of protein crystals obtained for the p85 (105-319) protein fragment. **D.** Overlay of the p85 (1-319) crystal structure (magenta) with the crystal structure solved to 2.40 Å for the p85 (105-319) protein fragment (green).

previously unseen interaction suggests that the region is potentially a novel binding pocket within the p85 BH domain.

Due to the absence of the SH3 domain in our obtained structure, and the presence of this potential novel binding pocket, efforts of future crystallization experiments were focused on the bovine p85 BH domain exclusively. To this end we used a p85 fragment containing amino acids 105-319 for further crystallization experiments.

Crystals of p85 (105-319) were grown in 0.1 M Sodium Cacodylate pH 6.0, 1.5 M Li_2SO_4, and 4% (w/v) glycerol. These crystals formed as triangular prisms, often in clusters, and reached maximum dimensions after approximately 7 days of incubation. An example cluster of crystals is shown in **Figure 4.2 C**. The analyzed crystal had unit cell dimensions of 85.14, 91.83, 93.27, 90, 90, 90; had $P2_12_12_1$ symmetry, and diffracted to 2.45 Å.

The solved crystal structure also appeared as a dimer of BH domains, and the potential novel binding pocket observed in the crystal structure from p85 (1-319) was present in p85 (105-319) structure as well. A comparison of the p85 (1-319) and p85 (105-319) crystal structures is shown in **Figure 4.2 D**.

The highest resolution structure of the bovine p85 BH domain obtained was using the p85 (105-319) protein fragment and the crystallization conditions 0.1 M Sodium Cacodylate pH 6.0, 1.5 M Li_2SO_4, 4% (w/v) glycerol, and 10 mM short chain soluble 8 carbon PI4P lipid. The crystal analyzed had unit cell dimensions of 85.83, 91.74, 93.78, 90, 90, 90; had $P2_12_12_1$ symmetry, and diffracted to a resolution of 2.25 Å. Residues 169-171 and 277-279 did not have visible electron density in either chain, and Pro 276 did not have visible electron density in Chain A. As this determined structure had the highest resolution collected we will refer to this structure determined as p85-BH and all other structures obtained were compared to this structure. The determined structure of p85-BH and a closer examination of the potential novel binding pocket observed are shown in **Figure 4.3**.

Data collection and refinement statistics for p85 (1-319), p85 (105-319), and p85-BH are provided in **Table 4.2**.

4.1.2 Crystallization of p85-BH containing cancer-associated point mutations

Having obtained the crystal structure for the bovine p85 BH domain our next step was to observe the structural changes caused by several human cancer-associated point mutations (E137K, I177N, E217K, R262T, K288Q, and E297K) (Cheung *et al.*, 2011; Ross *et al.*, 2013). In bovine p85 amino acid 177 is a phenylalanine in place of an isoleucine found in the human p85.

The p85-BH-F177N mutant crystal condition optimization is still ongoing. Currently the most promising condition obtained is 0.1 M Tris pH 7.0, 2.0 M $(NH_4)_2SO_4$, 0.2 M Li_2SO_4, leading to the formation of tiny crystals lacking in the smooth sides and defined corners that normally

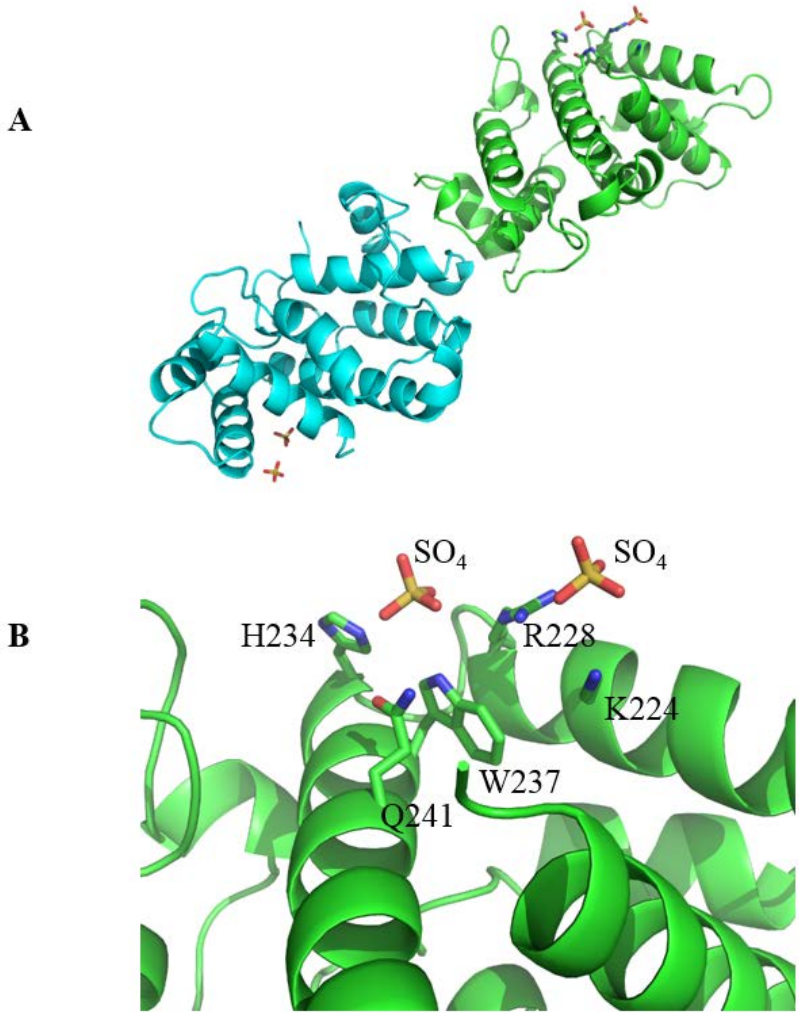

Figure 4.3 Crystal structure of p85-BH to 2.25 Å resolution highlighting residues that form the potential novel binding pocket. **A.** 2.25 Å resolution crystal structure obtained using p85-BH protein fragment treated with cryoprotectant containing 8 carbon chain PI4P. The two BH domains present in the homodimer are differentially coloured for easier differentiation. **B.** Close up view of the potential novel binding pocket observed in the p85-BH structure. Sulfate molecules and the sidechains of amino acids involved in their binding (K224, R228, H234, W237, and Q241) are shown in stick representation.

suggest crystals that may diffract well. None of the currently obtained crystals were suitable for X-ray diffraction data collection.

The p85-BH-K288Q fragment has been generated and produced in bacterial expression systems, but crystal condition trials have not been performed on this mutant.

For p85-BH-E137K, p85-BH-E217K, p85-BH-R262T, and p85-BH-E297K we have successfully crystallized, collected diffraction data, and determined their crystal structures. An

Table 4.2 Data collection and refinement statistics for p85 (1-319), p85 (105-319) and p85-BH

	p85 (1-319)	p85 (105-319)	p85-BH
Beamline	CMCF-ID	CMCF-BM	CMCF-ID
Resolution range (Å)	46.61 – 2.698 (2.795 – 2.698)	35.68 – 2.449 (2.537 – 2.449)	46.89-2.248 (2.329-2.248)
Space group	$P2_12_12_1$	$P2_12_12_1$	$P2_12_12_1$
Unit cell	84.798 92.505 93.222 90 90 90	85.142 91.826 93.274 90 90 90	85.825 91.737 93.778 90 90 90
Total reflections	153810	203440	264033
Unique reflections	20779 (2052)	27520 (2676)	35590 (3471)
Multiplicity	7.4 (7.5)	7.4 (7.5)	7.4 (7.2)
Completeness (%)	99.97 (99.66)	99.94 (99.37)	99.13 (97.86)
Mean I/sigma(I)	32.5 (4.74)	19.95 (3.68)	24.23 (3.00)
Wilson B-factor	52.36	40.36	33.63
R-merge	11.3 (53.4)	8.5 (60.2)	9.4 (63.8)
R-work	0.2085 (0.2611)	0.1955 (0.2412)	0.2011 (0.2239)
R-free	0.2424 (0.3229)	0.2363 (0.2945)	0.2263 (0.2517)
Number of non-hydrogen atoms	2769	2829	2924
macromolecules	2745	2804	2829
non-water solvent	20	20	20
water	4	5	75
Protein residues	349	360	358
RMS (bonds)	0.006	0.003	0.002
RMS (angles)	1.00	0.67	0.62
Ramachandran favoured (%)	94.26	92.73	93.57
Ramachandran outliers (%)	2.42	3.78	3.22
Rotamer outliers (%)	5.54	1.61	0.00
Clashscore	4.86	3.89	1.22
Average B-factor	51.17	46.40	44.25
macromolecules	50.68	46.04	44.03
non-water solvent	119.43	99.42	93.71
solvent	41.20	38.97	39.57

Statistics for highest-resolution shell are shown in parentheses

overlay of the crystal structures for p85-BH and the above mutant structures is shown in **Figure 4.4**.

The p85-BH-E137K crystals were grown in 0.1 M Sodium Cacodylate pH 6.0, 1.4 M Li_2SO_4, and 6% (w/v) glycerol. The analyzed crystal had unit cell dimensions of 85.36, 91.92, 93.27, 90, 90, 90; had $P2_12_12_1$ symmetry, and diffracted to a resolution of 2.40 Å. The p85-BH-

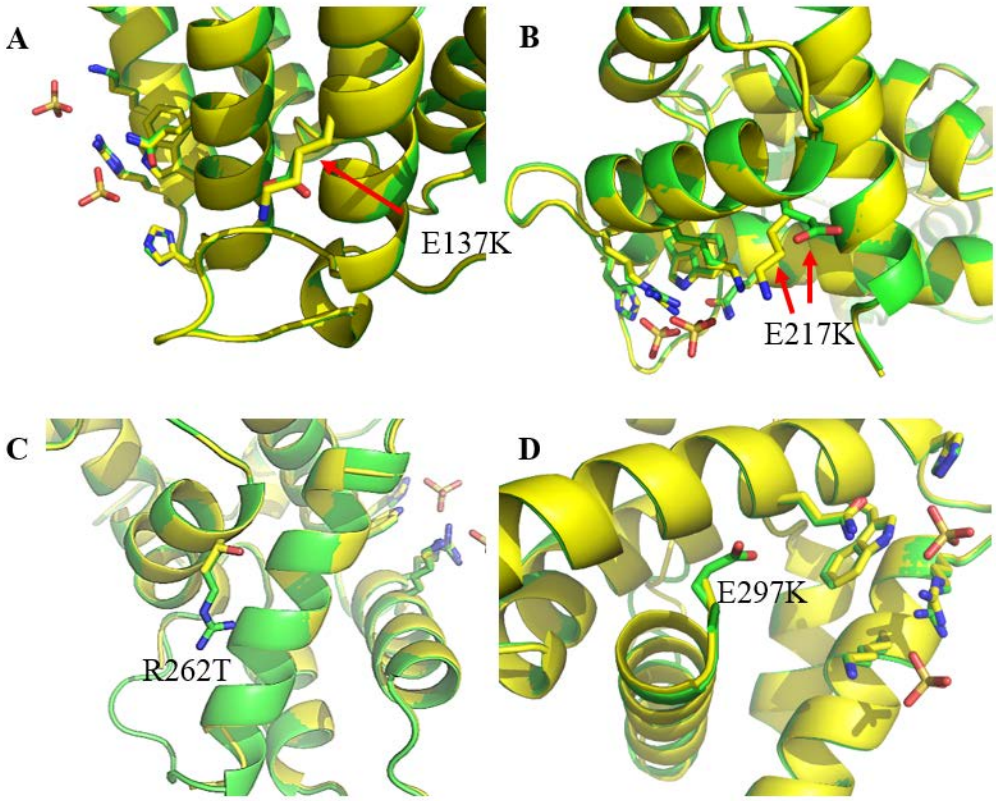

Figure 4.4 Overlays of the crystal structures for p85-BH wild-type and cancer-associated point mutants. Overlays of the crystal structures for p85-BH wild-type (green, 2.25 Å) and cancer-associated point mutants (yellow). Mutant sidechains and potential novel binding pocket residues are shown in stick representation. **A.** E137K mutant (2.40 Å). **B.** E217K mutant (2.20 Å). **C.** R262T mutant (2.70 Å). **D.** E297K mutant (2.30 Å). Lack of density for the K297 sidechain prevented inclusion of the sidechain, and a placeholder Ala replaces it in the structure.

E217K crystals were grown in 0.1 M Sodium Cacodylate pH 6.0, 1.3 M Li_2SO_4, and 6% (w/v) glycerol. The analyzed crystal had unit cell dimensions of 85.47, 91.65, 93.56, 90, 90, 90; had $P2_12_12_1$ symmetry, and diffracted to a resolution of 2.20 Å. The p85-BH-R262T crystals were grown in 0.1 M Sodium Cacodylate pH 6.2, 1.5 M Li_2SO_4, and 6% (w/v) glycerol which resulted in large numbers of very small crystals forming, with select crystals transferred to fresh crystallization drops as seed crystals to obtain larger crystals for data collection. The larger crystal analyzed had unit cell dimensions of 85.45, 91.64, 93.57, 90, 90, 90; had $P2_12_12_1$ symmetry, and diffracted to a resolution of 2.70 Å. The p85-BH-E297K crystals were grown in 0.1 M Sodium Cacodylate pH 6.2, 1.4 M Li_2SO_4, and 6% (w/v) glycerol which resulted in large numbers of very small crystals forming, with select crystals transferred to fresh crystallization

drops as seed crystals to obtain larger crystals for data collection. The larger crystal analyzed had unit cell dimensions of 85.64, 91.26, 93.32, 90, 90, 90; had $P2_12_12_1$ symmetry, and diffracted to a resolution of 2.30 Å. The K297 sidechain lacked electron density to be modeled, likely due to its highly flexible nature and the residue being present near the edge of our resolved structure, so an Ala residue serves as its placeholder. All four mutants lacked visible electron densities for residues 167-171 in both chains, and lacked density for residues 277-279 in Chain B. The p85-BH-E137K also lacked residue residues 276 and 280 in Chain B. The p85-BH-217K also lacked residues 167 and 280 in Chain B. The p85-BH-R262T also lacked residues 276-280 in Chain A. The p85-BH-E297K also lacked residue 298 at the terminus of Chain A.

No major structural differences were observed between these mutants and the wild-type protein.

Data collection and refinement statistics for p85-BH mutants are provided in **Table 4.3**.

4.1.3 Crystallization of p85-BH containing engineered point mutations

Having observed a potential novel binding pocket in the p85 BH domain, we generated a series of engineered point mutations to determine their structural effect on this region and the BH domain as a whole. The mutants p85-BH-K224E-K225E (p85-BH-K224-5E), p85-BH-R228E, p85-BH-H234D, and p85-BH-Q241D were generated and crystallized.

The p85-BH-K224-5E crystals were grown in 0.1 M Sodium Cacodylate pH 6.0, 1.6 M Li_2SO_4, and 4% (w/v) glycerol. X-ray diffraction data was not collected for these crystals.

The p85-BH-R228E crystals were grown in 0.1 M Sodium Cacodylate pH 6.0, 1.5 M Li_2SO_4, and 4% (w/v) glycerol. The crystal analyzed had unit cell dimensions of 85.19, 92.70, 93.12, 90, 90, 90; had $P2_12_12_1$ symmetry, and diffracted to a resolution of 2.4 Å. Visible densities were not present for residues 168-171 for both chains and residues 277-279 in Chain B. In this crystal structure one of the SO_4 ions clearly visible in the other structures was absent, and the remaining SO_4 ion reoriented itself within the pocket region. An overlay of the p85-BH and p85-BH-R228E crystal structures of the potential binding pocket region is shown in **Figure 4.5**. No other major structural differences were observed.

The p85-BH-H234D crystals were grown in 0.1 M Sodium Cacodylate pH 6.0, 1.5 M Li_2SO_4, and 4% (w/v) glycerol. These conditions formed small crystals that were transferred to fresh crystallization drops as seed crystals to obtain larger crystals for data collection. These

Table 4.3 Data collection and refinement statistics for p85-BH cancer-associated mutants

	p85-BH E137K	**p85-BH E217K**	**p85-BH R262T**	**p85-BH E297K**
Beamline	CMCF-BM	CMCF-BM	CMCF-BM	CMCMF-BM
Resolution range (Å)	35.76 - 2.407 (2.493 – 2.407)	35.79 – 2.203 (2.282 – 2.203)	35.8 – 2.7 (2.796 – 2.7)	35.8 – 2.301 (2.384 – 2.301)
Space group	$P2_12_12_1$	$P2_12_12_1$	$P2_12_12_1$	$P2_12_12_1$
Unit cell	85.364 91.924 93.274 90 90 90	85.474 91.647 93.556 90 90 90	85.449 91.637 93.574 90 90 90	85.643 91.26 93.324 90 90 90
Total reflections	214849	280322	153261	244247
Unique reflections	28760 (2716)	37651 (3647)	20646 (2012)	33018 (3189)
Multiplicity	7.5 (7.6)	7.4 (7.5)	7.4 (7.5)	7.4 (7.5)
Completeness (%)	98.88 (95.50)	99.62 (98.35)	99.35 (98.87)	99.80 (98.03)
Mean I/sigma(I)	23.65 (5.51)	24.43 (5.37)	19.91 (4.65)	22.45 (4.72)
Wilson B-factor	35.79	34.85	40.94	34.84
R-merge	7.0 (45.3)	6.0 (42.0)	8.9 (50.1)	6.9 (42.6)
R-work	0.2133 (0.2472)	0.2123 (0.2492)	0.2003 (0.2263)	0.2150 (0.2388)
R-free	0.2509 (0.2892)	0.2433 (0.2888)	0.2427 (0.2798)	0.2542 (0.3232)
Number of non-hydrogen atoms	2858	2907	2840	2877
macromolecules	2802	2812	2790	2808
non-water solvent	20	20	20	15
water	36	75	30	54
Protein residues	358	358	355	358
RMS (bonds)	0.026	0.004	0.003	0.004
RMS (angles)	1.56	0.78	0.69	0.87
Ramachandran favoured (%)	91.18	92.11	94.66	92.69
Ramachandran outliers (%)	3.82	3.22	2.97	4.39
Rotamer outliers (%)	0.00	0.64	0.63	0.00
Clashscore	6.53	4.91	2.30	6.35
Average B-factor	41.59	42.61	43.16	41.76
macromolecules	41.35	42.41	42.90	41.59
non-water solvent	87.18	84.47	92.74	91.63
solvent	34.49	38.99	34.36	36.86

Statistics for highest resolution shell are shown in parenthesis

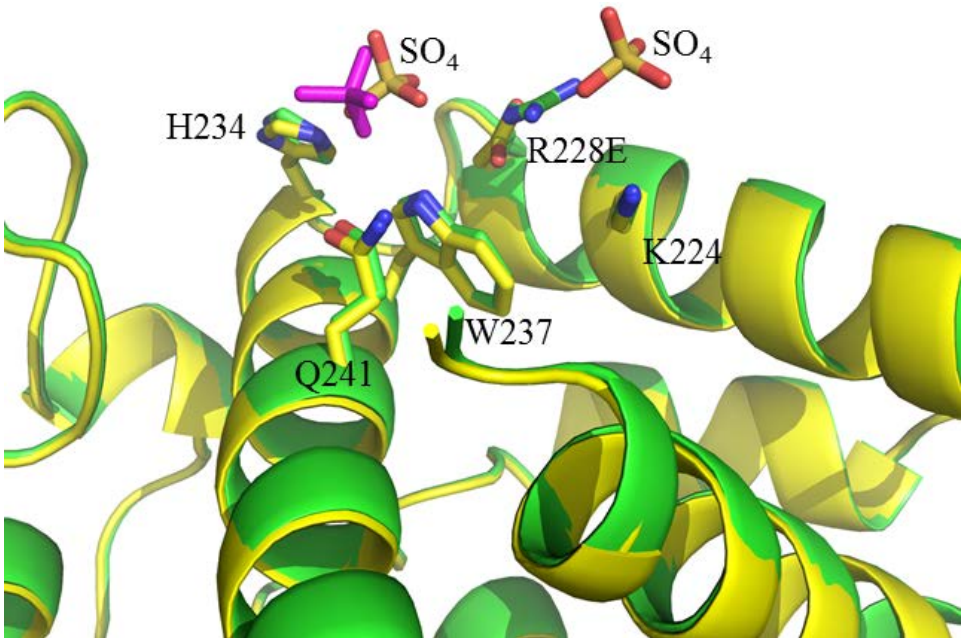

Figure 4.5 Potential binding pocket comparison between p85-BH and p85-BH-R228E. Overlay of the potential binding pocket region of the p85-BH wild-type (green, 2.25 Å) and p85-BH-R228E engineered mutant (yellow, 2.40 Å). Sidechains of pocket residues and SO_4 molecules are shown in stick representation, with the SO_4 present in the p85-BH-R228E coloured magenta for differentiation.

crystals only diffracted well across a 10° range of angles within the X-ray beam, preventing us from collecting enough X-ray diffraction data to solve its structure.

The p85-BH-Q241D crystals were grown in 0.1 M Sodium Cacodylate pH 6.0, 1.7 M Li_2SO_4, and 4% (w/v) glycerol. Diffraction data was not collected for these crystals.

Data collection and refinement statistics for p85-BH R228E are shown in **Table 4.4**.

4.1.4 Crystallization with addition of nucleotide, phosphoamino acids, or phospholipids

In order to identify physiological binding partners for the potential binding pocket observed we treated crystals with cryoprotectant solutions containing various mixtures of nucleotide, phosphoamino acids, or phospholipids, immediately prior to X-ray diffraction data collection. These phosphate containing compounds were chosen due to the structural similarity between PO_4 and the SO_4 ions observed within our crystal structures.

Structures for SO_4, cacodylate, PO_4, and the additives used for crystallization trials are shown in **Figure 4.6**.

Table 4.4 Data collection and refinement statistics for p85-BH R228E

Beamline	CMCF-ID
Resolution range (Å)	46.56-2.40 (2.44-2.40)
Space group	$P2_12_12_1$
Unit cell	85.187 92.697 93.117 90 90 90
Total reflections	217767
Unique reflections	29393 (1454)
Multiplicity	7.4 (7.5)
Completeness (%)	99.8 (99.8)
Mean I/sigma(I)	33.0 (4.84)
Wilson B-factor	40.39
R-merge	8.5 (60.1)
R-work	0.2073 (0.2368)
R-free	0.2287 (0.2853)
Number of non-hydrogen atoms	2850
macromolecules	2801
non-water solvent	10
solvent	39
Protein residues	360
RMS (bonds)	0.006
RMS (angles)	1.54
Ramachandran favoured (%)	92.73
Ramachandran outliers (%)	3.20
Rotamer outliers (%)	0.32
Clashscore	4.27
Average B-factor	49.37
macromolecules	49.03
non-water solvent	176.68
solvent	41.37

Statistics for highest resolution shell are shown in parenthesis

To test for binding of these additives crystals of p85-BH were treated with cryoprotectant solution containing either: 32 mM total nucleotides ATP, GTP and GppCp; 32 mM total phosphoamino acids pSer, pThr, and pTyr; or 12 mM total inositol lipid head groups inositol 1,3-bisphosphate, inositol 1,4-bisphosphate, inositol 1,5-bisphosphate, and inositol 1,3,5-trisphosphate as phospholipid representatives. Crystals were successfully obtained and X-ray diffraction data collected for all three additive soak conditions, and structures determined.

There were no electron densities present within any of the solved structures to suggest the presence of bound additives, but the high concentrations of SO_4 ions present in the crystallization solution may have prevented binding of the additives, which were present at much lower concentration.

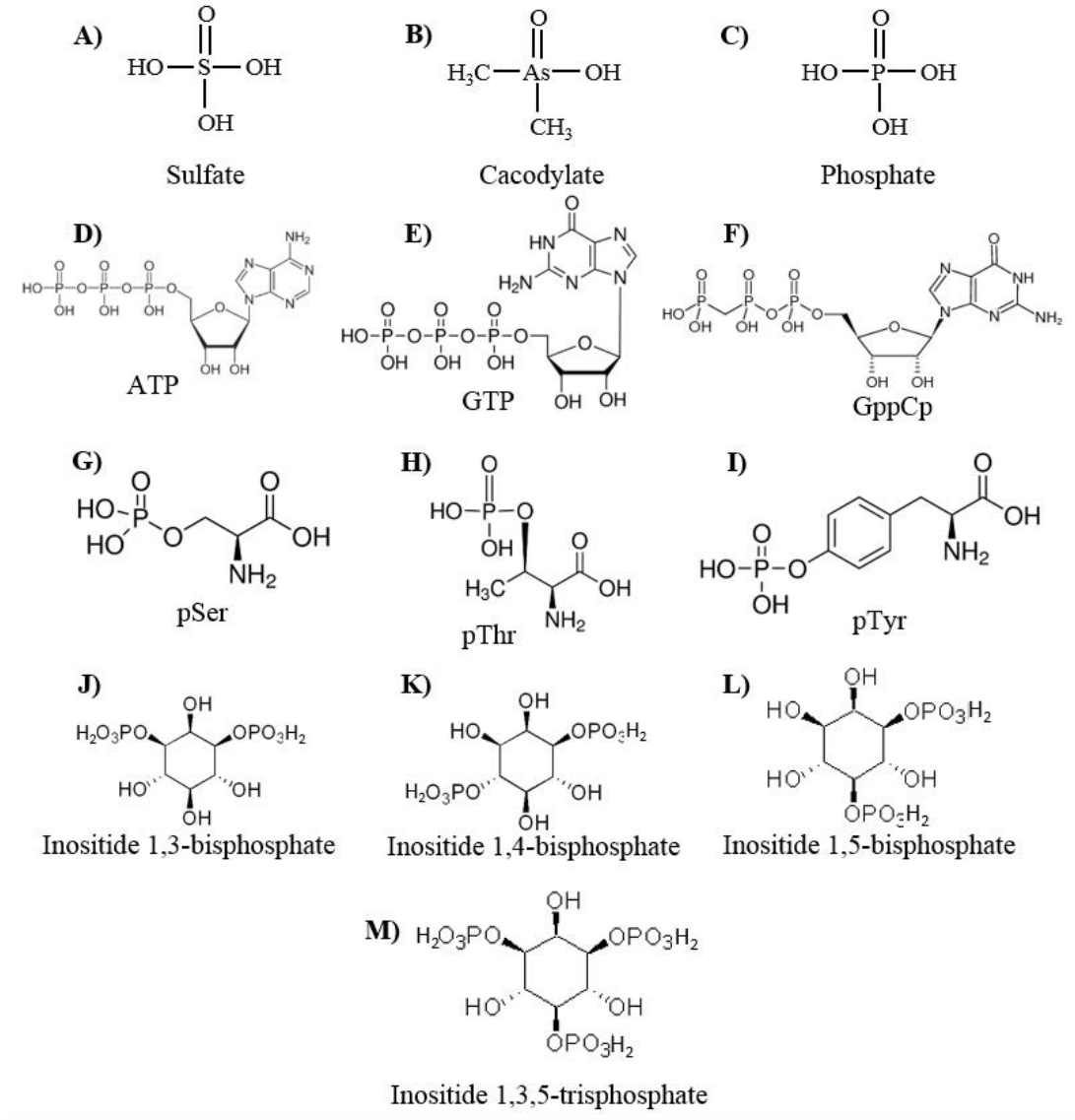

Figure 4.6 Structures of additives used in p85 crystallization solutions. Structures of sulfate **(A)** and cacodylate **(B)** present in our crystallization solution for all solved structures, with phosphate **(C)** for comparison of structural similarity. Other structures belong to nucleotides (**D-F**), phosphoamino acids (**G-I**), and phosphorylated inositol lipid head groups (**J-M**) used for additive cocktails to test binding of compounds with p85 protein. Structures obtained from www.sigmaaldrich.com **(D, E, G-I),** www.jenabiosciences.com **(F),** or www.echelon-inc.com **(J-M).**

Due to the role of the p85 protein in the PI3K/PTEN pathway we also treated p85-BH crystals with 10 mM individual short chain soluble 8 carbon PIP lipids. We hoped that the addition of the 8 carbon tail to the lipid head groups would increase the likelihood of the lipids binding despite the high SO_4 ion concentration present.

Structures of the 8 carbon tail PIP lipids investigated are shown in **Figure 4.7**.

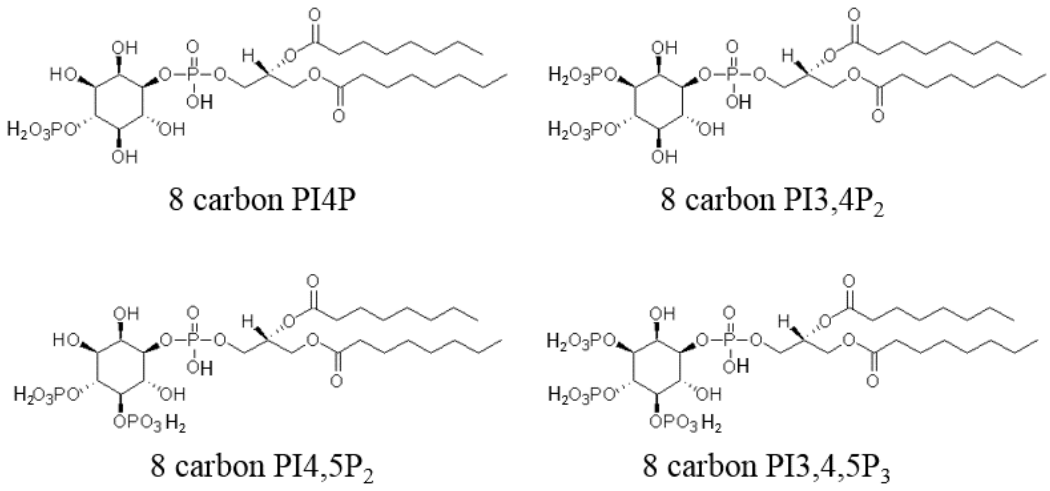

Figure 4.7 Structures of 8 carbon PIP lipids added to p85 crystallization solutions. Structures of short chain lipids added to cryoprotectant solutions prior to collection of X-ray diffraction data. Structures were obtained from www.echelon-inc.com

Crystals were successfully obtained for all four soluble 8 carbon PIP lipids pursued: PI4P, $PI3,4P_2$, $PI4,5P_2$, and $PI3,4,5P_3$. X-ray diffraction data was collected and crystal structures determined for each lipid soak and crystal structures were determined. For all four of these crystal structures there were no increased electron densities to suggest the presence of bound lipid. Once again the high concentrations of SO_4 ions may have out competed any binding that may have otherwise occurred.

4.1.5 Observations of C146 in the p85-BH protein structure

Within our p85-BH structure we noticed a region of extra electron density between amino acids C146 and H180. Based on the surrounding structure and allowed conformations of peptide bonds and sidechains C146 and H180 were unable to satisfactorily fill this excess density. We therefore began looking for explanations to this excess density.

To this end we examined possible post-translational modifications of the cysteine residue that would explain the observed density. In *Coot* software the C146 residue was replaced with the various oxidation states of cysteine; sulfenic acid (-SOH), sulfinic acid ($-SO_2H$), and sulfonic acid ($-SO_3H$). We also replaced them with the nitrosylated S-nitrosocysteine (-SNO). These modified structures then underwent batches of phenix.refine to determine the quality of their fit

within the experimentally determined electron density. To avoid bias of electron density fitting towards the selected modifications we also generated a structure in *Coot* by replacing Cys 146 with an Ala, and performed phenix.refine on this structure, allowing us to use the difference map from this analysis to validate our observations from the other modified structures. This allowed us to observe how well these various modifications fit within their own refined electron densities, as well as the difference density present from the Ala 146 refinement.

The initial unfilled electron density observed is shown in **Figure 4.8 A**. Electron difference density corresponding to the Ala 146 refinement, and the positioning of either Sulfenic Acid or S-nitrosocysteine at residue 146 are shown in **Figure 4.8 B-D**. The comparative electron densities observed with an S-nitrosocysteine positioned at residue 146 following structure refinement is shown in **Figure 4.8 E**.

By comparison of the various potential post-translational modifications applied to C146 in our structures, the S-nitrosocysteine showed the best correlation with the observed density differences. With the data available to us it is therefore most likely that the additional electron density detected between C146 and H180 corresponds to an S-nitrosocysteine residue.

Comparison of our p85-BH structures with the previously solved p85 BH domain structure (Musacchio *et al.*, 1996) shows good agreement between the orientations of residues within this region of the protein. However, in the structure by Musacchio *et al.* there is an unmodified cysteine residue at location 146. Without examination of their electron density data we are unable to know if any additional density were present around residue 146 in their structure to know if this residue frequently undergoes post-translational modification, or if our observed additional electron density present corresponds to an uncommon occurrence.

Based on these observations it will be important for future experiments to determine if nitrosylation of cysteine residues occurs under physiological conditions for the p85 protein, as such modifications can play important structural roles in stabilizing proteins or altering their activity.

4.1.6 Crystallization of p85 (78-319) in the presence of 8 carbon PI4,5P$_2$

To increase the available protein surface for potential binding partners to interact with we performed crystallization trials using a bovine p85 (78-319) protein fragment with 8 carbon PI4,5P$_2$ added to its crystallization buffer. We wished to see if the additional residues would

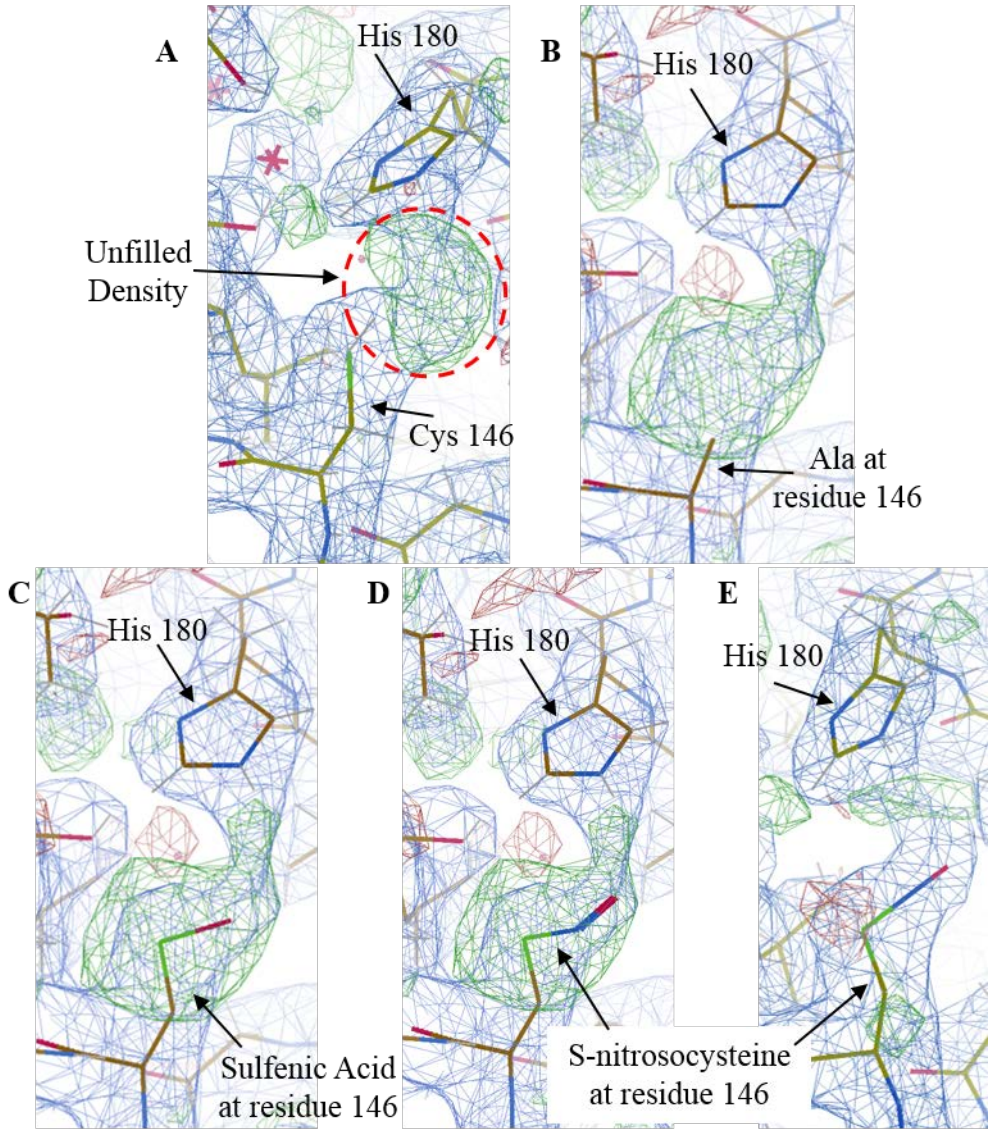

Figure 4.8 Examination of a modified cysteine at p85-BH residue 146. The region between residues C146 and H180 observed within our determined crystal structures visualized in *Coot*. Amino acids are shown as sticks, with the 2Fo-Fc electron density map shown as blue mesh contoured to 1.0 σ, and the electron density difference map shown as green and red mesh contoured to 3.0 σ. **A.** Unfilled density region observed in our p85-BH crystal structure. **B.** Electron density difference observed following replacing C146 with an Ala residue and performing phenix.refine. **C and D.** Sulfenic acid (**C**) or S-nitrosocysteine (**D**) positioned at residue 146 compared to the A146 electron density map**. E.** S-nitrosocysteine residue positioned at residue 146 positioned within electron density maps following phenix.refine.

improve the lipid binding in the presence of high SO_4 ion concentration in the crystallization solution.

Diffraction data was collected and the crystal had unit cell dimensions of 84.12, 91.56, 93.14, 90, 90, 90; had $P2_12_12_1$ symmetry and diffracted to a resolution of 2.75 Å.

Data collection and refinement statistics for p85 (78-319) with 8 carbon PI4,5P_2 are shown in **Table 4.5**.

Table 4.5 Data collection and refinement statistics for p85 (78-319) with 8 carbon PI4,5P_2

Beamline	CMCF-BM
Resolution range (Å)	46.57 – 2.75 (2.848 – 2.75)
Space group	$P2_12_12_1$
Unit cell	84.12 91.56 93.14 90 90 90
Total reflections	141928
Unique reflections	19249 (1889)
Multiplicity	7.4 (7.52)
Completeness (%)	99.70 (99.53)
Mean I/sigma(I)	22.6 (2.9)
Wilson B-factor	61.48
R-merge	7.8 (79.0)
R-work	0.2066 (0.2804)
R-free	0.2430 (0.3256)
Number of non-hydrogen atoms	2855
macromolecules	2813
non-water solvent	20
solvent	22
Protein residues	356
RMS (bonds)	0.003
RMS (angles)	0.81
Ramachandran favoured (%)	93.49
Ramachandran outliers (%)	3.25
Rotamer outliers (%)	0.63
Clashscore	4.20
Average B-factor	65.24
macromolecules	64.96
non-water solvent	117.78
solvent	52.19

Statistics for highest resolution shell are shown in parenthesis

Molecular replacement using our 2.25 Å resolution p85-BH structure was performed in order to locate our protein within the determined electron density. This was performed because the p85 (78-319) protein crystallized such that the BH domain dimer was oriented differently within the asymmetric unit. A comparison between the structure orientations of p85-BH and p85 (78-319) and an overlay of the two crystal structures are shown in **Figure 4.9**. Visible electron density was lacking for residues 168-171 and 277-279 in both Chains, as well as residue 280 in Chain A.

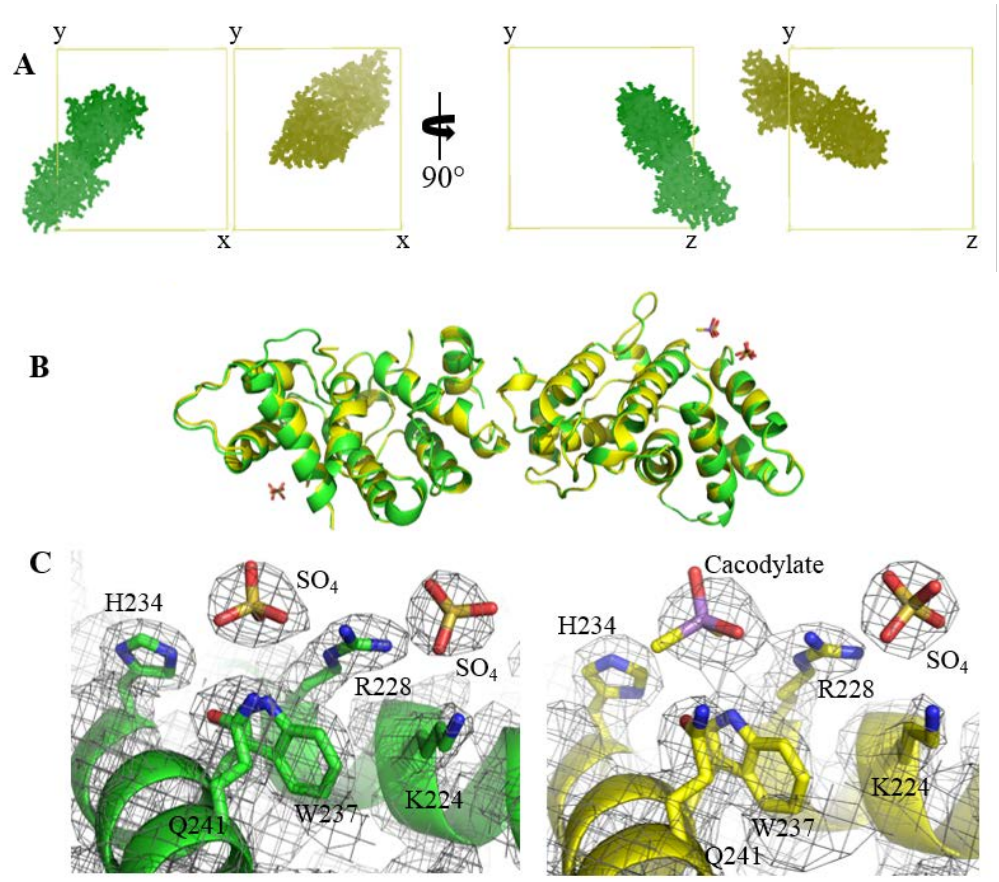

Figure 4.9 Comparison of p85-BH and p85 (78-319) crystal structures. Crystal structures of p85-BH to 2.25 Å (green) and p85 (78-319) to 2.75 Å (yellow). **A.** Comparison of the different orientations present within the unit cells of the p85-BH and p85 (78-319) crystals including a 90° rotation in *Coot*. Unit cell axes are labelled. **B.** Overlay of the crystal structures of p85-BH and p85 (78-319). Sulfate and cacodylate molecules are represented in stick format. **C.** Close up view of the potential binding pocket region with sidechains of involved residues, sulfate, and cacodylate in stick representation, and the 2Fo-Fc electron density map represented as a grey mesh and contoured to 1.0 σ.

Comparing the overlaid crystal structures of p85-BH and p85 (78-319) showed that the domain structure remained consistent between the two. The same residues of 113-297 were also visible between the two structures, no additional residues from the linker region were visible in the p85 (78-319) structure. There were no visible electron densities that would have corresponded to binding of the $PI4,5P_2$ to the p85 (78-319) structure. Of interest was an increase in the size of one of the electron densities present in the potential novel binding pocket. A cacodylate molecule, present within the crystallization buffer, fit well within this larger electron density region. The second density within this region remained consistent in its size. The potential binding pocket regions is shown with electron density map overlay in **Figure 4.9 C**.

4.2 Purification of PTEN (7-353, Δ286-309)

The p85 protein has previously been shown to interact with and stimulate the lipid phosphatase activity of the protein PTEN (Chagpar *et al.*, 2010; Rabinovsky *et al.*, 2009). Obtaining a crystal structure of the p85-BH:PTEN Crystal complex would better elucidate the residues involved in this interaction, and the mechanism of the catalytic stimulation. To pursue this we would need to generate quantities of PTEN Crystal suitable for complex formation and crystallization trials. We also generated a PTEN Crystal C124S catalytically dead mutant for these experiments.

Initial protein inductions of BL21-pGEX6P1-PTEN Crystal and PTEN Crystal C124S resulted in low protein yields that made pursuit of complex formation or co-crystallization experiments unfeasible. Due to these low protein yields we examined a variety of alternate growth conditions, to determine which resulted in the greatest protein yield.

Overnight incubations were performed at a temperature of 16 °C to slow the rate of PTEN induction with the intent of increasing total yields of soluble protein. We transformed Rosetta cells with expression plasmids for our protein of interest for use as our expression system. Rosetta cells contain plasmids that code for tRNAs for codons more frequently used for certain amino acids in eukaryotic proteins than bacterial proteins, which can improve expression of some eukaryotic proteins in bacteria. We also grew cultures in Hyper Broth in place of LB, with Hyper Broth containing a glucose supplement mixture to increase the available nutrients for bacteria growth to encourage larger bacterial yields.

Comparing results of cultures grown under combinations of the described conditions it was determined that growth using BL21 cells in Hyper Broth with our standard overnight incubation temperatures would be pursued for future growth. This combination resulted in substantial increases in total bacterial wet weight per litre (before ~4 g/L, altered conditions ~9 g/L) and a greater protein yield following harvesting.

For both individual batch protein purification and large scale ÄKTA Purifier Glutathione-Sepharose column purification the PTEN proteins suffered from extensive precipitation upon incubation with 3C Prescission Protease for cleavage of the GST-tag. During this 72 hour incubation at 4ºC, samples of the PTEN proteins that did not have 3C Prescission Protease also precipitated. These challenges were not resolved and attention was redirected to aspects of the project that were progressing well.

4.3 Size exclusion chromatography analysis of complex formation between bovine p85 fragments and Rab5

As the p85 protein has been shown to interact with Rab5 and stimulate the intrinsic GTPase activity of Rab5 (Chamberlain *et al.*, 2004) we wished to obtain structural information of this protein complex to better visualize the residues important for this interaction and catalytic function. In order to accomplish this we needed to purify a complex between the p85-BH domain and Rab5 so that we could prepare crystallization trials for the obtained complex.

Both p85-BH and Rab5 proteins were generated in BL21 cells as GST-tagged proteins, purifying these proteins by binding the GST-tag to Glutathione-Sepharose media and cleavage of the GST-tag. Protein concentrations were determined using NanoDrop analysis with concentrations checked via SDS-PAGE of the protein against known concentrations of BSA visualized with Coomassie Blue staining. Equimolar amounts of both proteins were mixed, incubated together at room temperature, and underwent SEC to separate protein complex formed.

Due to the similarity in MW between the p85-BH fragment (~24.15 kDa) and Rab5 (~23.66 kDa) identification of proteins present in the SEC fractions was determined using western blot analysis rather than Coomassie Blue stain gels. Differences were observed between Rab5 calculated concentrations using NanoDrop versus observed concentration based on Coomassie Blue stained gels loaded with known concentrations of BSA. Variation was also observed between batches for the fractions in which the Rab5 fragment eluted from the column, in some cases suggesting complex formation between p85-BH and Rab5, whereas others suggested co-elution of individual proteins without formation of complex. SEC chromatograms for different preparations of Rab5 mixed with p85-BH are shown in **Figure 4.10**. Western blots of elution fractions from these protein preparations are shown in **Figure 4.11**.

These results suggest that generation of a p85-BH:Rab5 complex may be possible, but that further optimizations will be required to obtain concentrations of the protein complex suitable for pursuing crystallization experiments. These were not pursued due to time constraints within my graduate studies program.

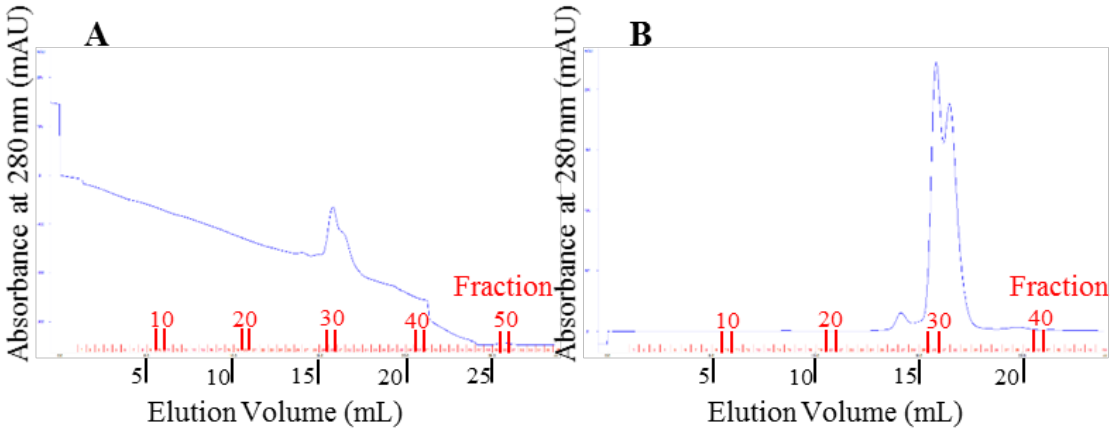

Figure 4.10 SEC chromatograms for p85-BH:Rab5 complex formation experiments. Purified samples of p85-BH and Rab5 proteins were mixed in equimolar amounts, incubated at room temperature, and underwent SEC to detect formation of a p85-BH:Rab5 protein complex. **A.** Chromatogram for SEC purification Experiment A. **B.** Chromatogram for SEC purification Experiment B.

4.4 Size exclusion chromatography and Native PAGE of recombinant full-length human p85 wild-type and mutants

In order to determine if mutations found in the p85 SH3 and BH domains alter protein oligomerization, we performed SEC coupled with Native PAGE. Identifying mutants that affect the protein oligomerization state might clarify some of the different crystallization behaviours observed for several of the p85-BH mutants.

To this end we analysed full-length human p85 protein wild-type, and containing cancer-associated or engineered point mutations. Cancer-associated mutations were located in the SH3 domain (L30F, F69L, I82F), or the BH domain (E137K, I177N, E217K, R262T, K288Q, or E297K) (Cheung *et al.*, 2011; Ross *et al.*, 2013). Engineered mutations examined (D168R, E212R, H234D, Q241D) were previously shown in our lab to decrease PTEN binding (**Figure 1.10**) and H234D and Q241D are both present within our potential novel binding pocket.

Samples of each protein at 0.70 mg/mL were loaded on the Superdex 200 SEC column connected to the ÄKTA Purifier, with their chromatograms recorded. Samples of the input and peak elution fraction based on the SEC chromatogram were loaded onto Native PAGE gels for analysis. The overlays of the various protein SEC chromatograms are shown in **Figure 4.12**. Corresponding Native PAGE gel images are shown in **Figure 4.13**. Elution volumes for each

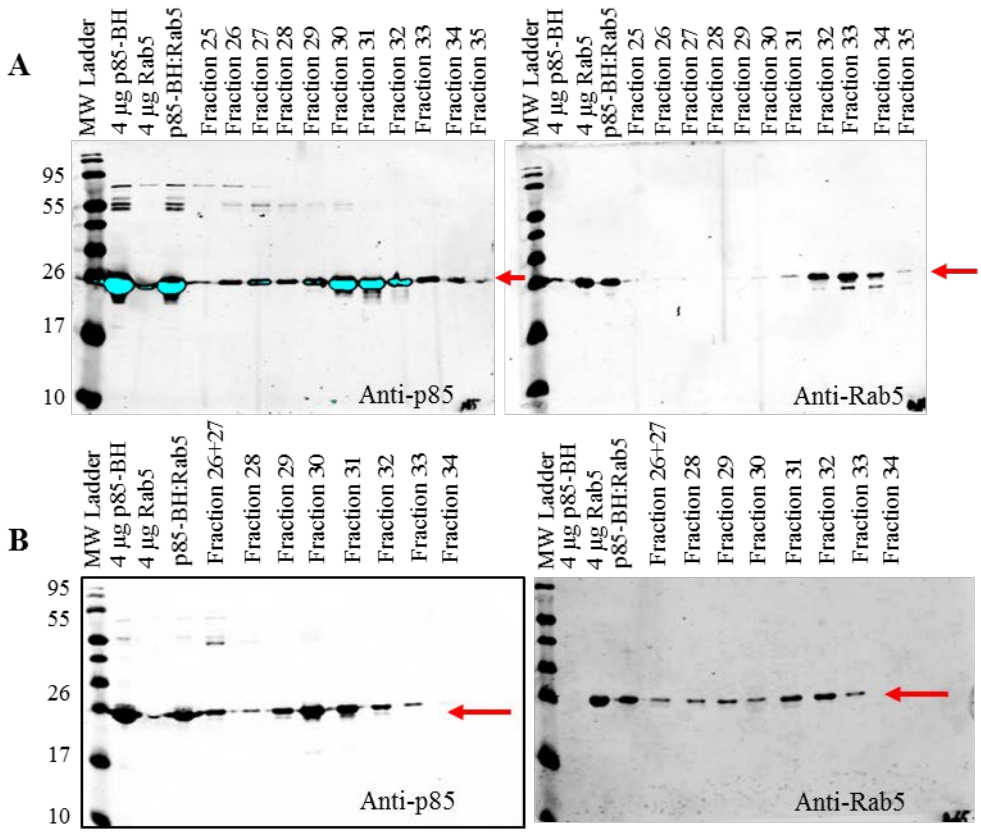

Figure 4.11 Western blot analysis of p85-BH and Rab5 complex formation SEC experiments. Equimolar quantities of p85-BH and Rab5 were incubated together at room temperature prior to SEC purification. Fractions were selected for Western blot analysis based on absorbance at 280 nm during SEC to check for presence of one or both proteins in the elution fractions. Western blots were probed with p85-specific or Rab5-specific antibodies and visualized using infrared secondary antibodies and a LICOR ODYSSEY infrared scanner. Protein bands of interest indicated using red arrows. **A.** Western blot using anti-p85-BH (left) or anti-Rab5 (right) primary antibodies from SEC Experiment A showing co-elution of p85-BH and Rab5 only in later fractions. **B.** Western blot using anti-p85 (left) or anti-Rab5 (right) primary antibodies from SEC Experiment B showing Rab5 eluting in early fractions as well as later fractions.

protein, and the corresponding MW, can be found in **Table 4.6**. The calculated elution volume for a p85 dimer (170 kDa) is 12.13 mL, and for a p85 monomer (85 kDa) is 13.63 mL.

All proteins examined had elution volumes that corresponded with molecular weights that best approximated those of a protein dimer. The p85 E137K and p85 R262T proteins both had more noise in their chromatogram signals potentially due to increased protein degradation, but still had their primary elution peak within the dimer range as well. Peak elution fractions were

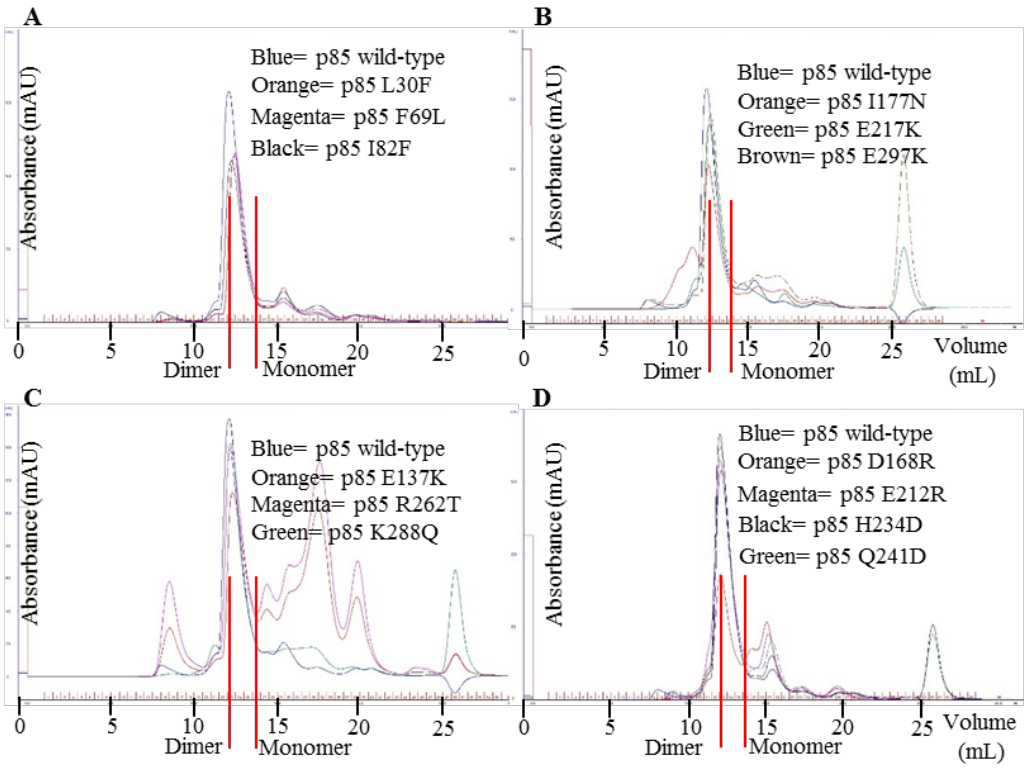

Figure 4.12 Size exclusion chromatography chromatograms for full-length human p85 and mutants. Overlay of SEC elution chromatograms of full-length human p85 wild-type and containing endometrial cancer mutations in the SH3 (L30F, F69L, I82F, **A**) or BH (I177N, E217K, E297K, **B**) domain, bladder cancer mutations (E137K, R262T, K288Q, **C**), or engineered BH domain mutations (D168R, E212R, H234D, Q241D, **D**) to observe the oligomerization state of the proteins. The expected elution volumes for a p85 dimer (170 kDa, 12.13 mL) and monomer (85 kDa, 13.63 mL) are displayed for reference.

further analysed using Native PAGE gels and these results were consistent with dimer formation (**Figure 4.13**).

At the protein concentrations we performed the SEC experiments at the mutants did not appear to significantly affect p85 oligomerization status.

4.5 MALS analysis of recombinant full-length human p85

In order to determine how the p85 concentration used in the SEC experiments may have affected the observed oligomerization state of our protein, we analyzed varying concentrations of full-length human p85 using the Wyatt MALS System with Refractive Index Measurement operated by the PCCF which was connected to a Superdex 200 Increase SEC column and an ÄKTA Purifier.

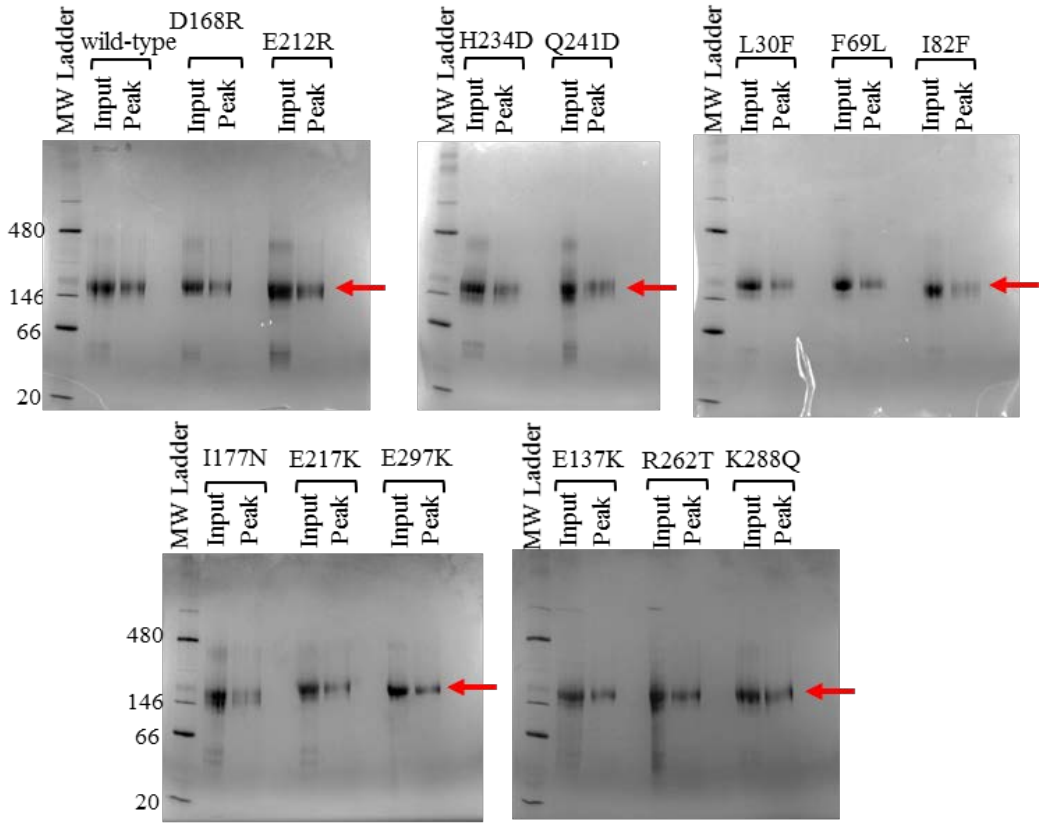

Figure 4.13 Native PAGE analysis of SEC fractions for full-length human p85 and mutants. Samples of the protein solution loaded for SEC analysis (Input) along with a sample from the elution fraction with the highest absorbance value (Peak) were analyzed using Native PAGE analysis to verify the oligomerization state determined by SEC. We examined full-length human p85 wild-type, as well as proteins containing point mutations that were BH domain engineered (D168R, E212R, H234D, Q241D), endometrial cancer associated mutations in the SH3 (L30F, F69L, I82F) or BH (I177N, E217K, E297K) domains, or bladder cancer associated mutations (E137K, R262T, K288Q). Protein was visualized by Coomassie blue staining. Dimer locations are indicated with red arrows.

We analyzed human p85 samples at concentrations of 4 mg/mL, 2 mg/mL, 1 mg/mL, 0.7 mg/mL, and 0.5 mg/mL. Overlays of the MALS chromatograms are shown in **Figure 4.14**. Summary of peak elution volume and determined MW for the different p85 concentrations are shown in **Table 4.7**.

For the 4 mg/mL p85 concentration there was a great deal of aggregation observed in the protein sample. Also observed in this sample was an elution peak that corresponded to a molecular weight of approximately 130 kDa. This elution peak was observed to have a tailing end, and the molecular weight distribution for the peak showed larger molecular weight population at the start of the peak, and lower molecular weight at the end of the peak, suggesting

Table 4.6 Elution volumes and corresponding MW for SEC analyzed p85

Protein Name	Elution Volume (mL)	Calculated MW (kDa)	Dimer/Monomer
$p85_{hu}$ wild-type	12.02	178.9	Dimer
$p85_{hu}$ L30F	12.44	147.5	Dimer
$p85_{hu}$ F69L	12.41	149.5	Dimer
$p85_{hu}$ I82F	12.29	158.0	Dimer
$p85_{hu}$ I177N	12.23	162.4	Dimer
$p85_{hu}$ E217K	12.27	159.5	Dimer
$p85_{hu}$ E297K	12.34	154.4	Dimer
$p85_{hu}$ E137K	12.32	155.8	Dimer
$p85_{hu}$ R262T	12.20	164.7	Dimer
$p85_{hu}$ K288Q	12.14	169.3	Dimer
$p85_{hu}$ D168R	12.01	179.7	Dimer
$p85_{hu}$ E212R	12.11	171.7	Dimer
$p85_{hu}$ H234D	11.9	181.4	Dimer
$p85_{hu}$ Q241D	12.05	176.5	Dimer

Table 4.7 Elution volumes and corresponding MW for MALS analysis of full-length p85

Concentration	Elution Volume (mL)	Calculated MW (kDa)	Dimer/Monomer
4 mg/mL	13.18	130	Mixture
2 mg/mL	11.7	128	Mixture
1 mg/mL	12.34	111	Mixture
0.7 mg/mL	12.65	72	Monomer
0.5 mg/mL	12.86	88	Monomer

a mixture of dimeric and monomeric population present within the same peak. The resolution of the column was not high enough to determine relative amounts of the different oligomeric states.

The 2 mg/mL concentration of p85 had much less aggregation present. The elution peak at this protein concentration suggested a molecular weight of approximately 128 kDa, once more potentially a mix of protein dimers and monomers. The 1 mg/mL p85 concentration had an elution peak corresponding to a molecular weight of approximately 111 kDa and had a very uniform molecular weight distribution. The 0.7 mg/mL p85 concentration had an elution peak corresponding to a molecular weight of approximately 72 kDa, which is smaller than the calculated molecular weight for the p85 monomer and there was a shifting molecular weight distribution across this peak. The 0.5 mg/mL p85 concentration had an elution peak corresponding to a molecular weight of between 80-90 kDa, suggesting monomeric p85.

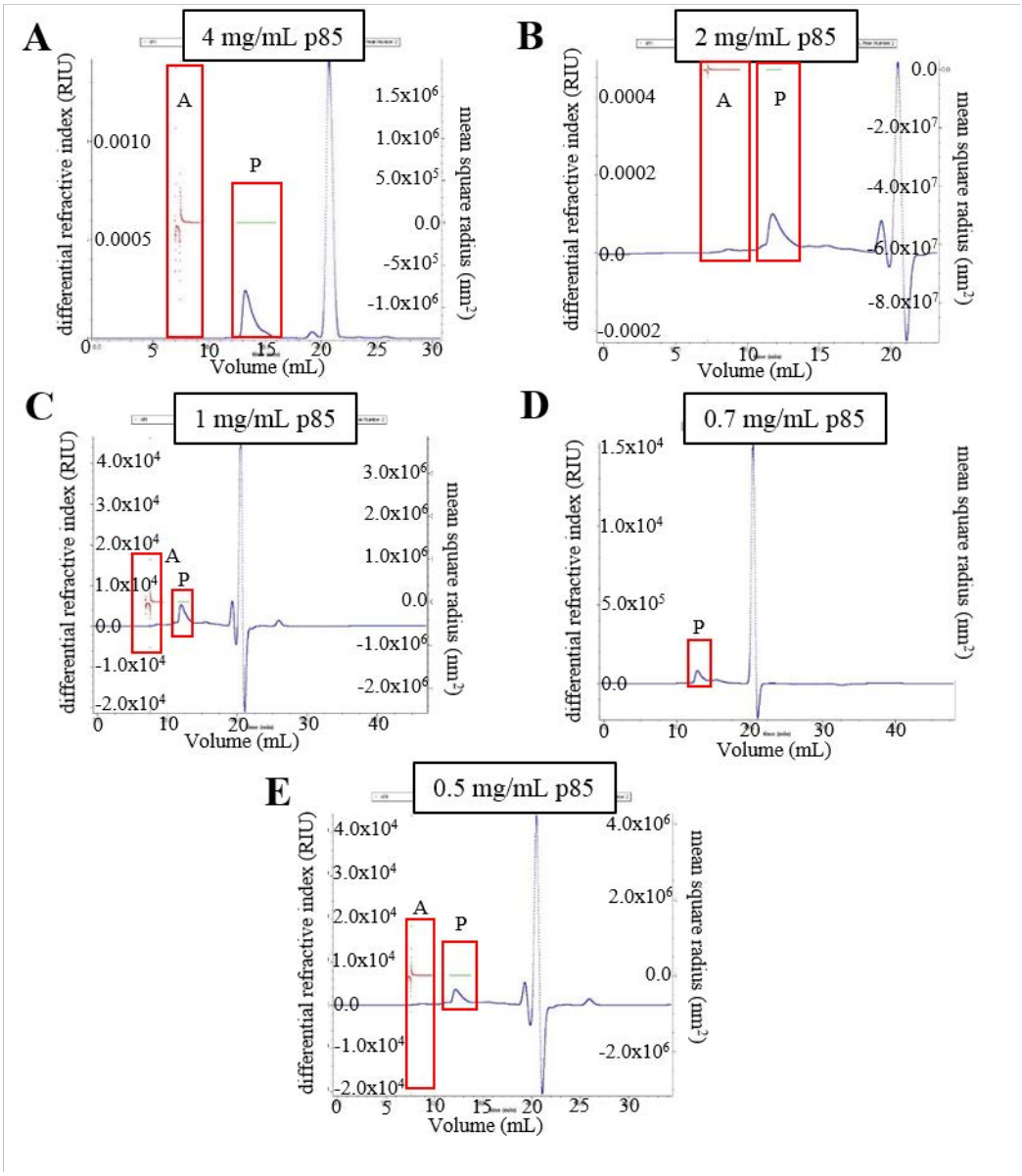

Figure 4.14 Multi-angle light scattering chromatograms for full-length p85. Chromatograms for the MALS results for full-length p85 at several concentrations. Differential refractive index (RIU) is the left y-axis, mean square radius (nm^2) is the right y-axis, elution volume (mL) is the x-axis, with the aggregate (A, red dots), and elution peak (P, green dots) are indicated in red boxes.

4.6 Lipid binding of p85 SH3 and BH domains using phosphatidylinositol phosphate lipid strips

The p85 protein is known to be a key regulatory protein of the PI3K/PTEN pathway, one of its mechanisms acting through binding to PTEN and facilitating the PTEN-mediated dephosphorylation of $PI3,4,5P_3$ to $PI4,5P_2$. Since the SO_4 ions observed in our p85-BH structures

could serve as a structural analogue for PO_4, and the lipids in the PI3K/PTEN pathway contain PO_4 groups, additional experiments were carried out to determine if the p85 BH domain could directly bind various phospholipids. Due to the high concentrations of SO_4 ions present within the crystallization solutions potentially preventing physiological binding partners from being able to bind within the potential novel binding pocket we wished to pursue binding experiments using soluble protein free of the high SO_4 concentrations. To these ends we performed PIP lipid strip analysis using several p85 protein fragments to check for binding between our protein and various lipids.

4.6.1 Determination of p85 regions required for lipid binding

To determine which regions of the p85 protein were required for any observed lipid binding we probed PIP lipid strips with 37 nM of p85 (1-319), p85 (78-319), or p85-BH protein. PIP strips probed with no protein were used as a control. Following anti-p85 antibody probing and visualization using LICOR ODYSSEY software we could clearly see signal indicating that p85 protein bound to several lipids.

The analyzed PIP Strips are shown in **Figure 4.15**.

All three p85 fragments showed binding to the following lipids: (PI3P, PI4P, PI5P) > (PI3,4P_2, PI3,5P_2, phosphatidic acid) > (PI4,5P_2, PI3,4,5P_3) > lysophosphatidic acid. Lipids grouped based on degree of binding observed. The p85 (1-319) protein fragment showed less signal but the same binding profile. As all three p85 fragments were able to bind to the lipid this demonstrates that the BH domain on its own is capable of lipid binding. All lipids that we observed binding were negatively charged and contained phosphate groups on the periphery, while we observed little binding for non-phosphorylated lipids such as PI and uncharged lipids or those without peripheral phosphates.

4.6.2 Determination of concentration dependence of observed p85 lipid binding

In order to determine that the lipid binding observed was concentration dependent, and would not provide the same signal intensity with lower protein concentrations used, we performed additional PIP strip analysis using 37 nM, 3.7 nM, and 0.37 nM of p85 (78-319).

PIP strips from the concentration dependence experiments are shown in **Figure 4.16**.

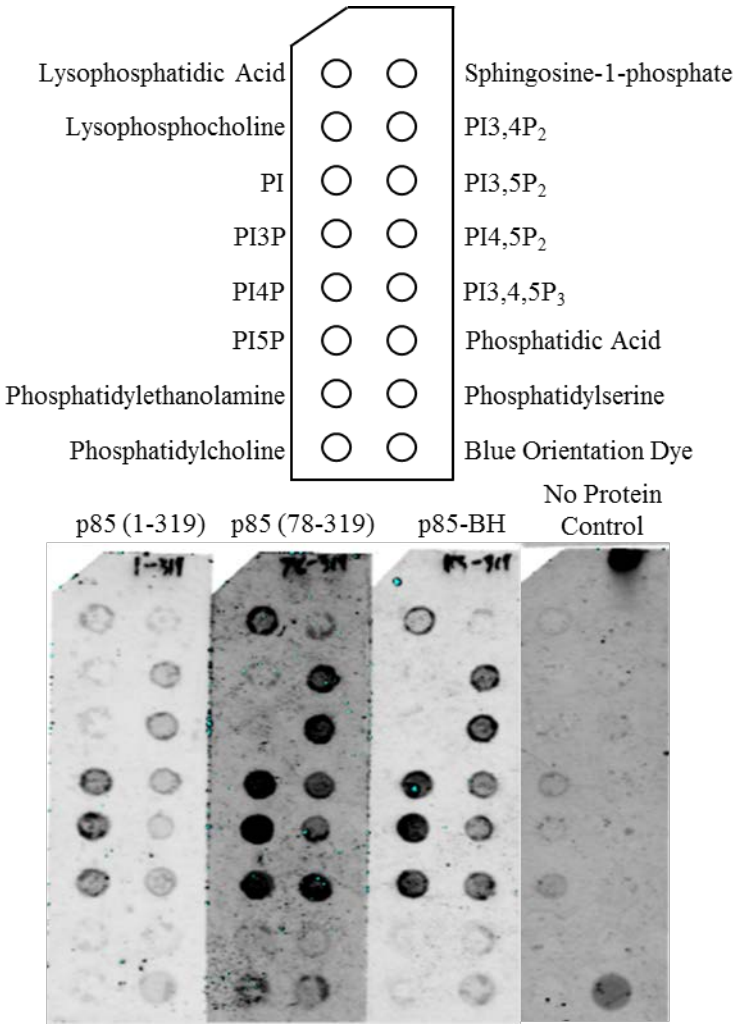

Figure 4.15 PIP strip analysis of p85 lipid binding. To test if p85 has lipid binding ability, and to determine which regions are required for any observed binding, we probed PIP strips containing various lipids bound to nitrocellulose with equimolar amounts of p85 (1-319), p85 (78-319) or p85-BH protein. PIP strips probed with no protein were used for control. Bound protein was detected using anti-p85-BH primary antibody, with an infrared secondary antibody and visualized using a LICOR ODYSSEY infrared scanner.

There was a clear correlation between the strength of signal observed and the concentration of p85 (78-319) that had treated the individual PIP strips. In addition, at the decreased protein concentrations the same lipid binding profile was seen for the p85 (78-319) protein fragment as at higher concentrations.

These results raise the interesting possibility that the potential new binding pocket seen within the p85 BH domain can bind phospholipids.

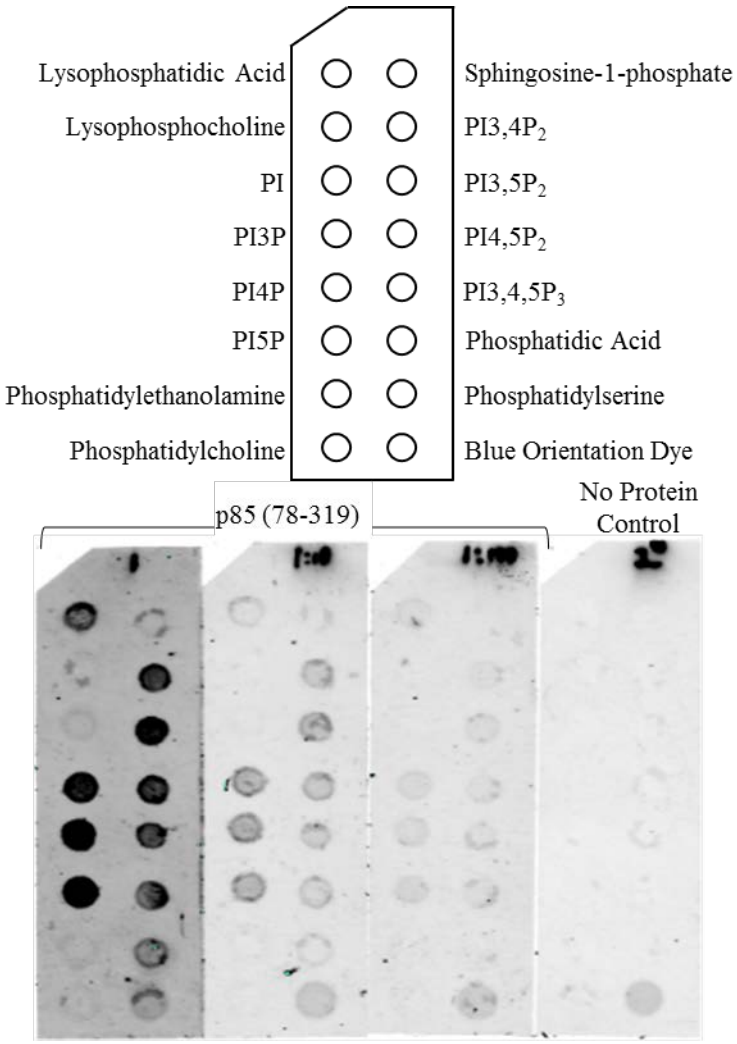

Figure 4.16 Concentration dependence of p85 (78-319) PIP strip binding. To determine if the observed lipid binding behaviour of p85 (78-319) was concentration dependent we incubated PIP strips containing various lipids bound to nitrocellulose with decreasing concentrations of p85 (78-319). PIP strips probed with no protein were used for control. Bound protein was detected using an anti-p85-BH primary antibody, with an infrared secondary antibody and visualized using a LICOR ODYSSEY infrared scanner.

5.0 Discussion

5.1 Combining High Resolution Structural Data with Protein Function Studies

The combination of high resolution structural data with the data collected from protein functional studies allows for a synergistic analysis of the data collected from both methods, resulting in more in depth understanding of the research subject. One excellent example, which served as an inspiration for the work pursued in this project, was Huang *et al.* crystallization of the p110α protein in complex with a p85 fragment containing the N-terminal SH2 domain and the inter-SH2 domain region important for p110 binding (Huang *et al.*, 2007). Based on the crystal structure obtained for the protein complex they examined the locations of various cancer-associated mutations in p110α to determine which would alter the interactions between p110α and the p85 fragment. One example was for mutations located in the p110 α C2 domain that had previously been thought to alter lipid binding affinity were located within hydrogen-bonding distance of several residues on the p85 inter-SH2 domain, meaning that mutations could likely alter the interaction between these two proteins rather than lipid binding affinity (Huang *et al.*, 2007).

Using these different techniques in tandem can allow for improved interpretation of experimental observations, granting deeper understanding to the mechanisms responsible for observed phenotypes. They can serve to reinforce theories on the potential mechanisms of interaction, and also help to correct misinterpretations that could be made from data from one technique in isolation. By observing disparities between the results of different techniques it can serve to guide further experiments in order to determine the correct interpretations. Agreement between data collected across different techniques can increase confidence in the interpretation of the data.

5.2 Insights from bovine p85 BH domain crystal structures

Crystallization progress for our various fragments of bovine p85 revealed identical visible residues despite the different length protein fragments used for crystallization. All of our crystal structures for p85-BH, p85 (78-319) and p85 (1-319) had residues 113-297 visible in both monomers of the BH domain homodimer within the asymmetric unit. These are consistent with the human p85 BH domain previously solved (PBI: 1PBW) where residues 115-298 were visualized (Musacchio *et al.*, 1996).

The similarity between the p85 (1-319) and p85-BH regions visible can most likely be explained by a proteolytic cleavage of the p85 (1-319) protein during the crystallization process. As the previous crystallization of the p85 SH3 domain (Liang *et al.*, 1996) revealed well defined structure we would expect this domain to be visible in a crystal containing both SH3 and BH domains. Another possibility is that the SH3 does not have a single orientation when expressed with the BH domain, so mobility of this domain may have prevented the visualization of the domain within the X-ray diffraction data. However, we note that all the p85 structures we determined shared nearly identical unit cell dimensions (~84, 92, 93, 90, 90, 90). If the SH3 domain was present within the crystal we would anticipate a difference in the observed unit cell dimensions to account for the additional domain present, so with no significant difference observed it is more likely that the SH3 domain was excluded during the crystallization process.

The reason behind the altered orientation of the p85 (78-319) protein within its asymmetric unit when compared to the p85-BH has several possibilities. Due to the consistency of the unit cell dimensions (84.12, 91.56, 93.14, 90, 90, 90) with the p85-BH crystals it is possible that the additional residues of the inter-domain linker region were cleaved similar to what is suspected of the SH3 domain for p85 (1-319). However, it is notable that examining the packing of molecules within the p85 (78-319) crystal X-ray diffraction data that a large region lacking protein molecules and electron density is located adjacent to the N-terminal region of the protein structure (**Figure 5.1**). It is also possible that the inter-domain linker region is present, but highly flexible, having no single predominant conformation, resulting in the lack of visible density in that region. However, the observed gaps could also correspond to solvent channels present within the protein crystals. With our current data collected a definitive answer to this difference in protein orientation cannot be made.

5.2.1 Observations from nucleotide, phosphoamino acid, and phospholipid additive analysis

Attempts to obtain structural information of the p85-BH with potential binding partners bound proved unsuccessful. None of our additive cocktails of nucleotides (ATP, GTP, and GppCp), phosphoamino acids (pSer, pThr, pTyr), or phospholipids (I1,3P_2, I1,4P_2, I1,5P_2, I1,3,5P_2) showed any notable regions of increased binding to suggest interaction between protein or additive. The same was true for our individual 8 carbon chain phosphatidylinositol lipids soaks (PI4P; PI3,4P_2; PI4,5P_2; PI3,4,5P_3) as well as our PI4,5P_2 soak with p85 (78-319).

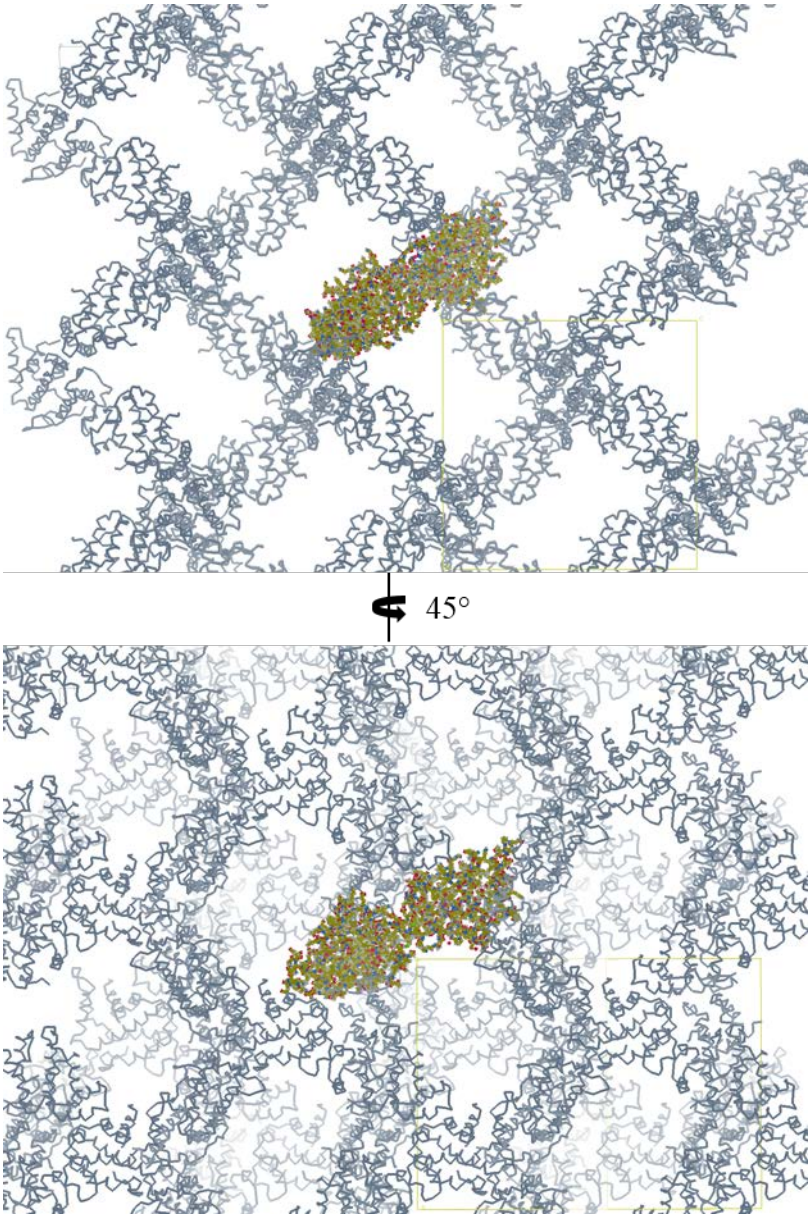

Figure 5.1 Crystal packing of p85 (78-319). Example region of packing between various BH domain dimers present in our p85 (78-319) protein structure. A homodimer of the p85 (78-319) is shown with yellow carbons, with symmetry molecules shown as strings of alpha-carbons in grey. Large open cavities are visible between the protein molecules, with channels that connect the cavities throughout the crystal. The lower image is rotated 45° relative to the top image to provide a different perspective of the crystal packing.

One possible explanation for this lack of observed binding is that these molecules do not interact with the p85 BH domain. All additives were selected as candidates based on the coordinated SO_4 ions observed within our structure, with PO_4 being a physiologically relevant

ion of a similar size and charge. These observed coordinated ions may not correspond to a physiological activity of the protein, and instead only exist as a crystallographic artifact.

Another explanation is that the high concentrations of SO_4 ions present within the crystallization screens (~1.5 M) excluded any physiologically relevant molecules from being able to bind to regions they interact with. Because the concentrations of additives we were using were in the ranges of 10 – 30 mM the SO_4 ions were present at a concentration at least 50 times greater than that of the additives. This excess may have forced the interaction with SO_4 ions to predominate over any physiologically relevant interactions that could normally occur in biological systems. Densities corresponding to SO_4 or cacodylate molecules were also observed for p85 (78-319) crystallization screens in which a 1:1 molar ratio of 8-carbon $PI4,5P_2$ was added to the protein solution prior to crystallization.

5.2.1.1 Future experiments to check for binding between additives and p85

In order to determine if any of the small molecules we have been examining bind to the p85 protein we will want to examine these interactions in solution and free of the high SO_4 ion concentration present under crystallization conditions. Several experimental techniques could be pursued to this end.

A technique that we will avoid using is surface plasmon resonance. Previous work performed by myself and others in the Anderson Lab have found the p85 protein does not yield good experimental data using this technique. The protein would bind to both activated and inactivated regions of the chips used for performing the experiments, causing significant background noise and preventing accurate baseline determination or data collection. Extensive attempts to optimize the activation and deactivation conditions of the experimental chip, concentrations of proteins used, buffers used for protein storage and experimental stages, as well as solutions for regeneration of the experimental chip failed to overcome these experimental difficulties. This high background prevented usable data collection using this method. We will place an emphasis on solution-based techniques for future binding experiments, to remove the challenges encountered when binding the protein to a surface.

One technique would be the use of isothermal titration calorimetry. Descriptions of the technique and various applications for protein interaction analysis by isothermal titration calorimetry are provided in (Ghai *et al.*, 2012; Liang, 2008; Velazquez-Campoy *et al.*, 2004).

Briefly, recording the changes in energy required to maintain a constant temperature for the calorimeter following addition of ligand to a vestibule containing our protein solution of interest (or adding protein to a vestibule of potential ligand). This allows determination of binding and dissociation constants of interactions, as well as the number of ligand molecules interacting with each protein molecule. Isothermal titration calorimetry has the advantages of using relatively small amounts of sample, not requiring any modification or immobilization of our protein of interest, and a large range of kinetic data that can be determined per experiment.

Another method for investigating potential interactions would be fluorescence anisotropy. A description of the experimental methodology, applications, and considerations is provided in (Heyduk *et al.*, 1996). Briefly, fluorescence anisotropy utilizes the behaviour of macromolecule rotation within solution, in which larger molecules rotate more slowly than smaller molecules. Coupling one type of molecule to a fluorophore and allowing it to bind to another molecule results in an increase in size and decreased rate of rotation. This leads to a measurable increase in the polarity of the light emitted which is recorded by the instrument. Using a fluorophore-bound potential ligand within the reaction chamber we can titrate in increasing amounts of our protein of interest (without fluorophore). If our protein of interest binds to the ligand it will lead to a decrease in the ligands rate of rotation, having bound to become part of a larger complex, observed by the change in polarity. From the observed change in polarity we can determine the binding constants for the interaction between protein and ligand. Fluorescence anisotropy has the advantages of using small amounts of sample, and the determination of binding kinetics through experimental data. Modification of the ligands is required, through coupling of the fluorophore, which could potential alter the binding behaviour, so control experiments of adding protein to fluorophore alone to test for non-specific interactions may be required. Fluorophore-coupled phosphatidylinositol lipids and DNA are commercially available, and techniques for fluorophore-coupling proteins are also well characterized and fluorophores with reactive groups commercially available (Waggoner, 1995; Echelon Biosciences Inc., Salt Lake City, UT; Thermo Fisher Scientific).

For both isothermal titration calorimetry or fluorescence anisotropy experiments we can use various fragments of p85 (full-length, SH3 and BH domains, BH domain alone) in order to also determine the regions important for observed interactions. The dissociation constants determined using these experiments can then be used to determine levels of ligand required to

improve our chances of visualizing it through crystallization, either to compete with the present SO_4 ions or through searching for different crystallization conditions containing lower concentrations of sulfate compounds.

If binding between the p85 BH domain and additives is observed, we can further characterize the residues important for the interaction through mutagenesis studies. Initial experiments could focus on the residues that compose the potential novel binding pocket observed (K224, R228, H234, W237, and Q241). Characterization of this region, including analysis of mutations, is discussed in later sections.

5.2.2 Interpretation and future analysis of potential post-translational modification of C146

The consistent presence of additional electron density between residues C146 and H180 in our various p85 BH domain structures was an unexpected observation. Our comparisons of various oxidized states of cysteine, as well as the nitrosylated S-nitrosocysteine, against the Fob-Foc difference map obtained during refinement of p85-BH with an Ala replacing C146 showed that S-nitrosocysteine best fit the electron density (**Figure 4.6**). For this reason further refinements of our determined structures used S-nitrosocysteine residues at amino acid 146.

A summary discussing cysteine nitrosylation and its roles in protein function and signalling pathways is provided in (Gould *et al.*, 2013). As a brief introduction to the roles of cysteine nitrosylation, S-nitrosylation is the addition of a –NO group to the thiol group of the cysteine sidechain. Nitrosylated cysteine residues have been identified in proteins belonging to a wide variety of tissues, with many present in mitochondrial enzymes important in various metabolic and energy producing pathways (Gould *et al.*, 2013). Due to the sensitivity of neuronal cells to excess levels of NO, neuronal cells have been specifically examined for the presence of nitrosylated cysteine residues, with proteins including GAPDH, glycogen phosphorylase, heat shock protein 72, ß-tubulin, and actin amongst others have been identified (Jaffrey *et al.*, 2001). The effect of excessive NO species and protein S-nitrosylation has also been examined for its role in various neurodegenerative diseases, reviewed in Nakamura and Lipton 2016, as well as cancers, reviewed in Monteiro *et al.* 2015 (Monteiro *et al.*, 2015; Nakamura and Lipton, 2016).

Examination of previously characterized post-translational modifications in p85 have identified polyubiquitination, acetylation, and phosphorylation, but no modification to cysteine

residues (UniProtKB ID P27986). If this is a physiologically occurring post-translational modification of the p85 protein it has, to our knowledge, not previously been characterized.

An important next step will be to determine whether this post-translational modification occurs in eukaryotic cells. Without such confirmation it is possible that the observed modification is an artifact of the bacterial expression of our protein fragment.

Some reviews that discuss cysteine nitrosylation and some of the methods of detecting these post-translational modification are provided in (Gould *et al.*, 2013; Murray and Van Eyk, 2012). One of the techniques used for detections of S-nitrosocysteine is the biotin switch assay (Jaffrey *et al.*, 2001). Briefly, unmodified cysteine residues are blocked, then S-nitrosocysteine is reduced by exposure to ascorbate and the exposed sidechains are reacted with biotin. This allows for purification of the previously nitrosylated protein through use of avidin or streptavidin purification of the biotin labelled proteins of interest. These proteins can then be identified using protein specific antibodies, or using mass spectrometry. There are also anti-S-nitrosocysteine antibodies commercially available that can be used for western blot detection of proteins containing S-nitrosocysteine (Abcam Cat# ab94930). These experiments can be performed with both full length p85, and our p85-BH fragment, as C146 is the only cysteine residue present within the p85 BH domain. Doing so will allow us not only to determine whether nitrosylation occurs to p85 in eukaryotic cells, but also if C146 is converted to S-nitrosocysteine.

If we detect nitrosylation of the p85 protein we can perform mutagenesis studies on C146 to determine the effect of such mutations on stability of the p85 protein. Further experiments could also be performed to determine how C146 mutation affects interaction with known protein binding partners p110, PTEN, and Rab5 through co-immunoprecipitation or pull down experiments (Carpenter *et al.*, 1990; Chagpar *et al.*, 2010; Chamberlain *et al.*, 2004). In addition, various functional assays can be performed to determine how a C146 mutation alters the activities of these various binding partners: kinase assays for p110 activity, GAP assay for Rab5, and lipid phosphatase assays for PTEN (Liu and Li, 1998; Myers *et al.*, 1997; Witt and Roskoski, 1975).

The results of these studies will provide us with a greater understanding of the role that cysteine nitrosylation plays in structural and functional regulation of the p85 protein, its interactions with various binding partners, and any role in the regulation of the PI3K/PTEN pathway.

5.2.3 Effect of cancer-associated and engineered mutations on the bovine p85 BH domain

Having collected X-ray diffraction data for p85-BH containing the cancer-associated mutations E137K, E217K, R262T, and E297K, as well as the engineered mutation R228E, we can examine any structural changes these mutations formed in the p85 BH domain.

None of the cancer-associated mutations crystallized resulted in any major structural changes for our protein. This is not surprising given the great similarity in crystallization conditions that were able to obtain crystals for the wild-type protein and these mutants. Crystallization condition trials had yet to be performed for the K288Q mutant, but if it were to also crystallize using very similar conditions to all the others this would lead us to suspect, prior to collecting X-ray diffraction data for confirmation, that the changes to the overall domain structure would be limited.

The I177N mutation (F177N in bovine) is a particularly interesting cancer-associated mutation that we had been working on. It did not crystallize using conditions similar to our previous p85-BH crystals, and currently crystallization condition screens are underway to identify conditions that will yield diffracting crystals. Due to the position of residue 177 being one of the residues that forms the BH domain dimerization pocket for the M176 of the opposite BH domain (Musacchio *et al.*, 1996) mutation of this residue could disrupt the dimerization interface in the crystal structure. Residues important for this BH domain dimerization site are shown in **Figure 5.2** for the bovine and human proteins. There is some debate regarding whether the dimerization between the BH domains exists in physiological systems, with a study by Harpur *et al.* showing a weak interaction with a dissociation constant in the mM range (Harpur *et al.*, 1999), whereas a more recent study by LoPiccolo *et al.* using a protein fragment containing p85 residues 78-322 did not detect any oligomerization (LoPiccolo *et al.*, 2015). It would be interesting to see if any disruption of that crystallographic BH domain interface would disrupt this site of homodimerization and require the formation of different crystal contacts for crystallization, or if it leads to any large changes to the overall structure of the BH domain.

As the crystal structures for the obtained cancer-associated mutations are all found on the surface of the p85 BH domain and cause negligible structural differences to the domain they may instead exert effects through alterations in interaction profiles with binding partners that could contribute to the associated cancerous phenotype. In order to examine this we can use proteins containing the mutations for isothermal titration calorimetry or fluorescence anisotropy

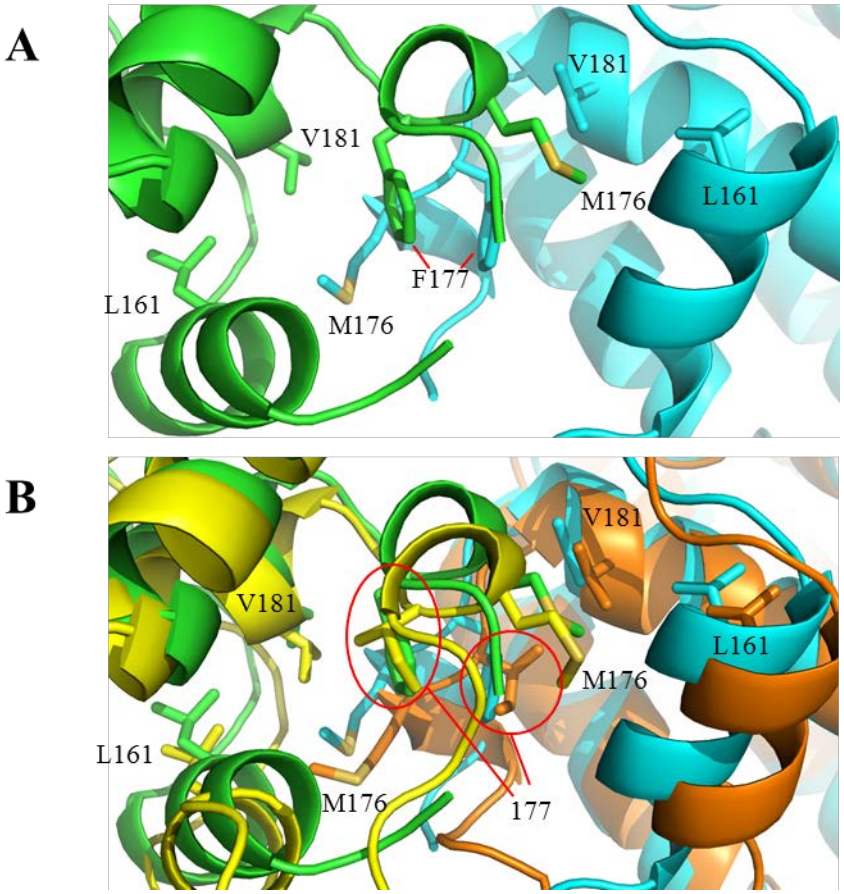

Figure 5.2 Homodimerization region overlay of human and bovine p85 BH domains. A. Examination of the BH domain homodimerization interface of bovine p85 proteins where M176 of one protein fits into a hydrophobic pocket generated by L161, F177, and V181 of the other protein. Sidechains are represented in stick format, and the two BH domains are coloured in green and cyan for differentiation. **B.** Overlay of the BH domain homodimerization interface between our bovine p85 BH domain structure and the previously solved human p85 BH domain structure (Musacchio *et al.*, 1996: PDB: 1PBW). Sidechains involved are represented in stick format, with F177 found in the bovine protein, and I177 found in the human protein. The two bovine BH domains are coloured in green and cyan, and the two human BH domains are coloured in yellow and orange for differentiation.

experiments as mentioned above. By comparing the experimental results of these mutant proteins with those of wild-type protein for molecules that showed detectable binding we can see if the mutants result in increased or decreased interaction with these binding partners.

In order to determine if the cancer-associated mutants detected in bioinformatics screens (Cheung *et al.*, 2011; Ross *et al.*, 2013) are sufficient to induce a cancerous phenotype we can knockout wild-type p85 from cells and transfect these cells with the various cancer-associated mutant p85 proteins and assay for their oncogenicity. For those mutants that result in

transformation we can examine altered phosphoAKT (the activated form; pAKT) levels, contact inhibition, motility, and colony formation in soft agar. Analysing results from these experiments will further elucidate the mechanism behind their oncogenicity and their biological effects.

5.2.4 Observed potential novel binding pocket

One of the most interesting observations made within our p85-BH structure were a pair of highly coordinated electron densities oriented by residues K224, R228, H234, W237, and Q241 in both BH domains. Based on the size of the electron densities seen, and the contents of our crystallization buffer, SO_4 ions have currently been modeled in these regions, and they agree well with the observed densities.

In our p85 (78-319) structure one of these observed electron densities was larger than in other structures. Based on the components of the crystallization buffer we modeled a cacodylate ion into this larger density and it agrees with this density better than the previously modeled SO_4. Based on this observation it is worth noting that the ions modeled within these densities are based on the best agreement of ions present in the crystallization solution with the X-ray diffraction data, but do not have further confirmation experiments. Therefore it is possible that cacodylate molecules were bound in our p85-BH structures, or that the p85 (78-319) increased density is a SO_4 that has larger mobility within the structure. We cannot confirm which ions were bound, but they are chosen based on agreement to the X-ray diffraction data.

The fitting of SO_4 ions within the observed densities served to guide our selection of potential binding partners that we treated the crystals with for our additive treatments discussed above. Due to the structural similarities between SO_4 ions and PO_4 ions, and the frequent usage of PO_4 in biological systems, we focused our additive screens on molecules containing PO_4 molecules (nucleotides, phosphoamino acids, and phospholipids).

5.2.4.1 Comparison of potential binding pocket region in bovine and human p85

An overlay of the bovine p85-BH crystal structure we have solved and the previously solved human p85 BH domain ((Musacchio *et al.,* 1996) PDB: 1PBW) is shown in **Figure 5.3**.

While there are shifts to the overall positions of structural features, the overall secondary structures and orientation are conserved between the human and bovine proteins. In the potential binding pocket region the important residues of K224, R228, H234, and W237 have largely

conserved final sidechain positions, with the R228 sidechains using different orientations in order to end in the same region despite a shift in the loop positions between structures. Residue Q241 displays different sidechain positioning between the two species, with bovine facing towards the coordinated SO_4 ions observed in the structure whereas in the human structure the Q241 sidechain is oriented directly away from this region. If this region is found to be important for binding to different partners, mutational studies of Q241 can determine if this residue plays a direct role in binding, adjusting sidechain orientation upon presence of ligand for example, or a nearby residue that does not have a role in binding.

5.2.4.2 Effect of mutations on the potential binding pocket

Comparison of the structures of p85-BH and p85-R228E it was observed that one of the coordinated densities around the potential binding pocket region vanished in the mutant structure. As this residue was identified as being important for the interaction between p85 and PTEN, this visible difference is of interest for further analysis.

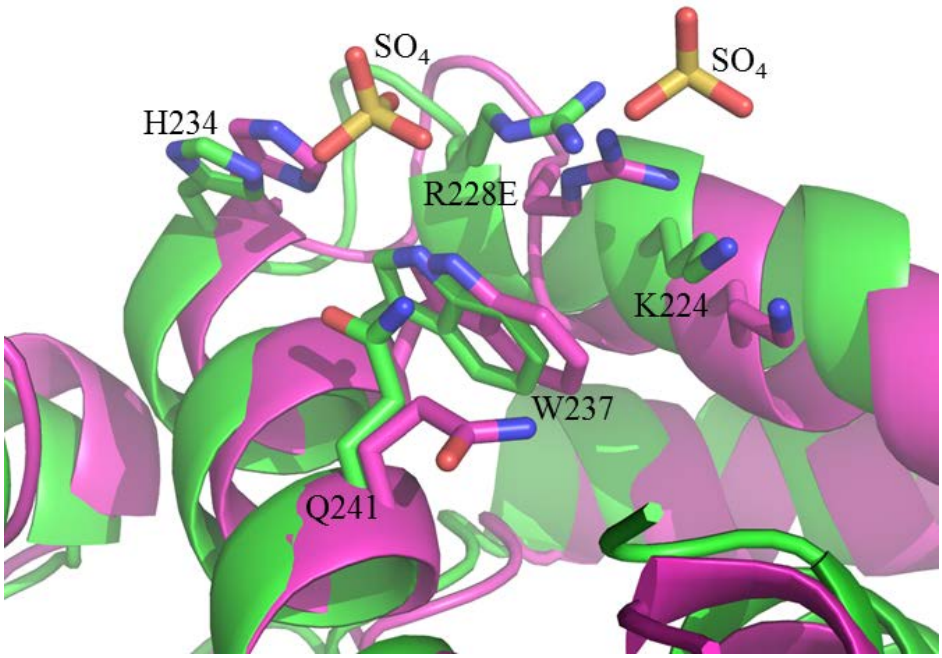

Figure 5.3 Overlay of potential binding pocket for bovine and human p85. Comparison of the sidechain orientation for residues involved in the potential binding pocket for both the bovine p85-BH structure (green), and the previously solved human p85 BH domain (magenta; Musacchio *et al.*, 1996; PDB: 1PBW). Structures are represented in cartoon format, with important sidechains, and SO_4 ions from the bovine structure, represented in stick format.

If this region is important for a direct interaction between PTEN and the p85 BH domain we would expect that our experiments described previously would show binding between the BH domain and phosphoamino acids. If this is the case we could use this information to search for residues that are phosphorylated on the surface of the PTEN protein that could be accessible for interaction, and use that information to assist modelling analysis prior to obtaining co-crystal structural information.

It would also be possible that the p85:PTEN interaction may be indirectly mediated through the presence of a phosphatidylinositol lipid at the protein interface, likely $PI4,5P_2$ or $PI3,4,5P_3$ due to their role in the PI3K/PTEN pathway. Observed interaction between the p85 BH domain and phospholipids determined by experiments described previously provides support for this possibility. If this is the case then for both modelling studies and co-crystallization trials it would be important to include this lipid in attempts to determine the structure of the p85:PTEN complex.

Determining the effect of mutations on any experimentally observed binding can provide further support and evidence for these analyses. We have p85-BH containing K224-5E, R228E, H234D, and Q241D, which could be used for isothermal titration calorimetry or fluorescence anisotropy to determine any changes to the kinetics of interaction caused by the mutations. Previously we obtained crystals for the p85-BH-K224-5E and p85-BH-Q241D mutations, but X-ray diffraction data was not collected for these mutants. Observing any effects that these mutations have on the potential binding pocket region could also provide additional insight into potential binding interactions. Crystals were obtained for p85-BH-H234D, but they did not diffract across a wide enough range to obtain an X-ray diffraction data set suitable for processing. Identification of new crystallization conditions for the p85-BH-H234D mutant could yield crystals of a different form that diffract better.

The mutants described above for the potential binding pocket residues are charge reversal mutations. It may be that this dramatic change of charge altered binding and lead to the observed electron density difference in our R228E mutant structure. If ligand binding is observed, and the above mutations affect this binding, examination of mutations of those residues to Ala may be warranted to ensure that it is the presence of the wild-type residue that is important in attracting the binding partner rather than an off-target repulsion from the mutant residue that is leading to the observed results.

5.2.4.3 Future experiments for characterization of the potential binding pocket

Many of the experiments to help further characterize the potential binding pocket were described previously. Experiments that displayed binding between the various compounds and p85 would be repeated with protein containing mutations of the various residues near the binding pocket; K224-5E, R228E, H234D, and Q241D, or mutating the residues to Ala. These would help to identify the roles these residues play with interacting to various binding partners.

Collection of X-ray diffraction data for the crystallized p85-BH-K224-5E and p85-BH-Q241D would allow us to see how these mutations affect the region around them. Identification of new crystallization conditions for p85-BH-H234D could yield crystals that diffract well enough for structure solution, allowing us to see the effects of this mutation as well.

5.3 Purification progress of PTEN (7-353, Δ286-309)

Improving yields of the bacteria expressing PTEN (7-353, Δ286-309) through growth in Hyper Broth has greatly increased our available protein following bacterial lysis. However, the consistent precipitation of the PTEN protein during the 4 °C incubation used for cleavage of the GST-tag has to be overcome to pursue further experiments.

With precipitation occurring during the 72 hour incubation at 4 °C during 3C Prescission Protease cleavage, solving this problem will be required in order to advance our experiments with this protein. As we have tested, in parallel, protein samples with 3C Prescission Protease added or only buffer added and observed precipitation in both cases it is unlikely the precipitation is triggered by removal of the GST-tag.

To determine the role that the incubation time and conditions have on the observed precipitation, we can alter these parameters to determine if this results in improved protein yield and quality. Decreasing the incubation times from 72 hours to a 16 hour overnight incubation, or even briefer 8 hour or 4 hour during the day, can allow us to extract various protein samples across these various time points. These samples can then be analyzed by SDS-PAGE to determine the amounts of proteins cleaved of the GST-tag after this time, and how much of the protein remains tagged. The incubation steps could also be performed at a higher temperature than the 4 °C used, such as incubating at room temperature for one of the decreased incubation times. Samples could be extracted and analyzed as above, and with a higher temperature

incubation it would also be important to determine that the protein does not denature or undergo major structural differences during incubation. One technique to ensure the secondary structures of the protein do not undergo significant changes is circular dichroism. Protein in solution is exposed to left and right circularly polarized light, which results in differential absorption between the left and right circularly polarized light based on the chiral nature of proteins and contributions of secondary structure features, forming a spectrum that can be interpreted to determine general ratios of various secondary structures features present in the protein structure (Greenfield and Fasman, 1969). The PCCF at the University of Saskatchewan has a Chirascan Plus CD Spectrometer (Applied Photophysics; Surrey, United Kingdom) instrument for performing circular dichroism experiments.

One potential reason for the observed precipitation would be due to high protein concentration of our initially Glutathione-Sepharose purified protein. As the precipitation at this step was noted following improving our protein yields through the Hyper Broth growth, it may be that the PTEN (7-353, Δ286-309) concentration at purification leads to spontaneous precipitation over time. In order to examine this possibility closely monitoring the concentration of our GST-PTEN (7-353, Δ286-309) at all stages of purification may allow us to observe if precipitation occurs at a certain concentration threshold. We can also dilute our protein in additional buffer, or add detergent to increase solubility, but for complex and crystallization experiments these solutions may decrease the chance of success. Low protein concentration could prevent crystallization, and presence of detergent molecules could interfere with complex formation between p85 and PTEN, as well as complicate co-crystallization condition determination.

Another potential reason for the precipitation could be the presence of a contaminating protease persisting through the purification protocol and slowly cleaving the PTEN over time. This could explain why the precipitation is observed during a longer incubation period, as it could provide the protease with the time required to degrade enough protein to lead to mass precipitation. One method to treat this problem would be the addition of additional purification steps to further remove any contaminating protein, some purification possibilities described below.

5.3.1 Additional purification steps for PTEN (7-353, Δ286-309)

In order to remove any possible contaminating proteases persisting through the initial purification steps of PTEN, additional purification may be required.

As the PTEN Crystal protein fragment has a calculated isoelectric point of 8.70, calculated using the ExPASy ProtParam tool, we could use cation exchange chromatography to further purify the protein.

Glutathione-Sepharose purified PTEN Crystal would be bound to a cation exchange column (potential column media of Source 15S, GE Healthcare, cat# 17-0944) based on the positive charge the protein possesses at pH 7.0. We can then elute the bound protein across a gradient of increasing NaCl, as described for our anion exchange purification of the p85 proteins above.

Based on the success of our anion exchange purifications of the p85 proteins use of cation exchange chromatography could assist in the removal of any contaminating proteins that may have been causing our PTEN Crystal to precipitate.

5.4 Complex formation progress between bovine p85 protein fragments and Rab5 as analyzed by SEC and Western blot analysis

Current attempts to form the complex between p85-BH and Rab5 have been hindered by the variation in behaviour between different preparations of the Rab5 protein. We have observed differences between protein preparations with some having small amounts of complex formation, and others showing separate elution of both proteins with no observable interaction. Identifying the source of this inconsistency will be important prior to pursuing further complex formation and co-crystallization experiments.

Previous research showed that presence or absence of bound nucleotide (GDP or GTP) did not significant alter the binding of Rab5 to p85 (Chamberlain *et al.*, 2004). These experiments were performed using ELISA and pull-down analysis, which may not take into account changes to the equilibrium of the complex formation. Because we need the protein complex, which may exist in a state of equilibrium with the proteins not in a complex, ensuring equal loading of nucleotide may increase the consistency of behaviour for the purified proteins.

It is also possible that contaminating proteins or proteases could have remained throughout the Glutathione-Sepharose purification. Additional purification steps could help to

solve this situation if additional proteins present are the source of the inconsistencies. Full-length Rab5 has a calculated isoelectric point of 8.32, calculated using the ExPASy ProtParam tool, which could make this protein another candidate for cation exchange chromatography, as mentioned above, as an additional purification step for PTEN Crystal. However if we use Rab5 (15-184), the protein fragment that previously had a crystal structure solved, this protein fragment has an isoelectric point of 6.93, which would make it unsuitable for purification using either anion exchange or cation exchange at pH 7. This would require different additional purification steps of the Rab5 (15-184) protein fragment, such as SEC to remove any contaminating proteins based on difference in MW.

5.4.1 Future experiments for p85-BH:Rab5 co-crystal screening

Upon optimization of large quantities of highly purified p85-BH:Rab5 protein complex we would begin our screening for crystallization conditions. To this end we will start with automated screens using the GRYPHON robot operated by the PCCF, testing our protein complex against the various commercially available crystallization screens as described above. Promising conditions can then be selected for optimization screens using the hanging drop vapour diffusion method as described above, with crystallization conditions pursued based on the automated sparse matrix screens.

One important consideration for observing initial promising crystallization conditions is the possibility of individual crystallization of the p85-BH or Rab5 protein. If a selected crystallization condition serves as an ideal condition for one protein this could result in the dissociation of that protein from the complex, to form a crystal with the free molecules of itself while excluding our other protein from the crystal. Visual inspection of crystals alone would not be enough to identify whether this individual crystallization had occurred, potentially resulting in the collection of X-ray diffraction data of crystals that only contain one protein rather than our complex of interest.

In order to identify the possibility of this individual crystallization, without collecting X-ray diffraction data of a crystal that doesn't contain the protein complex, comparison of the crystallization conditions previously used for the respective proteins could provide us with insight. If the crystallization conditions are the same as we used for p85-BH (0.1 M sodium cacodylate pH 6.0, 1.5 M Li_2SO_4, 4-8% [w/v] glycerol), that Musacchio *et al.* used for the human

p85 BH domain structure (3.6 M sodium formate pH 5.0) (Musacchio *et al.*, 1996), or that Zhu *et al.* used to solve the Rab5 (15-184) structure (50-100 mM 4-morpholineethanesulfonic acid pH 6.0, 0.2 M NaCl, 1 mM $MgCl_2$, 10% [w/v] PEG 6000, 0.1% [v/v] ß-mercaptoethanol) (Zhu *et al.*, 2003), closer examination of the crystals to determine presence of one or both proteins would be warranted. Crystallization under the same or similar conditions could result in the crystallization of an individual protein rather than the complex. Comparison of the crystal forms obtained under these conditions and for the individual proteins previously crystallized can allow us to observe additional similarities and differences prior to collecting X-ray diffraction data. For more quantitative analysis crystals could be removed from the crystallization drop, washed in fresh crystallization solution to remove proteins not incorporated into the crystal, dissolved in SDS, and then analyzed by SDS-PAGE followed by Western blotting to detect the presence of one or both proteins in the crystal. If both proteins are detected then collection of X-ray diffraction data at the CLS would be warranted.

Once X-ray diffraction data is collected we would process this data using HKL2000 software installed at the CLS (Otwinowski and Minor, 1997). Structure solution would be performed using PHENIX software (Adams *et al.*, 2010) with previously solved p85-BH and Rab5 structures used for molecular replacement search motifs. Improvement of the accuracy of the determined structure would be performed by using *Coot* software (Emsley *et al.*, 2010) and the phenix.refine operation in PHENIX.

5.5 Dimerization status of full-length human p85 wild-type and mutants using SEC and MALS

Following our SEC and MALS analysis of the full-length human p85 protein, the potential concentration dependent nature of protein dimerization requires further examination.

Having examined the dimerization state of human p85 wild-type and cancer-associated and engineered mutants (L30F, F69L, I82F, E137K, D168R, I177N, E212R, E217K, H234D, Q241D, R262T, K288Q, E297K) at 0.7 mg/mL concentration through SEC and Native PAGE we did not observe any significant effects of these mutants on dimerization. Our analysis of p85 wild-type through MALS analysis showed a decrease in determined MW to correspond with decreasing protein concentration (concentrations used were 4 mg/mL, 2 mg/mL, 1 mg/mL, 0.7 mg/mL, 0.5 mg/mL), suggesting mixed populations of dimer and monomer at 2 mg/mL and 1

mg/mL protein concentrations, and monomeric populations at 0.7 mg/mL and 0.5 mg/mL. The 4 mg/mL concentration showed extensive aggregation of protein. The determined oligomeric state at 0.7 mg/mL p85 is different when detected through SEC with Native PAGE (dimeric) and our MALS data (monomeric).

One possible reason for the discrepancy between the SEC and Native PAGE results as compared to the MALS results could be due to the shape of the p85 molecule. Molecular shape can affect the rate of movement through the media of the SEC column or gel matrix of Native PAGE, resulting in the calculated sizes based on elution volume or gel migration varying from what is actually biologically present. However, it seems unlikely that a monomeric p85 molecule would run so that it appears to be twice its actual MW. The MW determined by MALS is supposed to take into account the dimensions of the molecule in solution, avoiding such potential problems (Wyatt, 1993). However, our MALS analysis of 0.7 mg/mL p85 protein had a determined MW of 72 kDa, which is smaller than the 85 kDa MW for a p85 monomer.

5.5.1 Future experiments for examining the role of concentration and mutations in determining the oligomeric state of p85

Further experiments are required to better characterize the role of concentration and mutations on p85 oligomerization.

One experiment to provide comparison between the SEC and MALS results will be to perform SEC on a wider range of human p85 wild-type proteins to observe any changes in their elution volume, and therefore calculated MW. We will load 2 mg/mL, 1 mg/mL, and 0.5 mg/mL p85 concentrations for SEC analysis. Any observed changes in the elution volume could also help us to observe how significantly the protein shape affects the SEC results, for if we see a large increase in calculated MW at the higher protein concentrations this could suggest that the shape of the p85 protein significantly changes the elution volume for SEC experiments. If we do not observe a significant shift in elution volume at these different concentrations, we could also pursue these multiple concentrations of SEC experiments for the various p85 mutants to examine any changes to the oligomerization state.

Analysis of the p85 mutants via MALS at concentrations of 2 mg/mL, 1 mg/mL, 0.7 mg/mL, and 0.5 mg/mL can allow us to better characterize any changes to the dimerization status of the protein that these mutations might cause across the range of concentrations. These

experiments would be important for determining how these mutants affect the oligomerization state of p85 if we observe a significant difference in the elution volumes and calculated MW during the range of concentration experiments for SEC, as molecular shape should have less effect on the MALS results.

Results from these experiments can be further verified by Native PAGE, by running samples from across the various protein concentrations.

5.6 Binding of lipid by p85 through PIP strip analysis

Observed binding of various phosphorylated lipids by p85 was one of our most interesting results (**Figure 4.13, Figure 4.14**). With the observed potential novel binding pocket in our structure serving as the basis for our search for novel binding partners, the selective interaction between lipids containing solvent accessible phosphates was quite pronounced. The prevalence of PIP lipids that showed binding with p85, and that unphosphorylated phosphatidylinositol showed no appreciable binding, also raise interesting possibilities for physiological significance behind this lipid binding activity that is worth further examination.

5.6.1 Potential physiological significance for observed lipid binding

Based on the important regulatory role that the p85 protein plays in the PI3K/PTEN pathway, observing the ability of p85 to directly bind to various PIP lipids that play important roles in that pathway raises several exciting possibilities. One is that through direct binding to $PI4,5P_2$ and $PI3,4,5P_3$ the p85 protein brings these lipid substrate molecules into better proximity to its protein partners p110 or PTEN, helping to promote the catalytic activity of these proteins on their lipid substrates. If the lipids are bound in the potential novel binding pocket which contains several residues that were shown to be important for p85 binding to PTEN (**Figure 1.10**) it could also suggest that the interaction between p85 and PTEN may be enhanced by, or dependent on, the presence of lipid between the two proteins. If this is the case further considerations would need to be taken into account for characterization experiments based on purified p85 and PTEN proteins, as this lack of lipid present could alter the results of such experiments.

The fact that $PI4,5P_2$ and $PI3,4,5P_3$, the key PIP lipids in the PI3K/PTEN pathway, show less binding than the other PIP lipids tested against p85 is also interesting. As these lipids serve

as substrate and product for the reactions performed by p110, and in reverse PTEN, as the products for these reactions it makes sense for p85 to not bind them too tightly, to ensure their release and normal cellular function following catalysis, as well as to allow for binding of another substrate. It would be interesting to determine if interacting with p110 would alter the lipid binding profile of p85 to more strongly bind $PI4,5P_2$, or more weakly bind $PI3,4,5P_3$ to promote the p110 directed path of the reaction, and if the opposite would occur during p85 binding to PTEN.

5.6.2 Comparison of p85-BH SO_4 positions with inositol head groups

Due to the observed binding between the p85 BH domain and the various phosphorylated lipids through our PIP strip experiments, we wanted to compare the positions of the electron densities we assigned to SO_4 ions with the phosphates attached to PIP lipid head groups. This would allow us to compare the distances between the electron densities and the PIP phosphate groups to determine whether they would fit within this region.

To examine this we used the structure of inositol 1,3,4,5-tetrakisphosphate present in PDB ID# 1BWN (Baraldi *et al.*, 1999). We then positioned the inositol 1,3,4,5-tetrakisphosphate within our p85-BH structure near the potential binding pocket in *Coot*, and used the Real Space Refine Zone and Regularize Zone commands to finalize the position based on the previously calculated electron density (Emsley *et al.*, 2010). A resulting structure is provided in **Figure 5.4**. The phosphate groups located two carbons apart from each other on the six-carbon ring, carbon 3 and carbon 5 for example, fit extremely well within the calculated electron densities.

In **Figure 5.4** two possible orientations of the bound inositol 1,3,4,5-tetrakisphosphate have been presented. The first involves the binding at phosphates 1 and 3. As phosphate 1 would contain the lipid chain in PIP lipids, positioning the lipid chain adjacent to the p85 protein surface. This interaction orientation would be affected by membrane-bound PIP lipids, as binding to phosphate 1 would require the BH domain to be in very close proximity to the plasma membrane, which could result in steric interference depending on binding partners or the orientation of other domains of p85. The second orientation involves the binding at phosphates 3 and 5. As these phosphates are not involved in the lipid chain that serves to anchor PIP lipids to the plasma membrane they may be more easily accessible for the protein to bind and interact with.

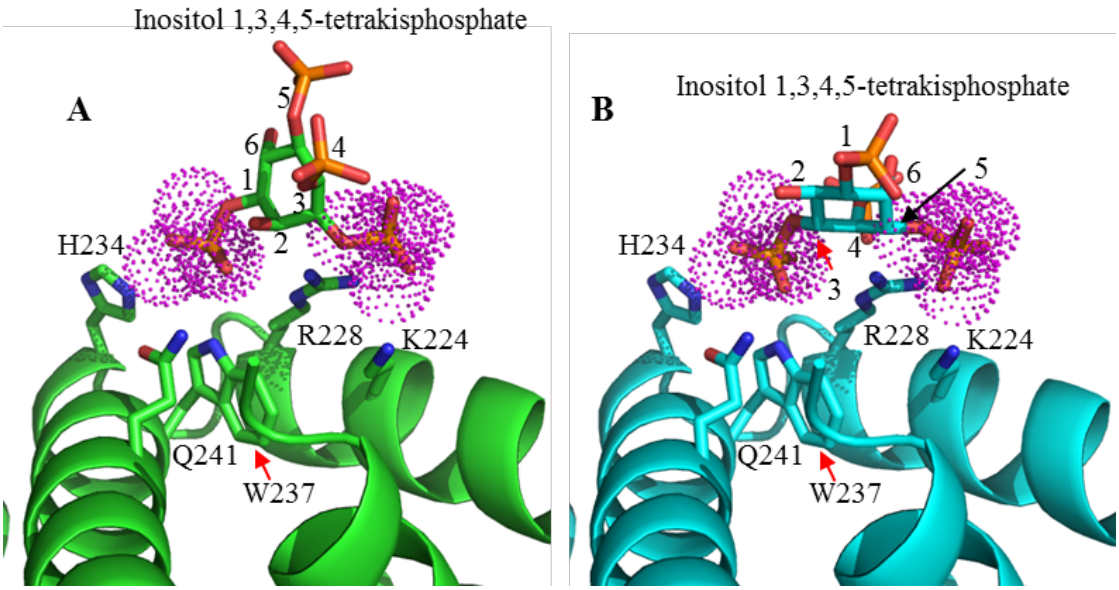

Figure 5.4 p85-BH potential binding pocket with overlaid inositol head group. Close up of the potential binding pocket of p85-BH with an inositol 1,3,4,5-tetrakisphosphate placed based on the positions of the SO_4 ion previously positioned. Side chains of involved residues and the inositol group are represented in stick format, and previously modelled SO_4 ion regions are represented as clouds of magenta dots. Inositol groups are positioned so that phosphates at positions 1 and 3 (**A**) or phosphates at positions 3 and 5 (**B**); are located where the electron densities assigned to SO_4 ions were present.

This examination suggests that the potential novel binding pocket could serve to bind PI3,4,5P_3 based on the positions of the calculated electron densities observed. The effect of mutations on lipid binding can provide biochemical evidence towards these initial observations.

5.7 Computer modelling of the p85-BH homodimer and PTEN complex

In order to determine a potential orientation between the p85 BH domain homodimer and the PTEN protein, we performed protein docking analysis using ClusPro server (Comeau *et al.*, 2004a, b; Kozakov *et al.*, 2006; Kozakov *et al.*, 2017). We selected this server due to its ease of use and its previous success in structural interaction competitions such as CAPRI (Critical Assessment of Predicted Interactions) (Kozakov *et al.*, 2017). Previous docking studies had been performed between the p85 BH domain and PTEN by Cheung *et al.* incorporating data from mutations that affected p85 homodimerization (I177N) or binding to PTEN (I127A, I133A, E137A) (Cheung *et al.*, 2015). This study did not include the residues important for p85 binding PTEN (our unpublished data; **Figure 1.10**), and so we wished to pursue this docking analysis incorporating this knowledge as well. This would help us to determine if the p85 protein could

have an uncharacterized role in helping orient lipid molecules that could explain the enhanced PTEN phosphatase activity we have observed upon p85 binding (Chagpar *et al.*, 2010).

Docking analysis was performed using the previously solved PTEN crystal structure, PDB ID# 1D5R, as our "receptor" molecule (Lee *et al.*, 1999). Our p85-BH structure was used as the "ligand" molecule, including both chains of the homodimer as homodimerization was shown to be important for p85:PTEN binding (Cheung *et al.*, 2015). Attraction residues were assigned for D168, E212, H234, Q241 of the A chain due to their role in p85 binding to PTEN in the purified protein binding experiments (**Figure 1.10**). We only assigned attraction residues to the A chain as the corresponding residues in the B chain of the p85 BH homodimer are oriented facing in opposite directions relative to the A chain residues, making it unlikely that a single PTEN protein would be interacting with these residues on both p85 BH domains at the same time. This prevented generation of additional possible structures of the same orientation on different protein chains, as the two chains have nearly identical structures. The ten output clusters of highest scoring arrangements were collected, the structures examined using PyMOL.

Summary of the ClusPro output clusters are provided in **Table 5.1**. A comparison of the various output clusters are shown in **Figure 5.5**.

Table 5.1 ClusPro output clusters statistics

		Representative Weighted Score	
Output Cluster	**Cluster Members**	**Center**	**Lowest Energy**
0	61	-713.4	-836.5
1	60	-751.2	-835.2
2	45	-740.4	-933.1
3	44	-736.2	-1004.3
4	43	-688.1	-895.0
5	36	-776.0	-908.5
6	32	-725.9	-770.4
7	32	-745.9	-748.1
8	26	-700.6	-808.3
9	26	-764.8	-764.8

For examining the ClusPro Output Clusters we used several criteria to determine which clusters to exclude from further analysis and which clusters to examine more thoroughly, based on biochemical analysis of the p85 and PTEN proteins. Cheung *et al.* have shown that PTEN binding to p85 is dependent of p85 dimerization, so we would expect the PTEN to interact with

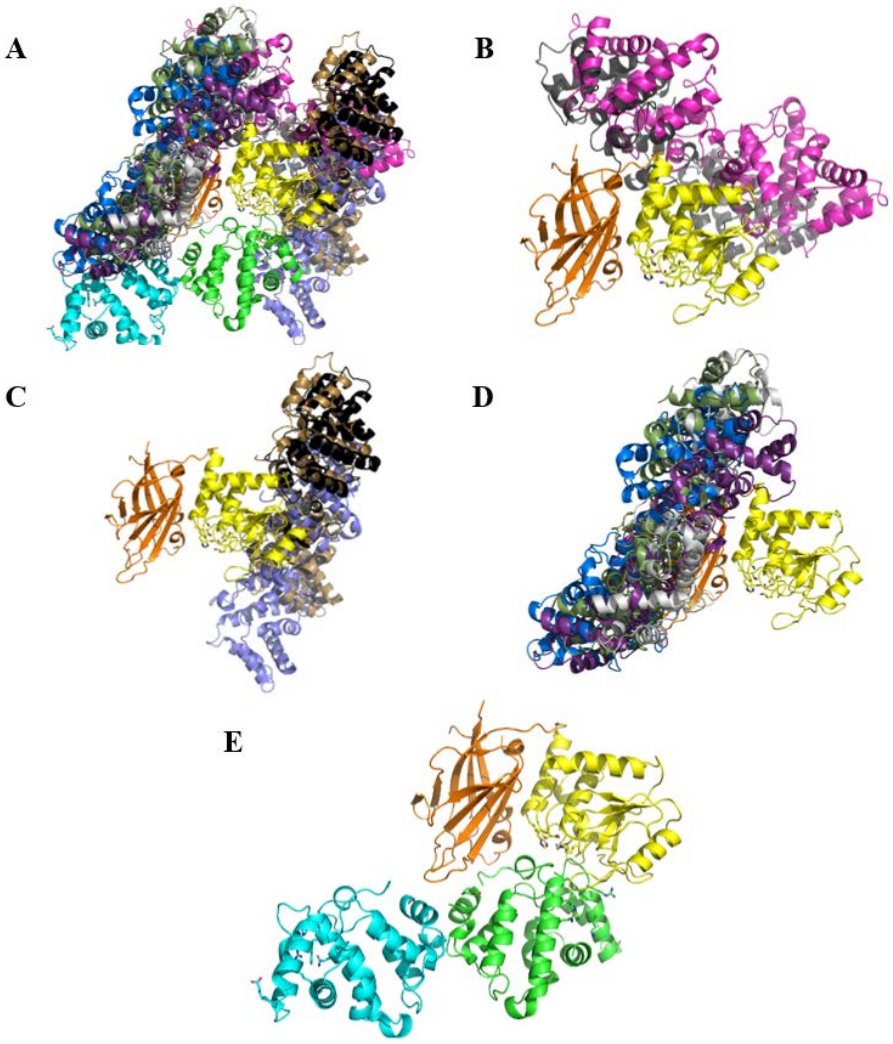

Figure 5.5 ClusPro docking results for p85 BH domain homodimer binding PTEN. Overlays of the calculated docking clusters of the p85 BH domain homodimer with PTEN (orange-C2 domain and yellow-phosphatase domain). Note the positions of the PTEN domains remains fixed, whereas the various possible orientations differ for the docked p85 BH domain homodimers. **A.** The ten most populous high scoring p85 BH docking clusters (0=magenta, 1=white, 2=lavender, 3=violet, 4=green and cyan, 5=blue, 6=olive, 7=brown, 8=grey, 9=black) with PTEN. **B.** Clusters 0 and 8. **C.** Clusters 2, 7 and 9. **D.** Clusters 1, 3, 5 and 6. **E.** Cluster 4

both members of the p85 BH homodimer (Cheung *et al.*, 2015). As p85 binding to PTEN stimulates PTEN phosphatase activity we would expect the p85 protein to bind near the catalytic pocket present in the PTEN phosphatase domain (Chagpar *et al.*, 2010). Das *et al.* determined that basic residues R161, K163, and K164 in the PTEN phosphatase domain are important for plasma membrane association, so we would expect these residues to not be concealed, and that

p85 proteins bound would not be oriented to extend into the plasma membrane (Das *et al.*, 2003). In addition we would expect the PTEN to associate with residues in p85 where mutation disrupted binding to PTEN, while not forming extensive interactions with residues where mutations did not alter PTEN binding (**Figure 1.10**).

All Output Clusters generated by ClusPro except for Cluster 4 show the PTEN protein interacting with the cleft formed at the homodimerization interface of the two p85 BH domains. Clusters 0 and 8 show this interaction primarily with the PTEN phosphatase domain on the opposite side of the protein from the catalytic pocket, with some minor contacts to the PTEN C2 domain, p85 is located on the opposite face of PTEN from the PTEN catalytic pocket, and many of the interaction sites are located around p85 residues that did not affect PTEN binding (**Figure 5.5 B**). Clusters 2, 7, and 9 interact exclusively with the PTEN phosphatase domain away from the catalytic pocket and are oriented such that they would extend into the plasma membrane (**Figure 5.5 C**). Clusters 1, 3, 5, and 6 interact exclusively with the PTEN C2 domain, are distant from the PTEN catalytic pocket, and are oriented so that they may extend into the plasma membrane (**Figure 5.5 D**). None of these observed interaction clusters are positioned to include residues D168, E212, H234, or Q241 within their interaction surfaces. In addition these interaction orientations often place the terminal S113 residue of the p85 BH domain tightly against the PTEN protein, which may not allow the addition of the inter-domain linker region that connects the p85 BH domain to the SH3 domain. Due to the lack of interaction with expected p85 residues, potential structural interference due to the orientation of the terminal p85 residues, and distance from the PTEN catalytic pocket, these Output Clusters are not consistent with the experimental data available.

The most interesting results from the ClusPro docking analysis are for Cluster 4 (**Figure 5.5 E, Figure 5.6**). Here both the C2 and phosphatase domains of the PTEN protein interact with the p85 protein, a loop of the C2 domain interacting with both of the monomers in the p85 BH domain homodimer and near the D168 residues for both p85 monomers as well. The PTEN C2 and phosphatase domains then continue to make contacts with a single p85 BH domain, in close proximity with p85 residues H234 and Q241, with these residues labeled in **Figure 5.6**. This orientation also positions the catalytic pocket of the PTEN phosphatase domain towards the p85 protein without obstructing the pocket. In addition, the PTEN protein is near the p85 potential binding pocket we had previously observed.

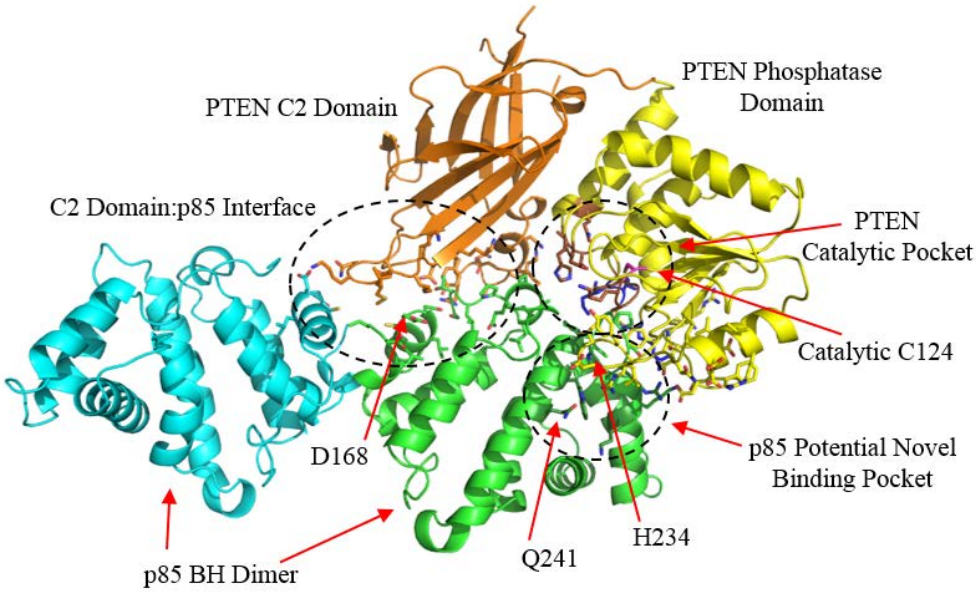

Figure 5.6 Examination of ClusPro Cluster 4 of p85 BH dimer PTEN complex. Orientation of Cluster 4 ClusPro server docking analysis between the p85 BH dimer and PTEN. The p85 BH domains are represented in green and cyan, PTEN C2 domain in orange, and PTEN phosphatase domain in yellow. Sidechains for protein function or potential interactions are represented in stick format, with PTEN residues important for membrane binding in blue, PTEN catalytic pocket residues in brown, and PTEN catalytic C124 in magenta.

The interface region between the PTEN C2 domain and the p85 BH dimer is shown in **Figure 5.7**. From the docking analysis there are a number of potential hydrogen bonding interactions between residues on PTEN and p85, either from side-chain to side-chain or side-chain to backbone. In addition, most of the PTEN residues involved in such interactions are found in flexible loop regions of the protein, which could allow for adjustments to their position to improve these possible interactions in the protein complex. A list of residues that have the potential to form hydrogen bonds can be found in **Table 5.2**.

D168 was one of the residues identified to be important for p85 binding to PTEN, and its presence in this region agrees with that, as does its sidechain belonging to a potential hydrogen bonding site (**Figure 1.10**). Determining if mutations to PTEN residues K263, K266, K327, R335, or Y336 affect the binding to p85 could clarify if this region is involved in complex formation. Furthermore, point-mutation of Y336 residue has been found in human cancers, as recorded in the Catalogue of Somatic Mutations in Cancer database (http://www.sanger.ac.uk/genetics/CGP/cosmic) and Y336 has been shown to be a site of

Table 5.2 Potential hydrogen binding sites between PTEN and p85 based on docking results

PTEN Residues	p85 Residues
Y336 (sidechain)	T114 (backbone nitrogen)
R335 (sidechain)	S113 (backbone oxygen)
K327 (sidechain)	T114 (backbone oxygen)
K266 (sidechain)	D166 (backbone oxygen)
L265 (backbone oxygen)	D168 (sidechain)
K263 (sidechain)	D166 (Chain B, backbone oxygen)
Q17 (sidechain)	S229, R228, K225 (sidechains)
D19 (sidechain)	R228, K225 (sidechains)
D22 (sidechain)	R228, K225 (sidechains)

phosphorylation by FRK, also called Rak (Yim *et al.*, 2009). Phosphorylation of PTEN Y336 by FRK was shown to protect PTEN from ubiquitin-mediated proteosomal degradation mediated by the E3 ubiquitin ligase Nedd4-1, while mutations of Y336F prevented PTEN phosphorylation and resulted in a significant increase in the rate of PTEN protein degradation (Yim *et al.*, 2009). Our current model of the interaction region between the p85 BH domain and PTEN, shown in **Figure 5.7**, there could be space for the Y336 residue to be phosphorylated following a reorientation of the p85 D166 sidechain, and the phosphate could potentially form hydrogen bonds with the backbone nitrogens of p85 S113 and T114. It is also possible that the increase in protein stability for PTEN by binding to p85 is due to this interaction interface preventing Nedd4-1 from binding to and ubiquitinating PTEN. If PTEN was not phosphorylated interaction with p85 could also prevent binding to and phosphorylation of PTEN by FRK.

Examination of the docking results from the perspective of the plasma membrane was performed, determined based on the location of PTEN residues R161, K163, and K164 which had been identified as important for PTEN to associate with the plasma membrane (Das *et al.*, 2003). As shown in **Figure 5.8** there is a cavity between the two proteins that allows access to the PTEN phosphatase catalytic pocket. To determine if this cavity would be large enough to accommodate a PI3,4,5P_3 molecule we manually modelled in a 4-carbon PI3,4,5P_3 obtained from the PDB (PDB ID# 4PT) using the ideal conformation for the ligand molecule. This 4-carbon PI3,4,5P_3 was successfully positioned within the observed cavity and into the PTEN phosphatase catalytic pocket.

A comparative view of the PTEN phosphatase catalytic pocket can be found in **Figure 5.9**, showing the tartrate molecule present within the crystal structure of PTEN solved by Lee *et*

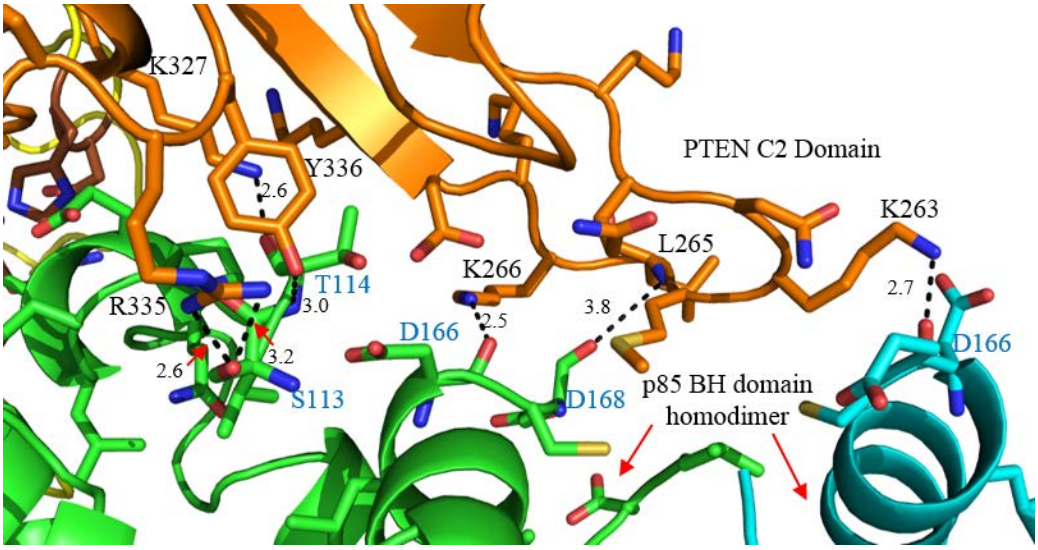

Figure 5.7 Docking analysis interface between p85 BH domain dimer and PTEN C2 domain. Close up view of the interface between the PTEN C2 domain (orange) and the p85 BH dimer (green and cyan) determined in ClusPro docking Cluster 4. Sidechains of residues near the protein interface are represented in stick format. Potential hydrogen bonding sites are indicated with dotted lines and their distances labelled in Angstoms. PTEN residues are labelled in black, p85 residues are labelled in blue. Potential hydrogen bonding sites are: PTEN R335 sidechain with p85 S113 backbone oxygen, PTEN K327 sidechain with p85 T114 backbone oxygen, PTEN Y336 with p85 T114 backbone nitrogen, PTEN K266 sidechain with p85 D166 backbone oxygen, PTEN L265 backbone oxygen with p85 D168 sidechain, PTEN K263 sidechain with p85 Chain B D166 backbone oxygen. Perspective rotated 180° relative to **Figure 5.6**.

al. (**Figure 5.9A**), or the manually modelled 4-carbon PI3,4,5P_3 molecule (**Figure 5.9B**) (Lee *et al.*, 1999).

For the manually modelled 4-carbon PI3,4,5P_3 it currently has the phosphate in the 4 position closest to the catalytic C124 residue, where we would expect the phosphate in the 3 position to be based on the catalytic function of PTEN. This is likely due to the rigidity of the idealized bond arrangement for the 4-carbon PI3,4,5P_3 used, and with the flexibility found in the actual molecule proper positioning of the phosphate in the 3 position could be possible within the catalytic pocket. It is also interesting to note that the p85 residues found near the PTEN catalytic pocket are in position to frame it, with the closest residues being prolines and a serine residue with its sidechain facing away from the pocket. These residues would not interfere with the entry of lipid molecules to this catalytic pocket and are positioned to frame the PTEN catalytic pocket, potentially helping to orient the bound lipid.

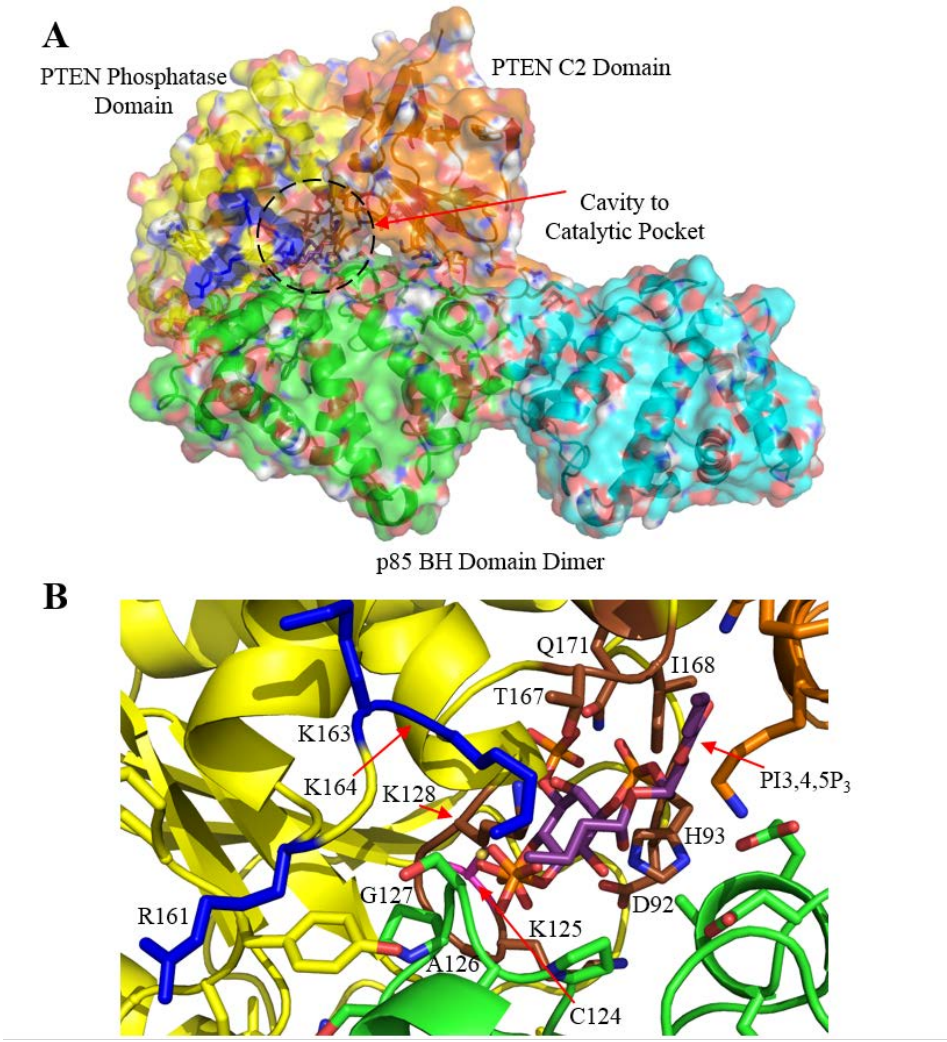

Figure 5.8 Potential cavity leading to PTEN catalytic pocket. A. View from the plasma membrane perspective of the ClusPro Docking Cluster 4, with p85 BH domains in green and cyan, PTEN phosphatase domain in yellow, PTEN C2 Domain in orange, and PTEN residues important for lipid binding in blue. A cavity containing a modeled 4-carbon PI3,4,5P_3 molecule is highlighted with a dashed circle. **B.** Close up view of the PTEN phosphatase catalytic pocket, shown in brown with the catalytic C124 in magenta, with the 4-carbon PI3,4,5P_3 shown in purple with its phosphate groups in orange shown in the same orientation as panel A.

Examining the positions of the PTEN catalytic pocket with the p85 potential binding pocket, shown in **Figure 5.9 C**, reveals that the two regions are separated from each other and not in direct contact. This means that it would be unlikely for the p85 potential binding pocket to assist PTEN catalytic function by helping to bind lipid and position it in the PTEN catalytic pocket.

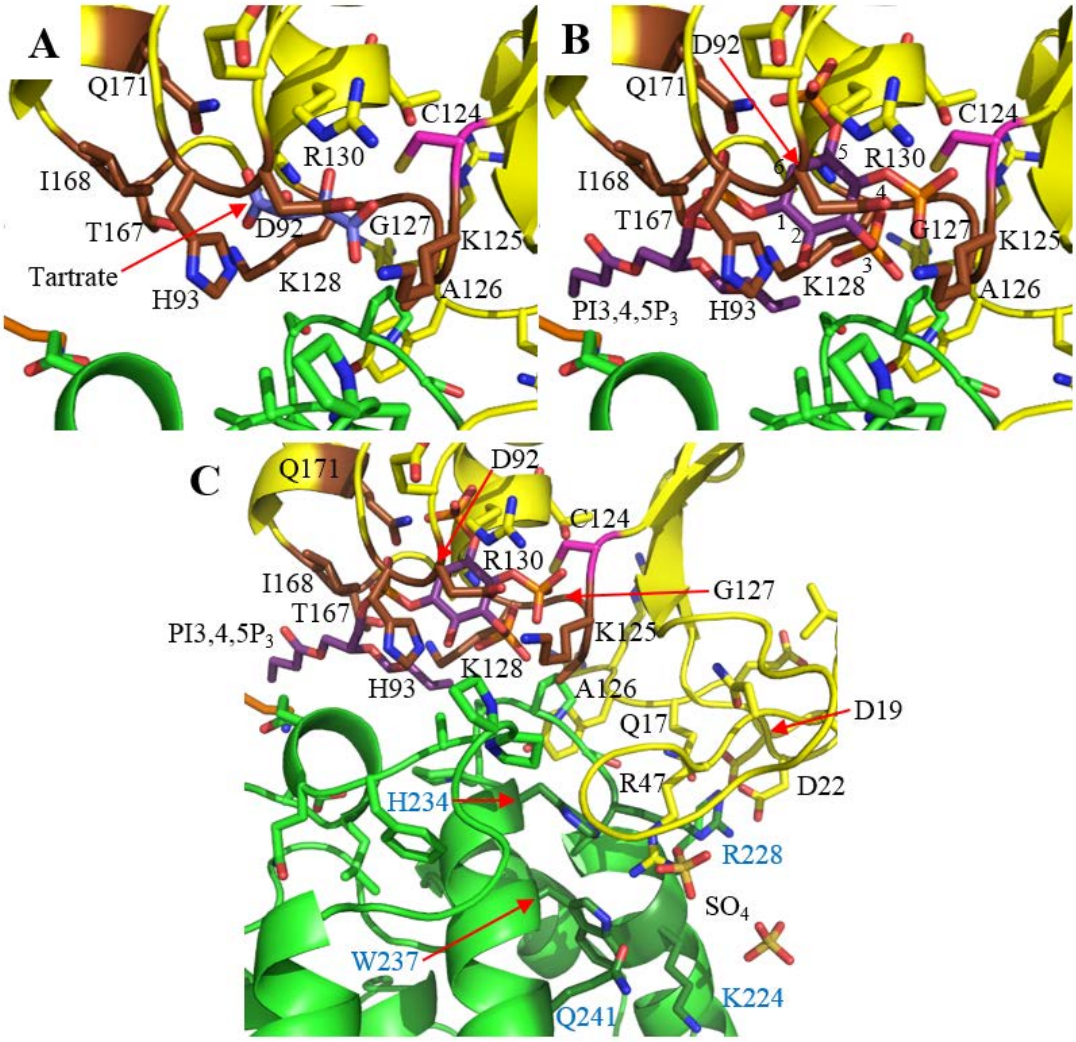

Figure 5.9 Examination of the PTEN phosphatase catalytic pocket, with spatial comparison to p85 BH domain potential binding pocket. PTEN phosphatase domain is shown in yellow, with catalytic pocket residues in brown and the catalytic C124 residue in magenta. Shown bound within the pocket are **A.** the tartrate (violet) present in the previously solved PTEN crystal structure (Lee *et al.*, 1999) **B.** Or the modelled 4-carbon PI3,4,5P_3 molecule (purple). **C.** A view showing the relative positioning between the PTEN catalytic pocket and the p85 BH domain potential binding pocket, including the SO_4 molecules that had been placed within the p85-BH structures solved.

A closer examination of the p85 potential binding pocket with respect to the PTEN phosphatase domain is shown in **Figure 5.10**.

Within the docking structure there is a large conformational adjustment of the p85 R228 sidechain, positioning itself to potentially form hydrogen bonds with Q17 or D22. Other potential hydrogen bonds can occur between p85 K225 with PTEN Q17 or D19, and the p85 S229 with Q17. It is possible that these residues play a role in binding between p85 and PTEN, as

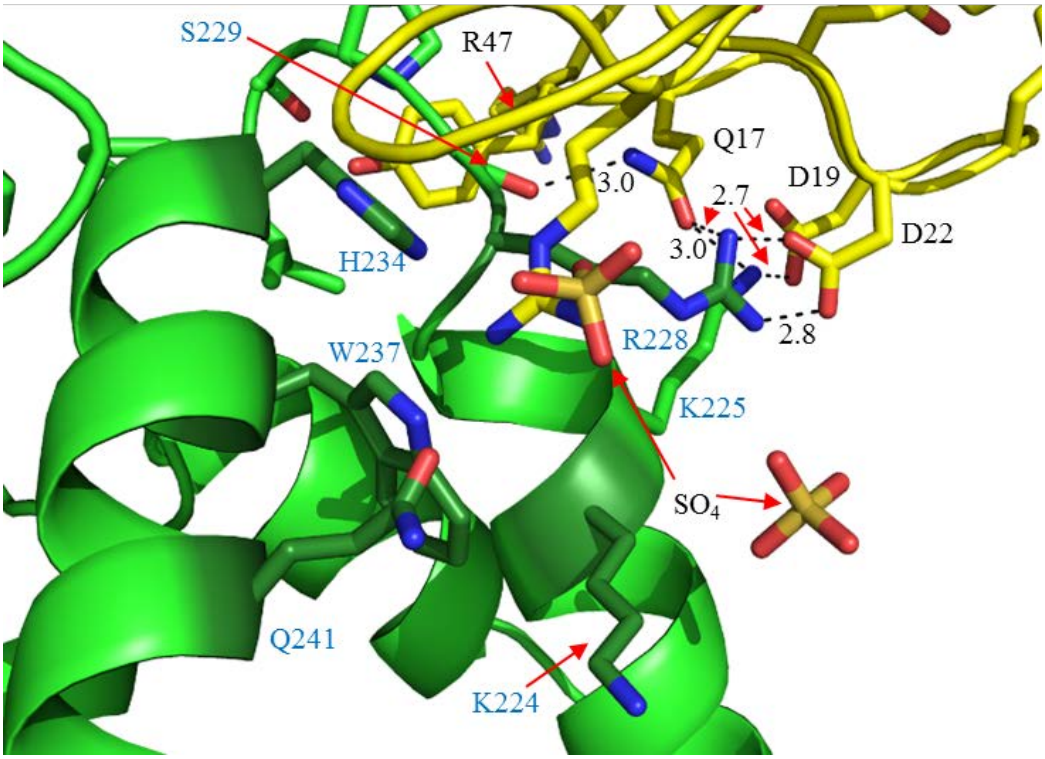

Figure 5.10 Interface between PTEN and p85 near the p85 potential binding pocket. ClusPro docking of PTEN:p85 BH domain dimer examining the interface near the p85 potential binding pocket. PTEN phosphatase domain is in yellow, and the p85 BH domain is in green. SO_4 molecules from the p85-BH crystal structure determined are also shown. PTEN residues are labelled in black and p85 residues are labelled in blue. Potential hydrogen bonding sites are shown as dashed lines with their distances labelled in Angstroms.

mutagenesis of p85 residues R228 and K225 showed decreased binding strength in the cell based binding assays previously performed by Ruan *et al.* (**Figure 1.10**). The sidechain of PTEN R47 is oriented towards the p85 potential binding pocket region, and may be able to replace the p85 R228 sidechain that has altered its orientation to interact with the PTEN protein. Comparison of the positions of involved sidechains between our previously solved p85-BH structure and the docking results show only minor adjustments to the positions of the other residues surrounding the potential binding pocket, K224, H234, W237, and Q241.

This docking model incorporates a number of the observations for residues important in the interaction between p85 and PTEN (**Figure 1.10**). The interaction between the PTEN C2 domain with both p85 BH domains in the homodimer also agrees with the observed dependence of p85 dimerization on PTEN binding (Cheung *et al.*, 2015). The positions of D168, K225, and R228 from p85 allowing for potential hydrogen bonding with PTEN residues offers a potential explanation for the observed effects of mutations to these residues on PTEN binding. H234 is

also located in close proximity to the p85:PTEN interface, although no potential binding interactions were observed for it in the observed model.

Examining the predicted interfaces between the two proteins provides additional mutagenesis targets to observe if they alter the binding between p85 and PTEN. The position of the PTEN catalytic pocket and the p85 potential binding pocket suggest that this region of p85 would not stimulate PTEN activity through additional coordination of lipid molecules for PTEN catalysis. Mutational studies of PTEN residues at the interface between p85 and the PTEN C2 domain, shown in **Figure 5.7** and **Table 5.2**, can help determine if they play a role in complex formation with p85.

This study has combined data collected from biochemical studies, high resolution structural data, and computation protein docking. From our protein experiments we have observed a novel function for the p85 protein, direct binding to lipid molecules. Examination of the structural data obtained provided us with a region of interest to examine regarding this novel biological function, the potential binding pocket observed in the p85 BH domain. Finally our docking studies have provided a potential orientation to the complex formed between the PTEN protein and the p85 BH domain homodimer, revealing additional residues worth examining through mutagenesis studies in order to support or disprove this possible orientation. Better understanding of how this interaction between PTEN and p85 regulates PTEN activity and protein stability may reveal a role in cancers with low PTEN protein levels but where PTEN expression levels are not altered.

6.0 References

Adams, P.D., Afonine, P.V., Bunkoczi, G., Chen, V.B., Davis, I.W., Echols, N., Headd, J.J., Hung, L.W., Kapral, G.J., Grosse-Kunstleve, R.W., *et al.* (2010). PHENIX: a comprehensive Python-based system for macromolecular structure solution. Acta Cryst. D *66*, 213-221.

Alessi, D.R., James, S.R., Downes, C.P., Holmes, A.B., Gaffney, P.R., Reese, C.B., and Cohen, P. (1997). Characterization of a 3-phosphoinositide-dependent protein kinase which phosphorylates and activates protein kinase Balpha. Curr. Biol. *7*, 261-269.

Ali, B.R., Wasmeier, C., Lamoreux, L., Strom, M., and Seabra, M.C. (2004). Multiple regions contribute to membrane targeting of Rab GTPases. J. Cell. Sci. *117*, 6401-6412.

Backer, J.M. (2010). The regulation of class IA PI 3-kinases by inter-subunit interactions. Curr. Top. Microbiol. Immunol. *346*, 87-114.

Baraldi, E., Djinovic Carugo, K., Hyvonen, M., Surdo, P.L., Riley, A.M., Potter, B.V., O'Brien, R., Ladbury, J.E., and Saraste, M. (1999). Structure of the PH domain from Bruton's tyrosine kinase in complex with inositol 1,3,4,5-tetrakisphosphate. Structure *7*, 449-460.

Batra-Safferling, R., Granzin, J., Modder, S., Hoffmann, S., and Willbold, D. (2010). Structural studies of the phosphatidylinositol 3-kinase (PI3K) SH3 domain in complex with a peptide ligand: role of the anchor residue in ligand binding. Biol. Chem. *391*, 33-42.

Beattie, E.C., Howe, C.L., Wilde, A., Brodsky, F.M., and Mobley, W.C. (2000). NGF signals through TrkA to increase clathrin at the plasma membrane and enhance clathrin-mediated membrane trafficking. J. Neurosci. *20*, 7325-7333.

Bonifant, C.L., Kim, J.S., and Waldman, T. (2007). NHERFs, NEP, MAGUKs, and more: interactions that regulate PTEN. J. Cell. Biochem. *102*, 878-885.

Bos, J.L., Rehmann, H., and Wittinghofer, A. (2007). GEFs and GAPs: critical elements in the control of small G proteins. Cell *129*, 865-877.

Brunet, A., Bonni, A., Zigmond, M.J., Lin, M.Z., Juo, P., Hu, L.S., Anderson, M.J., Arden, K.C., Blenis, J., and Greenberg, M.E. (1999). Akt promotes cell survival by phosphorylating and inhibiting a Forkhead transcription factor. Cell *96*, 857-868.

Cantley, L.C. (2002). The phosphoinositide 3-kinase pathway. Science *296*, 1655-1657.

Carnero, A. (2010). The PKB/AKT pathway in cancer. Curr. Pharm. Des. *16*, 34-44.

Carpenter, C.L., Duckworth, B.C., Auger, K.R., Cohen, B., Schaffhausen, B.S., and Cantley, L.C. (1990). Purification and characterization of phosphoinositide 3-kinase from rat liver. J. Biol. Chem. *265*, 19704-19711.

Carracedo, A., and Pandolfi, P.P. (2008). The PTEN-PI3K pathway: of feedbacks and cross-talks. Oncogene *27*, 5527-5541.

Chagpar, R.B., Links, P.H., Pastor, M.C., Furber, L.A., Hawrysh, A.D., Chamberlain, M.D., and Anderson, D.H. (2010). Direct positive regulation of PTEN by the p85 subunit of phosphatidylinositol 3-kinase. Proc. Natl. Acad. Sci. U.S.A. *107*, 5471-5476.

Chalhoub, N., and Baker, S.J. (2009). PTEN and the PI3-kinase pathway in cancer. Annu. Rev. Pathol. *4*, 127-150.

Chamberlain, M.D., Berry, T.R., Pastor, M.C., and Anderson, D.H. (2004). The p85alpha subunit of phosphatidylinositol 3'-kinase binds to and stimulates the GTPase activity of Rab proteins. J. Biol. Chem. *279*, 48607-48614.

Cherfils, J., and Zeghouf, M. (2013). Regulation of small GTPases by GEFs, GAPs, and GDIs. Physiol. Rev. *93*, 269-309.

Cheung, L.W., Hennessy, B.T., Li, J., Yu, S., Myers, A.P., Djordjevic, B., Lu, Y., Stemke-Hale, K., Dyer, M.D., Zhang, F., *et al.* (2011). High frequency of PIK3R1 and PIK3R2 mutations in endometrial cancer elucidates a novel mechanism for regulation of PTEN protein stability. Cancer Discov. *1*, 170-185.

Cheung, L.W., Walkiewicz, K.W., Besong, T.M., Guo, H., Hawke, D.H., Arold, S.T., and Mills, G.B. (2015). Regulation of the PI3K pathway through a p85alpha monomer-homodimer equilibrium. eLife *4*, e06866.

Comeau, S.R., Gatchell, D.W., Vajda, S., and Camacho, C.J. (2004a). ClusPro: a fully automated algorithm for protein-protein docking. Nucleic Acids Res. *32*, W96-99.

Comeau, S.R., Gatchell, D.W., Vajda, S., and Camacho, C.J. (2004b). ClusPro: an automated docking and discrimination method for the prediction of protein complexes. Bioinformatics *20*, 45-50.

Das, S., Dixon, J.E., and Cho, W. (2003). Membrane-binding and activation mechanism of PTEN. Proc. Natl. Acad. Sci. U.S.A. *100*, 7491-7496.

del Peso, L., Gonzalez-Garcia, M., Page, C., Herrera, R., and Nunez, G. (1997). Interleukin-3-induced phosphorylation of BAD through the protein kinase Akt. Science *278*, 687-689.

Desbois-Mouthon, C., Blivet-Van Eggelpoel, M.J., Beurel, E., Boissan, M., Delelo, R., Cadoret, A., and Capeau, J. (2002). Dysregulation of glycogen synthase kinase-3beta signaling in hepatocellular carcinoma cells. Hepatology *36*, 1528-1536.

Diekmann, D., Brill, S., Garrett, M.D., Totty, N., Hsuan, J., Monfries, C., Hall, C., Lim, L., and Hall, A. (1991). Bcr encodes a GTPase-activating protein for p21rac. Nature *351*, 400-402.

Emsley, P., Lohkamp, B., Scott, W.G., and Cowtan, K. (2010). Features and development of Coot. Acta Cryst. D *66*, 486-501.

Fodje, M., Grochulski, P., Janzen, K., Labiuk, S., Gorin, J., and Berg, R. (2014). 08B1-1: an automated beamline for macromolecular crystallography experiments at the Canadian Light Source. J. Synchrotron Radiat. *21*, 633-637.

French, A.R., Sudlow, G.P., Wiley, H.S., and Lauffenburger, D.A. (1994). Postendocytic trafficking of epidermal growth factor-receptor complexes is mediated through saturable and specific endosomal interactions. J. Biol. Chem. *269*, 15749-15755.

Garcia-Echeverria, C., and Sellers, W.R. (2008). Drug discovery approaches targeting the PI3K/Akt pathway in cancer. Oncogene *27*, 5511-5526.

Ghai, R., Falconer, R.J., and Collins, B.M. (2012). Applications of isothermal titration calorimetry in pure and applied research--survey of the literature from 2010. J. Mol. Recogn. *25*, 32-52.

Goh, L.K., and Sorkin, A. (2013). Endocytosis of receptor tyrosine kinases. Cold Spring Harb. Perspect. Biol. *5*, a017459.

Gorden, P., Carpentier, J.L., Cohen, S., and Orci, L. (1978). Epidermal growth factor: morphological demonstration of binding, internalization, and lysosomal association in human fibroblasts. Proc. Natl. Acad. Sci. U.S.A. *75*, 5025-5029.

Gould, N., Doulias, P.T., Tenopoulou, M., Raju, K., and Ischiropoulos, H. (2013). Regulation of protein function and signaling by reversible cysteine S-nitrosylation. J. Biol. Chem. *288*, 26473-26479.

Greenfield, N., and Fasman, G.D. (1969). Computed circular dichroism spectra for the evaluation of protein conformation. Biochemistry *8*, 4108-4116.

Grochulski, P., Fodje, M.N., Gorin, J., Labiuk, S.L., and Berg, R. (2011). Beamline 08ID-1, the prime beamline of the Canadian Macromolecular Crystallography Facility. J. Synchrotron Radiat. *18*, 681-684.

Gschwind, A., Fischer, O.M., and Ullrich, A. (2004). The discovery of receptor tyrosine kinases: targets for cancer therapy. Nat. Rev. Cancer *4*, 361-370.

Haigler, H.T., McKanna, J.A., and Cohen, S. (1979). Rapid stimulation of pinocytosis in human carcinoma cells A-431 by epidermal growth factor. J. Cell Biol. *83*, 82-90.

Hanahan, D., Jessee, J., and Bloom, F.R. (1991). Plasmid transformation of Escherichia coli and other bacteria. Methods Enzymol. *204*, 63-113.

Harpur, A.G., Layton, M.J., Das, P., Bottomley, M.J., Panayotou, G., Driscoll, P.C., and Waterfield, M.D. (1999). Intermolecular interactions of the p85alpha regulatory subunit of phosphatidylinositol 3-kinase. J. Biol. Chem. *274*, 12323-12332.

Heyduk, T., Ma, Y., Tang, H., and Ebright, R.H. (1996). Fluorescence anisotropy: rapid, quantitative assay for protein-DNA and protein-protein interaction. Methods Enzymol. *274*, 492-503.

Hoedemaeker, F.J., Siegal, G., Roe, S.M., Driscoll, P.C., and Abrahams, J.P. (1999). Crystal structure of the C-terminal SH2 domain of the p85alpha regulatory subunit of phosphoinositide 3-kinase: an SH2 domain mimicking its own substrate. J. Mol. Biol. *292*, 763-770.

Hojlund, K. (2014). Metabolism and insulin signaling in common metabolic disorders and inherited insulin resistance. Dan. Med. J. *61*, B4890.

Huang, C.H., Mandelker, D., Schmidt-Kittler, O., Samuels, Y., Velculescu, V.E., Kinzler, K.W., Vogelstein, B., Gabelli, S.B., and Amzel, L.M. (2007). The structure of a human p110alpha/p85alpha complex elucidates the effects of oncogenic PI3Kalpha mutations. Science *318*, 1744-1748.

Huang, F., Khvorova, A., Marshall, W., and Sorkin, A. (2004). Analysis of clathrin-mediated endocytosis of epidermal growth factor receptor by RNA interference. J. Biol. Chem. *279*, 16657-16661.

Huang, F., Kirkpatrick, D., Jiang, X., Gygi, S., and Sorkin, A. (2006). Differential regulation of EGF receptor internalization and degradation by multiubiquitination within the kinase domain. Mol. Cell. *21*, 737-748.

Ingmundson, A., Delprato, A., Lambright, D.G., and Roy, C.R. (2007). Legionella pneumophila proteins that regulate Rab1 membrane cycling. Nature *450*, 365-369.

Jaffrey, S.R., Erdjument-Bromage, H., Ferris, C.D., Tempst, P., and Snyder, S.H. (2001). Protein S-nitrosylation: a physiological signal for neuronal nitric oxide. Nat. Cell Biol. *3*, 193-197.

Jia, Z., Barford, D., Flint, A.J., and Tonks, N.K. (1995). Structural basis for phosphotyrosine peptide recognition by protein tyrosine phosphatase 1B. Science *268*, 1754-1758.

Kashiwagi, A., Verso, M.A., Andrews, J., Vasquez, B., Reaven, G., and Foley, J.E. (1983). In vitro insulin resistance of human adipocytes isolated from subjects with noninsulin-dependent diabetes mellitus. J. Clin. Invest. *72*, 1246-1254.

Kong, R., Yi, F., Wen, P., Liu, J., Chen, X., Ren, J., Li, X., Shang, Y., Nie, Y., Wu, K., *et al.* (2015). Myo9b is a key player in SLIT/ROBO-mediated lung tumor suppression. J. Clin. Invest. *125*, 4407-4420.

Kozakov, D., Brenke, R., Comeau, S.R., and Vajda, S. (2006). PIPER: an FFT-based protein docking program with pairwise potentials. Proteins *65*, 392-406.

Kozakov, D., Hall, D.R., Xia, B., Porter, K.A., Padhorny, D., Yueh, C., Beglov, D., and Vajda, S. (2017). The ClusPro web server for protein-protein docking. Nat. Protoc. *12*, 255-278.

Laemmli, U.K. (1970). Cleavage of structural proteins during the assembly of the head of bacteriophage T4. Nature *227*, 680-685.

Lee, J.O., Yang, H., Georgescu, M.M., Di Cristofano, A., Maehama, T., Shi, Y., Dixon, J.E., Pandolfi, P., and Pavletich, N.P. (1999). Crystal structure of the PTEN tumor suppressor: implications for its phosphoinositide phosphatase activity and membrane association. Cell *99*, 323-334.

Li, N., Lorinczi, M., Ireton, K., and Elferink, L.A. (2007). Specific Grb2-mediated interactions regulate clathrin-dependent endocytosis of the cMet-tyrosine kinase. J. Biol. Chem. *282*, 16764-16775.

Liang, J., Chen, J.K., Schreiber, S.T., and Clardy, J. (1996). Crystal structure of P13K SH3 domain at 20 angstroms resolution. J. Mol. Biol. *257*, 632-643.

Liang, Y. (2008). Applications of isothermal titration calorimetry in protein science. Acta Biochim. Biophys. Sin. *40*, 565-576.

Liaw, D., Marsh, D.J., Li, J., Dahia, P.L., Wang, S.I., Zheng, Z., Bose, S., Call, K.M., Tsou, H.C., Peacocke, M., *et al.* (1997). Germline mutations of the PTEN gene in Cowden disease, an inherited breast and thyroid cancer syndrome. Nat. Genet. *16*, 64-67.

Liu, K., and Li, G. (1998). Catalytic domain of the p120 Ras GAP binds to RAb5 and stimulates its GTPase activity. J. Biol. Chem. *273*, 10087-10090.

Liu, P., Cheng, H., Roberts, T.M., and Zhao, J.J. (2009). Targeting the phosphoinositide 3-kinase pathway in cancer. Nat. Rev. Drug. Discov. *8*, 627-644.

Liu, S., Knapp, S., and Ahmed, A.A. (2014). The structural basis of PI3K cancer mutations: from mechanism to therapy. Cancer Res. *74*, 641-646.

LoPiccolo, J., Kim, S.J., Shi, Y., Wu, B., Wu, H., Chait, B.T., Singer, R.H., Sali, A., Brenowitz, M., Bresnick, A.R., *et al.* (2015). Assembly and Molecular Architecture of the Phosphoinositide 3-Kinase p85alpha Homodimer. J. Biol. Chem. *290*, 30390-30405.

Maru, Y., and Witte, O.N. (1991). The BCR gene encodes a novel serine/threonine kinase activity within a single exon. Cell *67*, 459-468.

Masui, H., Castro, L., and Mendelsohn, J. (1993). Consumption of EGF by A431 cells: evidence for receptor recycling. J. Cell Biol. *120*, 85-93.

McPherson, A., Jr. (1976). The growth and preliminary investigation of protein and nucleic acid crystals for X-ray diffraction analysis. Methods Biochem. Anal. *23*, 249-345.

Mellman, I., and Yarden, Y. (2013). Endocytosis and cancer. Cold Spring Harb. Perspect. Biol. *5*, a016949.

Miled, N., Yan, Y., Hon, W.C., Perisic, O., Zvelebil, M., Inbar, Y., Schneidman-Duhovny, D., Wolfson, H.J., Backer, J.M., and Williams, R.L. (2007). Mechanism of two classes of cancer mutations in the phosphoinositide 3-kinase catalytic subunit. Science *317*, 239-242.

Mishra, A., Eathiraj, S., Corvera, S., and Lambright, D.G. (2010). Structural basis for Rab GTPase recognition and endosome tethering by the C2H2 zinc finger of Early Endosomal Autoantigen 1 (EEA1). Proc. Natl. Acad. Sci. U.S.A. *107*, 10866-10871.

Monteiro, H.P., Costa, P.E., Reis, A.K., and Stern, A. (2015). Nitric oxide: Protein tyrosine phosphorylation and protein S-nitrosylation in cancer. Biomed. J. *38*, 380-388.

Murray, C.I., and Van Eyk, J.E. (2012). Chasing cysteine oxidative modifications: proteomic tools for characterizing cysteine redox status. Circ. Cardiovasc. Genet. *5*, 591.

Musacchio, A., Cantley, L.C., and Harrison, S.C. (1996). Crystal structure of the breakpoint cluster region-homology domain from phosphoinositide 3-kinase p85 alpha subunit. Proc. Natl. Acad. Sci. U.S.A. *93*, 14373-14378.

Myers, M.P., Stolarov, J.P., Eng, C., Li, J., Wang, S.I., Wigler, M.H., Parsons, R., and Tonks, N.K. (1997). P-TEN, the tumor suppressor from human chromosome 10q23, is a dual-specificity phosphatase. Proc. Natl. Acad. Sci. U.S.A. *94*, 9052-9057.

Nakamura, T., and Lipton, S.A. (2016). Protein S-Nitrosylation as a Therapeutic Target for Neurodegenerative Diseases. Trends Pharmacol. Sci. *37*, 73-84.

Nassar, N., Hoffman, G.R., Manor, D., Clardy, J.C., and Cerione, R.A. (1998). Structures of Cdc42 bound to the active and catalytically compromised forms of Cdc42GAP. Nat. Struct. Biol. *5*, 1047-1052.

Nolte, R.T., Eck, M.J., Schlessinger, J., Shoelson, S.E., and Harrison, S.C. (1996). Crystal structure of the PI 3-kinase p85 amino-terminal SH2 domain and its phosphopeptide complexes. Nat. Struct. Biol. *3*, 364-374.

Ogawara, Y., Kishishita, S., Obata, T., Isazawa, Y., Suzuki, T., Tanaka, K., Masuyama, N., and Gotoh, Y. (2002). Akt enhances Mdm2-mediated ubiquitination and degradation of p53. J. Biol. Chem. *277*, 21843-21850.

Orth, J.D., Krueger, E.W., Weller, S.G., and McNiven, M.A. (2006). A novel endocytic mechanism of epidermal growth factor receptor sequestration and internalization. Cancer Res. *66*, 3603-3610.

Otwinowski, Z., and Minor, W. (1997). Processing of X-ray diffraction data collected in oscillation mode. Methods Enzymol. *276*, 307-326.

Papa, A., Wan, L., Bonora, M., Salmena, L., Song, M.S., Hobbs, R.M., Lunardi, A., Webster, K., Ng, C., Newton, R.H., *et al.* (2014). Cancer-associated PTEN mutants act in a dominant-negative manner to suppress PTEN protein function. Cell *157*, 595-610.

Pawson, T., and Gish, G.D. (1992). SH2 and SH3 domains: from structure to function. Cell *71*, 359-362.

Peck, J., Douglas, G.t., Wu, C.H., and Burbelo, P.D. (2002). Human RhoGAP domain-containing proteins: structure, function and evolutionary relationships. FEBS Lett. *528*, 27-34.

Rabinovsky, R., Pochanard, P., McNear, C., Brachmann, S.M., Duke-Cohan, J.S., Garraway, L.A., and Sellers, W.R. (2009). p85 Associates with unphosphorylated PTEN and the PTEN-associated complex. Mol. Cell. Biol. *29*, 5377-5388.

Rahdar, M., Inoue, T., Meyer, T., Zhang, J., Vazquez, F., and Devreotes, P.N. (2009). A phosphorylation-dependent intramolecular interaction regulates the membrane association and activity of the tumor suppressor PTEN. Proc. Natl. Acad. Sci. U.S.A. *106*, 480-485.

Rani, C.S., Wang, F., Fuior, E., Berger, A., Wu, J., Sturgill, T.W., Beitner-Johnson, D., LeRoith, D., Varticovski, L., and Spiegel, S. (1997). Divergence in signal transduction pathways of platelet-derived growth factor (PDGF) and epidermal growth factor (EGF) receptors. Involvement of sphingosine 1-phosphate in PDGF but not EGF signaling. J. Biol. Chem. *272*, 10777-10783.

Ross, R.L., Burns, J.E., Taylor, C.F., Mellor, P., Anderson, D.H., and Knowles, M.A. (2013). Identification of Mutations in Distinct Regions of p85 Alpha in Urothelial Cancer. PloS One *8*, e84411.

Scott, P.H., Brunn, G.J., Kohn, A.D., Roth, R.A., and Lawrence, J.C., Jr. (1998). Evidence of insulin-stimulated phosphorylation and activation of the mammalian target of rapamycin mediated by a protein kinase B signaling pathway. Proc. Natl. Acad. Sci. U.S.A. *95*, 7772-7777.

Soldati, T., Riederer, M.A., and Pfeffer, S.R. (1993). Rab GDI: a solubilizing and recycling factor for rab9 protein. Mol. Biol. Cell *4*, 425-434.

Sorkin, A., Krolenko, S., Kudrjavtceva, N., Lazebnik, J., Teslenko, L., Soderquist, A.M., and Nikolsky, N. (1991). Recycling of epidermal growth factor-receptor complexes in A431 cells: identification of dual pathways. J. Cell Biol. *112*, 55-63.

Stephens, L., Anderson, K., Stokoe, D., Erdjument-Bromage, H., Painter, G.F., Holmes, A.B., Gaffney, P.R., Reese, C.B., McCormick, F., Tempst, P., *et al.* (1998). Protein kinase B kinases that mediate phosphatidylinositol 3,4,5-trisphosphate-dependent activation of protein kinase B. Science *279*, 710-714.

Streuli, M., Krueger, N.X., Tsai, A.Y., and Saito, H. (1989). A family of receptor-linked protein tyrosine phosphatases in humans and Drosophila. Proc. Natl. Acad. Sci. U.S.A. *86*, 8698-8702.

Takahashi, Y., Morales, F.C., Kreimann, E.L., and Georgescu, M.M. (2006). PTEN tumor suppressor associates with NHERF proteins to attenuate PDGF receptor signaling. EMBO J. *25*, 910-920.

Tamguney, T., and Stokoe, D. (2007). New insights into PTEN. J Cell Sci. *120*, 4071-4079.

Tamura, M., Gu, J., Matsumoto, K., Aota, S., Parsons, R., and Yamada, K.M. (1998). Inhibition of cell migration, spreading, and focal adhesions by tumor suppressor PTEN. Science *280*, 1614-1617.

Terzyan, S., Zhu, G., Li, G., and Zhang, X.C. (2004). Refinement of the structure of human Rab5a GTPase domain at 1.05 A resolution. Acta Cryst. D *60*, 54-60.

Toker, A., and Cantley, L.C. (1997). Signalling through the lipid products of phosphoinositide-3-OH kinase. Nature *387*, 673-676.

Tolkacheva, T., Boddapati, M., Sanfiz, A., Tsuchida, K., Kimmelman, A.C., and Chan, A.M. (2001). Regulation of PTEN binding to MAGI-2 by two putative phosphorylation sites at threonine 382 and 383. Cancer Res. *61*, 4985-4989.

Tzeng, H.T., and Wang, Y.C. (2016). Rab-mediated vesicle trafficking in cancer. J. Biomed. Sci. *23*, 70.

Vasudevan, K.M., and Garraway, L.A. (2010). AKT signaling in physiology and disease. Curr. Top. Microbiol. Immunol. *347*, 105-133.

Vazquez, F., Grossman, S.R., Takahashi, Y., Rokas, M.V., Nakamura, N., and Sellers, W.R. (2001). Phosphorylation of the PTEN tail acts as an inhibitory switch by preventing its recruitment into a protein complex. J. Biol. Chem. *276*, 48627-48630.

Vazquez, F., Matsuoka, S., Sellers, W.R., Yanagida, T., Ueda, M., and Devreotes, P.N. (2006). Tumor suppressor PTEN acts through dynamic interaction with the plasma membrane. Proc. Natl. Acad. Sci. U.S.A. *103*, 3633-3638.

Velazquez-Campoy, A., Ohtaka, H., Nezami, A., Muzammil, S., and Freire, E. (2004). Isothermal titration calorimetry. Current protocols in cell biology / editorial board, Juan S. Bonifacino ... [et al.] *Chapter 17*, Unit 17 18.

Vivanco, I., and Sawyers, C.L. (2002). The phosphatidylinositol 3-Kinase AKT pathway in human cancer. Nat. Rev. Cancer *2*, 489-501.

Vogt, P.K., Hart, J.R., Gymnopoulos, M., Jiang, H., Kang, S., Bader, A.G., Zhao, L., and Denley, A. (2010). Phosphatidylinositol 3-kinase: the oncoprotein. Curr. Top. Microbiol. Immunol. *347*, 79-104.

Winn, M.D., Ballard, C.C., Cowtan, K.D., Dodson, E.J., Emsley, P., Evans, P.R., Keegan, R.M., Krissinel, E.B., Leslie, A.G., McCoy, A., *et al.* (2011). Overview of the CCP4 suite and current developments. Acta Cryst. D *67*, 235-242.

Witt, J.J., and Roskoski, R., Jr. (1975). Rapid protein kinase assay using phosphocellulose-paper absorption. Anal. Biochem. *66*, 253-258.

Wong, K.K., Engelman, J.A., and Cantley, L.C. (2010). Targeting the PI3K signaling pathway in cancer. Curr. opin. Genet. Dev. *20*, 87-90.

Woodman, P.G. (2000). Biogenesis of the sorting endosome: the role of Rab5. Traffic *1*, 695-701.

Wu, X., Hepner, K., Castelino-Prabhu, S., Do, D., Kaye, M.B., Yuan, X.J., Wood, J., Ross, C., Sawyers, C.L., and Whang, Y.E. (2000a). Evidence for regulation of the PTEN tumor suppressor by a membrane-localized multi-PDZ domain containing scaffold protein MAGI-2. Proc. Natl. Acad. Sci. U.S.A. *97*, 4233-4238.

Wu, Y., Dowbenko, D., Spencer, S., Laura, R., Lee, J., Gu, Q., and Lasky, L.A. (2000b). Interaction of the tumor suppressor PTEN/MMAC with a PDZ domain of MAGI3, a novel membrane-associated guanylate kinase. J. Biol. Chem. *275*, 21477-21485.

Yim, E.K., Peng, G., Dai, H., Hu, R., Li, K., Lu, Y., Mills, G.B., Meric-Bernstam, F., Hennessy, B.T., Craven, R.J., *et al.* (2009). Rak functions as a tumor suppressor by regulating PTEN protein stability and function. Cancer Cell *15*, 304-314.

Yu, J., Zhang, Y., McIlroy, J., Rordorf-Nikolic, T., Orr, G.A., and Backer, J.M. (1998). Regulation of the p85/p110 phosphatidylinositol 3'-kinase: stabilization and inhibition of the p110alpha catalytic subunit by the p85 regulatory subunit. Mol. Cell. Biol. *18*, 1379-1387.

Yuan, T.L., and Cantley, L.C. (2008). PI3K pathway alterations in cancer: variations on a theme. Oncogene *27*, 5497-5510.

Zhao, L., and Vogt, P.K. (2008). Class I PI3K in oncogenic cellular transformation. Oncogene *27*, 5486-5496.

Zhu, G., Liu, J., Terzyan, S., Zhai, P., Li, G., and Zhang, X.C. (2003). High resolution crystal structures of human Rab5a and five mutants with substitutions in the catalytically important phosphate-binding loop. J. Biol. Chem. *278*, 2452-2460.

Zhu, G., Zhai, P., Liu, J., Terzyan, S., Li, G., and Zhang, X.C. (2004). Structural basis of Rab5-Rabaptin5 interaction in endocytosis. Nat. Struct. Mol. Biol. *11*, 975-983.